POLARIZATION DIVERSITY PLANAR ANTENNA FOR PORTABLE MOBILE DEVICES

KOMSAK MEKSAMOOT

A THESIS SUBMITTED IN PARTIAL FULFILLMENT OF
THE REQUIREMENT FOR THE DEGREE OF
DOCTOR OF ENGINEERING IN ELECTRICAL ENGINEERING
SCHOOL OF GRADUATE STUDIES
KING MONGKUT'S INSTITUTE OF TECHNOLOGY LADKRABANG
2001

ISBN 974-648-479-6

หัวข้อวิทยานิพนธ์	**สายอากาศระนาบแบบแยกการโพลาไรซ์สำหรับอุปกรณ์สื่อสารเคลื่อนที่แบบพกพา**
นักศึกษา	**นายคมศักดิ์ เมฆสมุทร**
รหัสประจำตัว	40060003
ปริญญา	**วิศวกรรมศาสตรดุษฎีบัณฑิต**
สาขาวิชา	**วิศวกรรมไฟฟ้า**
พ.ศ.	2544
อาจารย์ผู้ควบคุมวิทยานิพนธ์	รศ.ดร.โมไนย ไกรฤกษ์

บทคัดย่อ

วิทยานิพนธ์นี้นำเสนอสายอากาศระนาบรูปตัวเอฟกลับหัวแบบแยกการโพลาไรซ์สำหรับโทรศัพท์เคลื่อนที่แบบพกพา เพื่อแก้ปัญหาเฟดดิงหลายวิถีโดยที่สายอากาศยังคงมีโครงสร้างกระทัดรัด ด้วย สายอากาศมีโครงสร้างประกอบด้วยแผ่นโลหะสี่เหลี่ยมจัตุรัสที่มีขนาดในแนวทแยงมุมประมาณหนึ่งในสี่ของความยาวคลื่น ทำหน้าที่เป็นตัวแผ่คลื่น ที่มุมหนึ่งของตัวแผ่คลื่นจะลัดวงจรด้วยแท่งตัวนำ ส่วนด้านข้างทั้งสองที่มุมจะมีอาร์เอฟสวิตช์ต่ออยู่เพื่อทำหน้าที่เป็นตัวสวิตช์เลือกสาขาการโพลาไรซ์เป็นแบบแผนคลื่นการโพลาไรซ์แนวตั้งเป็นใหญ่หรือแนวนอนเป็นใหญ่ อย่างใดอย่างหนึ่ง

ในการวิเคราะห์ได้ใช้วิธีแบบจำลองเส้นลวดร่วมกับวิธีเชิงโมเมนต์โดยจะเริ่มวิเคราะห์จากโครงสร้างของสายอากาศบนระนาบกราวด์ จากนั้นจะเป็นสายอากาศบนแบบจำลองโทรศัพท์มือถือและสุดท้ายจะเพิ่มแบบจำลองของตัวผู้ใช้โทรศัพท์เพื่อจำลองแบบให้เสมือนสภาวะการใช้งานจริง

คุณสมบัติพื้นฐานของสายอากาศจะแสดงด้วยอิมพีแดนซ์ขาเข้า การกระจายกระแสบนโครงสร้างสายอากาศ แบบรูปการแผ่พลังงาน และประสิทธิภาพ ซึ่งประสิทธิภาพในการแผ่พลังงานสายอากาศระนาบรูปตัวเอฟกลับหัวแบบแยกการโพลาไรซ์จะมีค่าประมาณ 50% โดยจะสูงกว่ากรณีของสายอากาศโมโนโพลเล็กน้อย ส่วนสมรรถนะเชิงการสื่อสารของสายอากาศบนโทรศัพท์มือถือที่มีแบบจำลองของผู้ใช้อยู่ด้วยภายใต้สภาพแวดล้อมหลายวิถี สามารถแสดงในเชิงปริมาณด้วยพารามิเตอร์เชิงไดเวอร์ซิตีซึ่งได้แก่อัตราขยายประสิทธิผลเฉลี่ย สัมประสิทธิ์สหสัมพันธ์ อัตราขยายไดเวอร์ซิตีและอัตราขยายสายอากาศเชิงไดเวอร์ซิตี ซึ่งอัตราขยายสายอากาศเชิงไดเวอร์ซิตีจะมีค่าลดลงประมาณ 4 dB เมื่อมีร่างกายของผู้ใช้ร่วมด้วย หรือกล่าวอีกอย่างหนึ่งได้ว่าร่างกายผู้ใช้จะลดสมรรถนะเชิงการสื่อสารลงประมาณครึ่งหนึ่ง

Thesis Title	Polarization Diversity Planar Antenna for Portable Mobile Devices
Student	Mr. Komsak Meksamoot
Student ID.	40060003
Degree	Doctor of Engineering
Programme	Electrical Engineering
Year	2001
Thesis Advisor	Assoc.Prof. Dr. Monai Krairiksh

ABSTRACT

This thesis proposes a polarization diversity planar inverted-F antenna (PIFA) —to be a built-in antenna for a portable mobile telephone—to mitigate the short-term multipath fading of the received signal at mobile terminal while the antenna dimension maintains compactness. The antenna comprises a square metallic patch, as a radiator of approximate quarter-wavelength in diagonal dimension, with one permanent short-pin at one corner and two RF-switches at two beside corners. These RF-switches perform as the polarization branch switches for either dominantly vertical polarization (VP) or dominantly horizontal polarization (HP) modes.

The wire-grid modeling based on the Method of Moments is utilized for the analysis. Antenna analysis begins with the structure of antenna on a ground plane, then antenna on portable telephone and, eventually, including a user's body to realize the practical situation.

Fundamental characteristics of the antenna are shown in terms of input impedance, current distribution, radiation patterns, and efficiency. The radiation efficiency of the polarization diversity PIFA is approximately 50%, which is a few percents higher than that of the monopole antenna case. Communication performance of the antenna on portable telephone with the user's model under multipath environment can be quantitatively revealed in terms of mean effective gain, correlation coefficient, diversity gain and diversity antenna gain. The diversity antenna gain of the antenna is 4 dB inferior if the user's body is included. In other words, the presence of the user's body degrades the communication performance by a half.

ACKNOWLEDGEMENTS

I would like to express my gratitude and sincere thanks to many people involved in various aspects with this thesis.

First of all, my deep and grateful thanks is dedicated to Assoc.Prof. Dr. Monai Krairiksh, my supervisor, for his support, helpful suggestions, continuous attention and stimulation the progress of this research. I also profoundly appreciate Assoc.Prof. Dr. Jun-ichi Takada of TITech (Tokyo Institute of Technology), Japan for his invaluable guidance, useful discussion, and for his arrangement to provide me the visiting research scholarships to TITech.

I am particularly grateful to Prof. Dr. Wiwat Kiranon for his encouragement to pursue the advanced study since my undergraduate course. His great personality, humanity and understanding have impressed me and made my experiences in KMITL really invaluable. I would also like to thank Assist.Prof. Dr. Sompol Kosulvit for his hospitality and kind advice on additional knowledge.

In addition, I would like to thank my friends in Wireless Communication Laboratory: Dr. Chuwong Phongcharoenpanich, Mr. Chanchai Thongsopa, and Mr. Rangsan Wongsan for sharing and lessening depressive emotion sometimes occured during doctoral course; Mr. Chaiwat Leekpai, Mr. Duang-arthit Srimoon, Mr. Anat Mearnchu, Mr. Phaisan Ngamjanyaporn, and Ms. Wanlika Buasomboon for their partial contributions to the experiment. Especially, my thank goes to Ms. Panisa Keowsawat for her assistance in manipulating diversity data as well as her discussion that deepen our knowledge in diversity technology. Also, I wish to thank all members of Takada Laboratory, TITech for having created a friendly environment and for their patient advices during my training there supported by JICA (Japanese International Cooperation Agency) in 1998.

For long time spending life while pursuing graduate studies, I appreciate my room-mates: Mr. Amorn Jiraseree-amornkun, Mr. Nayot Kurukitkoson, and Mr. Arkhom Suvannakita for their cheerfulness and their inevitable patience with my behavior.

Special thank is to Dr. Koichi Ogawa of Matsushita Electric Industrial Co., Ltd., Osaka, Japan for the invitation to visit his laboratory to observe the research facilities and methodologies, and for his helpful discussion on the diversity parameters. Thank is also to Prof. Dr. Kiyomichi Araki of TITech for his constructive comments during his being as a short-term expert of JICA at KMITL in year 2000.

I wish to thank INCOCSAT (International Cooperation Center for Science and Technology), TITech for awarding me the visiting research scholarships, which made contributions to my research knowhow. The support for computers and measuring instrument, the essential infrastructures to conduct research, from the Japanese Government via JICA is very appreciated.

My gratitude is due to NSTDA (National Science and Technology Development Agency), Thailand for awarding me the doctoral scholarship under the local graduate scholarship program, which made this thesis possible. A partial support from NSTDA via IMT-2000 Research and Development Project, is also appreciated.

Finally, this thesis is dedicated to my parents, who have been constant support throughout my life.

TABLE OF CONTENTS

LIST OF TABLES

Tables **Page**

Figures **Page**

Chapter 1

Introduction

1.1 Background of Antennas in Mobile Systems

The development of antennas for mobile communications may be classified according to progress in system development into five generations as shown in Tab. 1.1. The first generation is (generally accepted and) traced back to nearly the end of the 19th century, when wireless telegraphy by means of electrostatic coupling was developed by Thomas Edison and used for communication between trains and railway stations. The *metal strip* was used as an antenna at that time, hence it could be considered as *the first type of mobile antennas*. In early 1900, the wireless telegraphs in HF band were practically used in ship communications. Many linear antennas were invented such as inverted-L antennas (ILA), fan antennas, and top-loaded monopoles during this time.

Just after the World War II (second generation), the utilization of frequency bands were gradually raised from HF to VHF and then lower UHF bands. Consequently, it led to the significant progress of antenna technology, i.e., the development of the inverted-F antenna (IFA), the normal mode helical antenna (NMHA), and the very small rectangular-loop antenna for various mobile applications.

The advances in antenna design associated with propagation and systems started in the middle of the 1970s (third generation). It is relevant to the first generation (1G-) mobile communications (FDMA, analog system). Intensive study of propagation problems, especially *multipath propagation phenomena*, was done and *diversity systems* have been developed to cope with the multipath fad-

Table 1.1 Progress of antennas for mobile systems.

Generation	I	II	III	IV	V
Year	~1900~	1950~	1975~	1990~	2000~
Frequency	LF–HF	< 400 MHz	< 1.5 GHz	< 3 GHz	~ELF
System	Telegraph/ Telephony for Train, Ship, Aircraft, Police Car	Voice System for Business, Navigation, Taxi	Paging, Portable Tx. & Rx., NTT, NMT, AMPS	SatCom— Voice and Data Ch. for Aircraft, PCS, PDC, GSM	WPAN (Blue Tooth), LMDS, MMDS, HAP, ITS, IMT-2000
Antenna	*Metal Strip*, Monopole, Whip, ILA ⇒	Blade, Ferrite Loop, NMHA, IFA ⇒	Dipole, Collinear, LCX, MSA, PIFA ⟹	Bifilar/ Quadrifilar Helix	Antenna System with Signal Processing

ing problem, which is very serious in urban area communication. The antennas used for mobile terminals had been developed during this time were: microstrip antenna (MSA), planar inverted-F antenna (PIFA) and so forth. In particular applications, such as train communication, the leaky coaxial cable (LCX) had been invented and used at the railway station side.

The fourth generation (from 1990) of mobile antennas correspond to the 2G-mobile communications (TDMA, digital system). The mobile terminals were getting smaller and mobile antenna also had to be miniaturized.

The mobile antennas are now moving to the fifth generation (relevant to the 3G-mobile communications, CDMA, digital system) where broad-band, multi-band, and built-in antennas are required for modern multi-mode mobile terminals. Antenna may be closely integrated with system employing advanced signal processing.

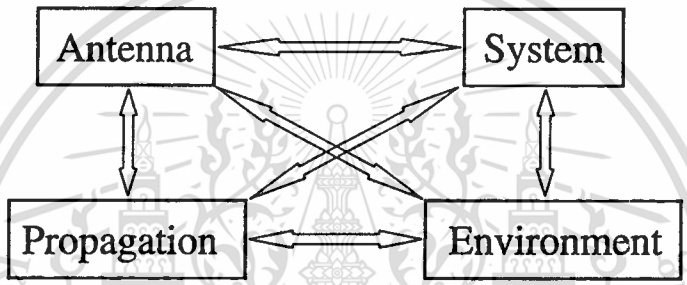

Figure 1.1 Antenna and related factors in mobile communication systems.

At present, personal communications can be considered as a part of daily-life essence. Antenna technology has made a great contribution to the progress of mobile communications. Key devices for transmitting and receiving signal between portable unit and base station are antennas. The real significant antenna design in mobile communication systems seems to have gained new understanding and the important roles of antennas has been recognized [1, 2]. *The antenna is a critical element that can either enhance or constrain system performance* [3]. Consequently, antenna performance and characteristics have come to be studied extensively, specifically taking mobile environment conditions into account. Design of antenna today not only concerns its element, but also includes consideration of factors related to propagation, systems, and environment conditions (Fig. 1.1). Those factors are in general closely interrelated and treated systematically when an antenna is designed.

Antenna classification by applications from a system exposition can be land, maritime, aeronautical, and satellite systems. This thesis only focuses on land (terrestrial) mobile system.

The following topics briefly review the antennas used in land mobile systems. The land mobile antennas can be categorized into three major groups; base station antennas, vehicular mobile antennas, and portable mobile antennas. However, here focuses on only the polarization diversity antenna types.

The detailed reasons on the necessities of polarization diversity scheme for enhancing the mobile antenna system performance will be given in Sec. 5.2.1.

1.1.1 Base Station Antennas

The base station antenna configurations depend on the size and shape of the service area and the number of cells and channels. In a private mobile communication systems whose service area is small, the base station antenna is as small as the vehicle-mount antenna used in automobile telephone systems. If the service area is limited within a restricted angle in the horizontal plane, a corner reflector antenna or bi-directional antenna are often used [4, 5, 6]. When the service area is wide, as in a pager system, maritime telephone system, or aeronautical telephone system, a linear array antenna, which has large directivity in vertical plane, is often used as in cellular systems [7, 8, 9, 10].

1.1.2 Vehicular Mobile Antennas

The antenna widely used for vehicular terminal is whip antenna (flexible version of monopole antenna). In specific satellite-mobile system, a circularly polarized conical beam spherical slot array antenna [11] is an interesting candidate due to its low-profile property which pertinent to aerodynamic constrain of the vehicle. While in land-mobile system, a notch-wire composite antenna for polarization diversity reception [12] is used instead.

1.1.3 Portable Mobile Antennas

The trend of the portable telephone technology in the last few years has been dramatically decreased in the size and the weight of the unit as illustrated in Fig. 1.2. In the initial offering (early 1980s), the portable cellular phone was about 6,600cc in volume (including batteries). Today (2001), the most recent cellular portable telephones have a volume of 90cc. These dramatic weight and volume improvements have necessitated a rapid evolution of the antennas used for the telephones. The design efforts have been to maintain approximately the same antenna performance in terms of gain coverage area, and bandwidth in the face of rapidly decreasing size requirements [13].

Monopole antenna is often used in portable telephone or laptop computer [14] due to its low cost and simple structures. However, the monopole antenna are easily damaged, due to its nonrigid and protruding structure. Also, more than a half of radiated power from a portable-mounted monopole antenna may be absorbed in the user's body [15, 16, 17, 18]. Loop antenna is seldom used to replace monopole antennas due to its low radiation efficiency and need of matching circuit limits its popularity [19], except for received performance in pager system [20]. Microstrip antennas are an alternative to monopole and loop antennas that can be designed to reduce these problems. They can be made conformal with the portable telephone for protection from damage. They can

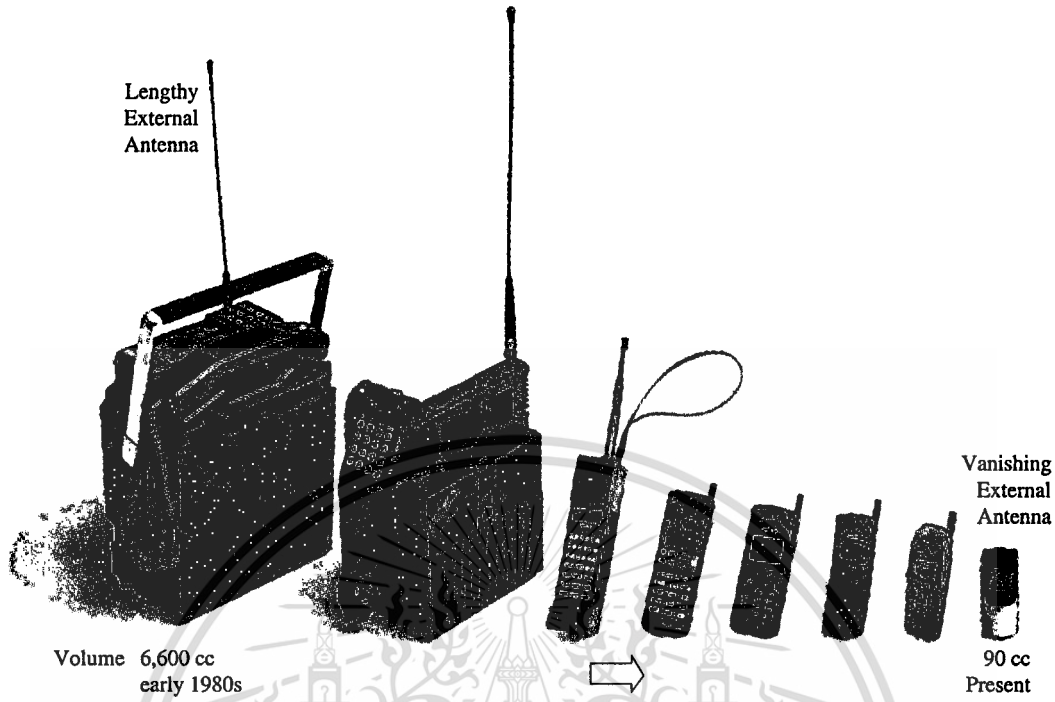

Figure 1.2 Evolution and miniaturization of portable mobile telephones with attached antenna [from *Wireless Asia Mag.*, vol. 2, no. 9].

also be positioned away from the head and hand to reduce power deposition in the user's body. Many microstrip antenna configurations have been developed for portable telephone [21, 22, 23, 24]. For the very small portable telephone, the shorted circuit microstrip antenna known as planar inverted-F antenna(PIFA) operated on quarter-wavelength principle is used instead due to its very compact size [25, 26, 27, 28, 29, 30, 31, 32, 33, 34].

1.2 Purpose and Scope of the Study

This thesis proposes a polarization diversity planar inverted-F antenna (PIFA) —to be a built-in antenna for a portable mobile telephone—to mitigate the short-term multipath fading of the received signal at mobile terminal while the antenna is capable to maintain the compact dimension. The most interesting aspect of the PIFA [33] is its low-profile and most fundamental resonance on quarter-wavelength mode. The wire-grid modeling based on the Method of Moments is utilized for the analysis. This thesis also investigates the external field interaction between the polarization diversity PIFA on a portable telephone and the operator's body, from the chest to the head, under the mobile urban environment.

The diversity performance of this antenna on a ground plane have been first

theoretically studied in [35], and then the semi-empirical results have been confirmed in [36]. The ground plane was replaced by a portable telephone in [37], and [38] compared the performance of the antenna on the ground plane with the antenna on the portable telephone. The simple model of user's body has been taken into account in [39], more realistic user's and propagation models have been analyzed and reported in [40] successively. This thesis compiles the results presented in [35, 36, 37, 38, 39, 40] and thoroughly analyzes the problem in more interesting aspects. The results are revealed in two categories; first, fundamental characteristics in terms of input impedance, current distribution, radiation patterns, and efficiency; later, diversity characteristics in terms of mean effective gain, correlation coefficient, diversity gain, and diversity antenna gain quantitatively.

1.3 Thesis Outline

This thesis is mainly concerned with portable mobile antenna applied with polarization diversity scheme and propagation characteristics in mobile urban environment. Additionally, the user's body is taken into account in the analysis of the antenna performance. The thesis is composed of six chapters. Some literature surveys are also provided at the beginning of each chapter. Their contents will be outlined as follows:

Chapter 1 gives an introduction and outline of the thesis. The history of mobile communication systems, necessity of antennas to the system are described. The introduction of diversity techniques to improve the mobile systems is briefed. Also the motivations and aims of conducting that part of research is included.

Chapter 2 describes the radiowave propagation characteristics in mobile environment and explains the diversity techniques with combining methods commonly used in mobile communications to mitigate the received signal fading caused by the multipath propagation.

Chapter 3 mainly deals with theoretical expressions of mobile antenna performance, i.e., angular distribution model of incident waves, mean effective gain, correlation characteristics, diversity gain which is based on the improvement of received bit error rate (BER), and diversity antenna gain which is the product between diversity gain and the maximum mean effective gain.

Chapter 4 provides the methodology needed for simulating the effects of radiated structure as well as absorbing material. The canonical examples relevant to the practical problem are described. Knowhow for properly modeling is discussed and considered as accuracy analysis. The numerical method used throughout this thesis is also explained in this chapter.

Chapter 5 is concerned with the modeling and fundamental characteristics of the polarization diversity PIFA from on the ground plane to on portable telephone with user's body.

Chapter 6 renders the communication performance of polarization diversity PIFA in terms of diversity parameters, i.e., mean effective gain, correlation co-

efficient, diversity gain, and diversity antenna gain, in statistical sense.

The thesis conclusions are given in Chap. 7, where some suggestions are also given for further research works in the field.

Chapter 2

Mobile Propagation and Diversity Techniques

2.1 Introductory Remarks

This chapter introduces the mobile propagation characteristics from the large- to small-scales. The small-scale propagation will be discussed deeply in details. To mitigate the signal deep fading resulted from multipath propagation, various diversity techniques together with combining methods are described as the remedies.

2.2 Mobile Radiowave Propagation

The radiowave propagation places fundamental limitations on the performance of mobile communication systems. The transmission path between the transmitter and the receiver can vary from simple line-of-sight to one that is severely obstructed by buildings, mountains, foliage and other various kinds of surroundings. Unlike wired transmission of which channels are static and predictable, radio channels are extremely random and very difficult to analyze deterministically.

The electromagnetic wave propagation mechanisms in multipath environment can generally be attributed to random scattering as illustrated in Fig. 2.1. Most mobile radio systems operate in urban areas where there is no direct line-of-sight path between transmitter and receiver, and where the presence of tall buildings causes severe diffraction loss. Due to multiple reflections from surroundings, the electromagnetic waves travel along different paths of varying path lengths. The interaction between these waves causes *multipath fading* (small-scale propagation) at a specific location, and the strengths of waves decrease as the distance between the transmitter and receiver increases (large-scale propagation) as depicted in Fig. 2.2.

2.2.1 Large-Scale Propagation: Path Loss

Propagation models that predict the mean signal strength for an arbitrary transmitter-receiver separation distance are useful in estimating the radio coverage area of a transmitter and are called large-scale propagation model. As the mobile moves away from the transmitter over much larger distance, the local average

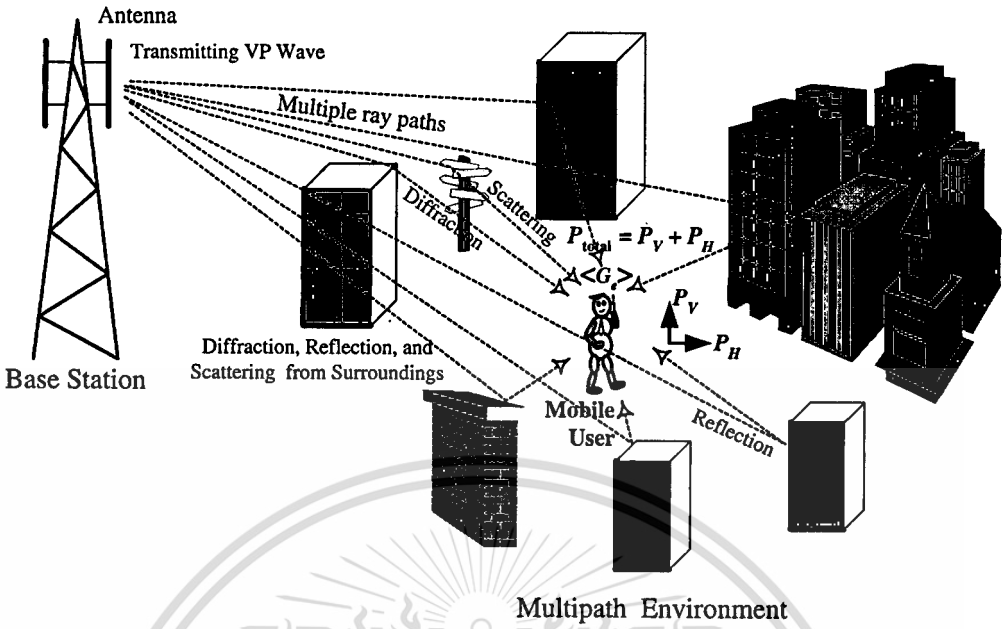

Figure 2.1 Radiowave propagation mechanisms which cause fading signal at mobile user in multipath environment.

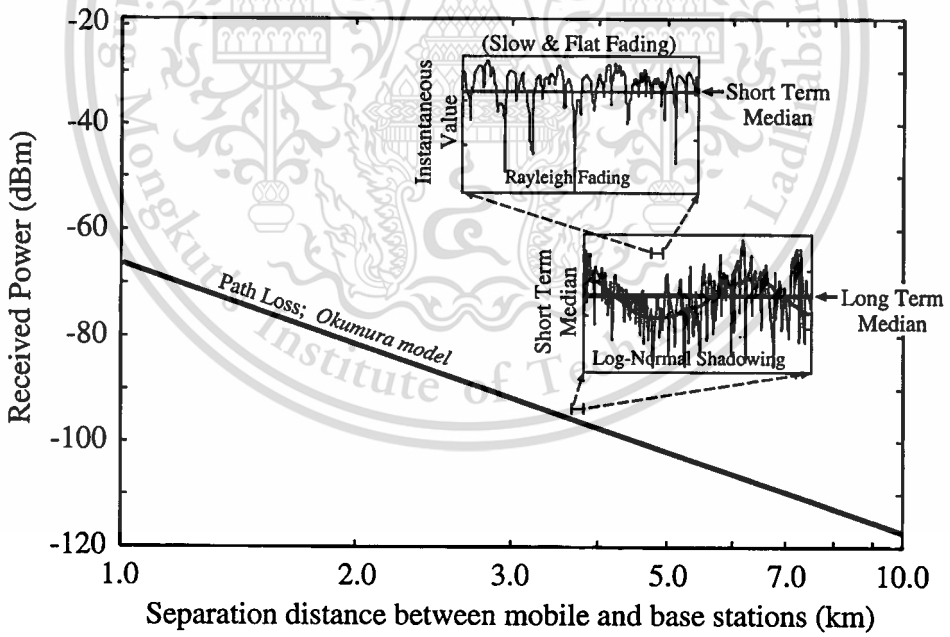

Figure 2.2 Large-scale (path loss) and small-scale (shadowing and fading) propagation characteristics.

received signal will gradually be decreased as depicted in Fig. 2.2, and it is this local average signal level that is predicted by large-scale propagation model.

Both theoretical and measurement-based propagation models indicate that average received dB signal power decreases logarithmically with distance, whether in outdoor or indoor environments. The average large-scale path loss, L, for an arbitrary transmitter-receiver separation, r, is expressed as a function of distance by using a path loss exponent, n,

$$L = L(r_0) + 10\log(\frac{r}{r_0})^n \qquad [\text{dB}] \tag{2.1}$$

where the path loss exponent index n equals 2 for free-space, 3–5 for urban cellular radio, 4–6 for obstructed in building, and 1.6–1.8 for line-of-sight in building environments [41]. r_0 is the close-in reference distance which is determined from the measurements close to the transmitter. In large coverage cellular system, 1 km reference distances are commonly used, whereas in microcellular systems, much smaller distances (such as 100 m or 1 m) are used. The reference distance should always be in far-field of the antenna. However, (2.1) does not consider the difference of the surrounding environments between two locations having the same distance.

The most widely used path loss model is Hata's model [42] which is for signal prediction in urban areas. This model is an empirical formulation of the geographic path loss provided by Okumura, and is valid from 150 to 1500 MHz. The European Co-operative for Scientific and Technical research (EURO-COST) formed the COST-231 working committee to develop an extended version of the Hata model. The proposed path loss model to be applicable to the personal communication services (PCS) is

$$\begin{aligned} L_{urban} &= 46.3 + 33.9\log f - 13.82\log h_{base} - a(h_{mobile}) \\ &\quad + (44.9 - 6.55\log h_{base})\log r + C_M, \end{aligned} \tag{2.2}$$

where f is the frequency (in MHz) from 1,500–2,000 MHz, h_{base} is the effective base station antenna height (in meters) ranging from 30 m to 200 m, h_{mobile} is the effective mobile antenna height (in meters) ranging from 1 m to 10 m, r is the transmitter-receiver separation distance (in km), and $a(h_{mobile})$ is the correction factor for effective mobile antenna height which is a function of the size of the coverage area. For a small to medium sized city, the mobile antenna correction factor is given by

$$a(h_{mobile}) = (1.1\log f - 0.7)h_{mobile} - (1.56\log f - 0.8) \tag{2.3}$$

and for a large city, it is given by

$$a(h_{mobile}) = 3.2(\log 11.75h_{mobile})^2 - 4.97, \tag{2.4}$$

and

$$C_M = \begin{cases} 0 \text{ dB} & \text{for medium sized city and suburban area,} \\ 3 \text{ dB} & \text{for metropolitan center.} \end{cases} \tag{2.5}$$

The above path loss models are sufficiently accurate for prediction of the macrocellular systems which radius of the cell is more than 1 km, whereas the smaller radius (< 1 km) microcellular systems have different characteristics. The studies of microcellular propagation characteristics have just been received attentions less than ten years before. At the beginning, the microcell propagation was studied by the measurement as by Rappaport et. al. [43] for factory environments, and by Xia et. al. [44] for urban and suburban environments. Just previous years, the simulation tools such as *ray tracing technique* and the *uniform theory of diffraction* (UTD) [45], or even recently the *finite-difference time-domain* (FD-TD) method have been introduced to effectively predict the propagation characteristics of micro-, nano-, or picocellular systems. However, propagation simulations need very long simulation time and high performance computer, that has been available recently, due to the large volume of computational space.

2.2.2 Small-Scale Propagation: Fading and Multipath

Small-scale fading, or simply *fading*, is used to describe the rapid fluctuation of the amplitude of radio signal over a short period of time or travel distance, so that the large-scale path loss effects may be ignored. Fading is caused by interference between two or more versions of the transmitted signal which arrive the receiver at slightly different times. These waves, called *multipath waves* as shown in Fig. 2.1, combine at the receiver antenna to give a resultant signal which can vary widely in amplitude and phase, depending on the distribution of intensity and relative propagation time of the waves and the bandwidth of the transmitted signal. In small-scale fading, the received signal power may vary by as much as three or four order of magnitude (30 or 40 dB) when the receiver is moved by only a fraction of wavelength as illustrated in the inset of Fig. 2.2. There were a number of researchers interested in small-scale fading modeling. Many fading models were briefly described and analyzed in [46], whereas [47] unified the approaches to the performance analysis of digital communication over generalized fading channels.

Due to the constructive and destructive effects of multipath waves summing at various points in space, a receiver moving at high speed can pass through several fades in small period of time, as depicted in the inset of Rayleigh fading in Fig. 2.2. In more serious case, a receiver may stop at a particular location at which the received signal is in a deep fade. To maintain good communications, antenna diversity techniques can alleviate deep fading nulls, as being discussed in the next section.

2.2.2.1 Types of Small-Scale Fading

I. **Fading effects due to multipath time delay spread**

A. **Flat Fading**

The received signal will undergo flat fading if the mobile radio channel has a constant gain and linear phase response over a bandwidth which is greater than the bandwidth of the transmitted signal. In flat fading, the multipath structure of the channel is such that the spectral characteristics of the transmitted signal are preserved at the receiver. However the strength of the received signal changes with time, due to fluctuations in gain of the channel caused by multipath. The distribution of the instantaneous gain of flat fading channels is important for designing radio link, and the most common amplitude distribution is the Rayleigh distribution.

B. **Frequency Selective Fading**
The channel creates frequency selective fading on received signal if the channel possesses a constant gain and linear phase response over a bandwidth which is smaller than the bandwidth of the transmitted signal. Specifically, the channel is called frequency selective when the delay spread is larger than $\frac{1}{10}$ of symbol duration, from the viewpoint of modem design. Frequency selective fading is due to *time dispersion* (multipath delay spread) of the transmitted symbols within channel. Hence, the channel induces *intersymbol interference* (ISI).

II. **Fading effects due to Doppler spread**

A. **Fast Fading**
In a fast fading channel, the channel impulse response changes rapidly within the symbol duration. Specifically, $f_d T_s$ is used as a measure of the fast/slow fading; where f_d is the maximum Doppler frequency, and T_s is the symbol duration. When this value is greater than 10^{-3}, the channel is said to be fast fading channel. In practice, fast fading only occurs for very low data rates.

B. **Slow Fading**
The channel impulse response changes at a rate much slower than the transmitted baseband signal.

2.2.2.2 Rayleigh and Nakagami-Rice Distributions

In a slow fading channel, to describe the statistical time varying nature of the received signal envelope in mobile communications, two fundamental types of distribution are utilized.

I. **Rayleigh Distribution**
In mobile communications, Rayleigh distribution is commonly used to explain the characteristic of signal envelope (r) of flat fading under non-line-of-sight condition. The Rayleigh distribution has a probability density

function (PDF) given by

$$p(r) = \begin{cases} \frac{r}{\sigma^2} e^{-\left(\frac{r^2}{2\sigma^2}\right)} & (0 \le r \le \infty), \\ 0 & (r < 0) \end{cases} \tag{2.6}$$

where σ is the RMS (root mean square) value of the received voltage signal before envelope detection, and σ^2 is the time-average power of the received signal before envelope detection.

The probability that the envelope of the received signal does not exceed a specified value or equivalently, the probability that the signal envelope, r, falls below a certain specified threshold, R, is the *outage probability* which is given by the corresponding cumulative distribution function (CDF)

$$P(R) = P_r(r \le R) = \int_0^R p(r)dr = 1 - e^{-\left(\frac{R^2}{2\sigma^2}\right)}. \tag{2.7}$$

The mean or expected value ($E\{\cdot\}$) of r of the Rayleigh distribution is given by

$$E\{r\} = \int_0^\infty r\, p(r)dr = \sigma\sqrt{\frac{\pi}{2}} = 1.2533\sigma. \tag{2.8}$$

II. Nakagami-Rice Distribution

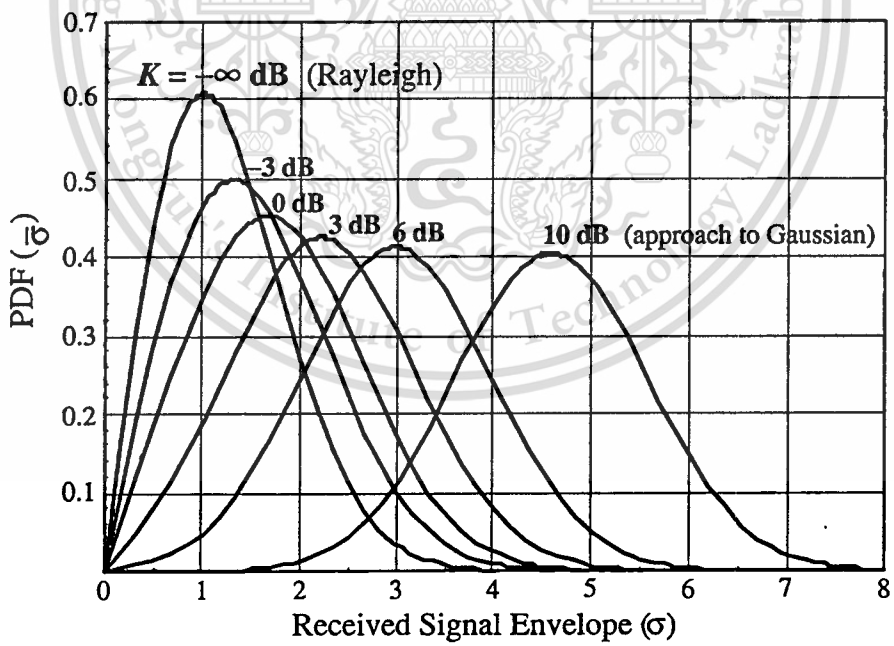

Figure 2.3 Probability density function of Nakagami-Rice distribution.

Nakagami-Rice distribution is commonly used to explain the characteristic of signal envelope of flat fading under line-of-sight condition. Sometimes it

is referred as Nakagami-n or Rician distributions. The PDF of Nakagami-Rice distribution is given by

$$p(r) = \begin{cases} \frac{r}{\sigma^2} e^{-\left(\frac{r^2+A^2}{2\sigma^2}\right)} \cdot I_0\left(\frac{Ar}{\sigma^2}\right) & (A \geq 0, r \geq 0), \\ 0 & (r < 0). \end{cases} \tag{2.9}$$

The parameter A denotes the peak amplitude of the dominant signal and $I_0(\cdot)$ is the zeroth-order modified Bessel function of the first kind.

The mth-order modified Bessel function of the first kind can be expressed as the integral

$$I_m(z) = \frac{1}{2\pi} \int_{-\pi}^{\pi} (-je^{-j\theta})^k e^{-z\sin\theta} d\theta, \tag{2.10}$$

where $j = \sqrt{-1}$.

The Nakagami-Rice distribution is often described in terms of a parameter K which is defined as the ratio between the deterministic signal power and the variance of the multipath. It is given by

$$K = \frac{A^2}{2\sigma^2}. \tag{2.11}$$

The parameter K is known as the Rician factor (related to Nakagami-n distribution via $n^2 = K$) and specifies the Nakagami-Rice distribution. As $A \to 0, K \to 0$, and as the dominant path decreases in amplitude, the Nakagami-Rice distribution degenerates to a Rayleigh distribution.

The Nakagami-Rice CDF can be expressed by [48]

$$\begin{aligned} P(R) &= 1 - e^{-\left(\frac{R^2+A^2}{2\sigma^2}\right)} \sum_{m=0}^{\infty} \left(\frac{A}{R}\right)^m \cdot I_m\left(\frac{RA}{\sigma^2}\right) \\ &= 1 - e^{-\left(\frac{R^2}{2\sigma^2}+K\right)} \sum_{m=0}^{\infty} \left(\frac{\sigma\sqrt{2K}}{R}\right)^m \cdot I_m\left(\frac{R\sqrt{2K}}{\sigma}\right). \end{aligned} \tag{2.12}$$

This formulation is very difficult to evaluate due to the summation of an infinite number of terms. Practically, it is sufficient to increase m to a value, where the last term's contribution becomes less than 0.1%.

2.2.2.3 Level Crossing Rate and Average Fade Duration

The level crossing rate (LCR) and average fade duration (AFD) are regarded as secondary-order statistic, since it is time-dependent. They are illustrated in Fig. 2.4: the LCR is the number of positive-going crossings of a reference level $\bar{r}$ in unit time, while the AFD is the average time between negative and positive level-crossings.

It is clear from Fig. 2.4 that the signal spends most of its time crossing signal levels just below the reference value, and that deep fades below this value have far

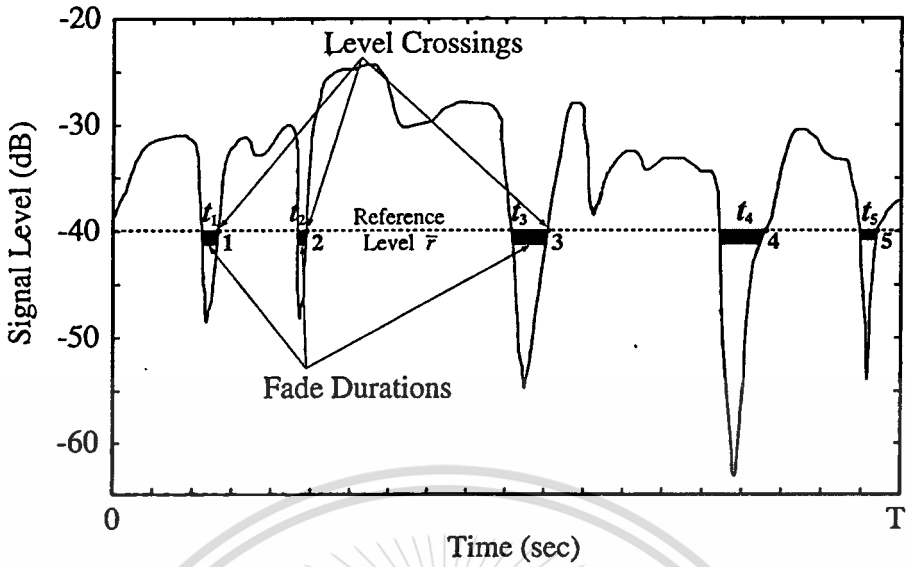

Figure 2.4 Level crossings and fade durations.

shorter duration than enhancements above it. This means that, although *outages* may be frequent, they will not be last for very long. The simple expressions of LCR and AFD pertinent to Fig. 2.4 can be respectively shown as

$$\text{LCR}: \qquad N_{(\text{at } \bar{r})} = 5_{(\text{over T sec.})}, \tag{2.13}$$

$$\text{AFD}: \qquad \tau_{\bar{r}} = \frac{\sum_{k=1}^{5} t_k}{5}. \tag{2.14}$$

where t_k is time duration (of the kth crossing) that the received signal is below the reference level $\bar{r}$.

2.3 Diversity Techniques in Mobile Systems

Large-scale fading is caused by shadowing due to variations in both the terrain profile and the nature of the surroundings. In deep shadowed conditions, the received signal strength at a mobile can drop well below that of free-space. By selecting a base station which is not shadowed when others are, the mobile can improve substantially the average CNR on the *downlink* (base station transmitting, mobile receiving). This is called *macroscopic diversity*, it is also useful at the base station receiver. By using base station antennas that are sufficiently separated in space, the base station is able to improve the *uplink* by selecting the antenna with strongest signal from mobile.

As is well known, the benefit of a *microscopic diversity* reception is that it overcomes deep short-term fading of the received signal. This can reduce the required transmission power as well as cochannel interference protection ratio. Furthermore, it has been shown that the antenna diversity could improve

the capacity of mobile communication systems [49] without the need of larger frequency bands.

Over the past ten years there has been an increasing demand for development of diversity systems to reduce multipath fading for both mobile [50] and base stations [51, 52, 53]. It can take the form of *space diversity*, *directional diversity*, *field component diversity*, and *polarization diversity*, each of which will be described below. The diversity performance depends on the number of diversity branches and on the correlation coefficient between the received branches. Each diversity scheme can reach the same performance if the branch correlation coefficients are the same. Two diversity signals are received from two antennas if space, directional, and polarization schemes are used, or from one antenna if field diversity are used.

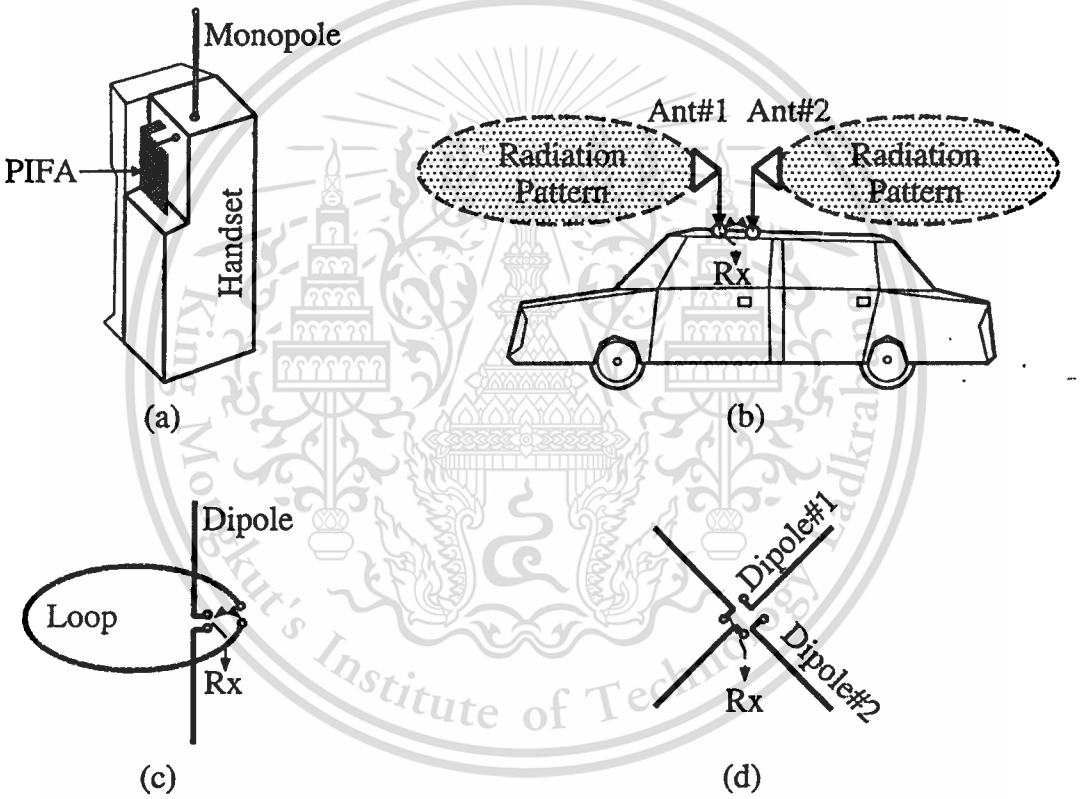

Figure 2.5 Antenna diversity techniques for two diversity branches
(a) space diversity of monopole antenna and PIFA
(b) directional diversity of two opposite directional antennas
(c) field component diversity of dipole and loop antennas
(d) polarization diversity of cross-dipole antenna.

2.3.1 Space Diversity

Space diversity has been most commonly used in practice [54]. It has also been applied to portable telephone, in which a monopole antenna and a PIFA constitute the diversity elements [53] as shown in Fig. 2.5(a), or the diversity combined from two PIFA's [50]. However, space diversity needs large space for multiple antenna locations.

2.3.2 Directional Diversity

In a non-line-of-sight condition, the directivity of a received antenna does not increase the average received power, but signal fading is reduced for a narrower beam. The effect of directional (or directivity) diversity has been tested in the mobile radio environment [55]. It is suitable for vehicular mobile, where antennas can be installed on the roof-top to be in-line with the motion of the vehicle, as shown in Fig. 2.5(b).

2.3.3 Field Component Diversity

Multiple scattering and fading effects can create cross-polarization such that it is desirable for the antenna to receive both E- and H-field components. This is called an *energy diversity antenna*. An advantage of this technique is that only one location is needed and transmitting antenna need only have E-field [56]. However, the antenna itself is bulky as its structure occupies three-dimensional space volume, as shown in Fig. 2.5(c).

2.3.4 Polarization Diversity

Polarization diversity is another useful scheme for reducing multipath fading [57, 58, 59]. Measurement of co-polarization and cross-polarization of received signal power in urban areas without line-of-sight to base stations showed that two polarizations are statistically independent to each other as depicted in Fig. 2.6(a) [60]. While the difference between the received signal levels of co-polarization and cross-polarization is large in line-of-sight environment as depicted in Fig. 2.6(b) so that the polarization diversity becomes less effective. In urban area, it is often observed that the polarization at receiver is not necessarily the same as at the transmitter [61]. By combining differently polarized waves effectively, diversity performance can be realized and fading can be reduced. This type of diversity possesses an advantage over three diversity schemes because the antennas can be placed at the same position (collocation), as shown in Fig. 2.5(d). The antenna elements can also be chosen to be low-profile. Therefore, the polarization diversity is the most appropriate scheme to apply with antennas on portable telephone [62, 63]. Polarization diversity has also been received very high attention for base stations [7, 8, 9, 10], as well as for vehicle mobile [12].

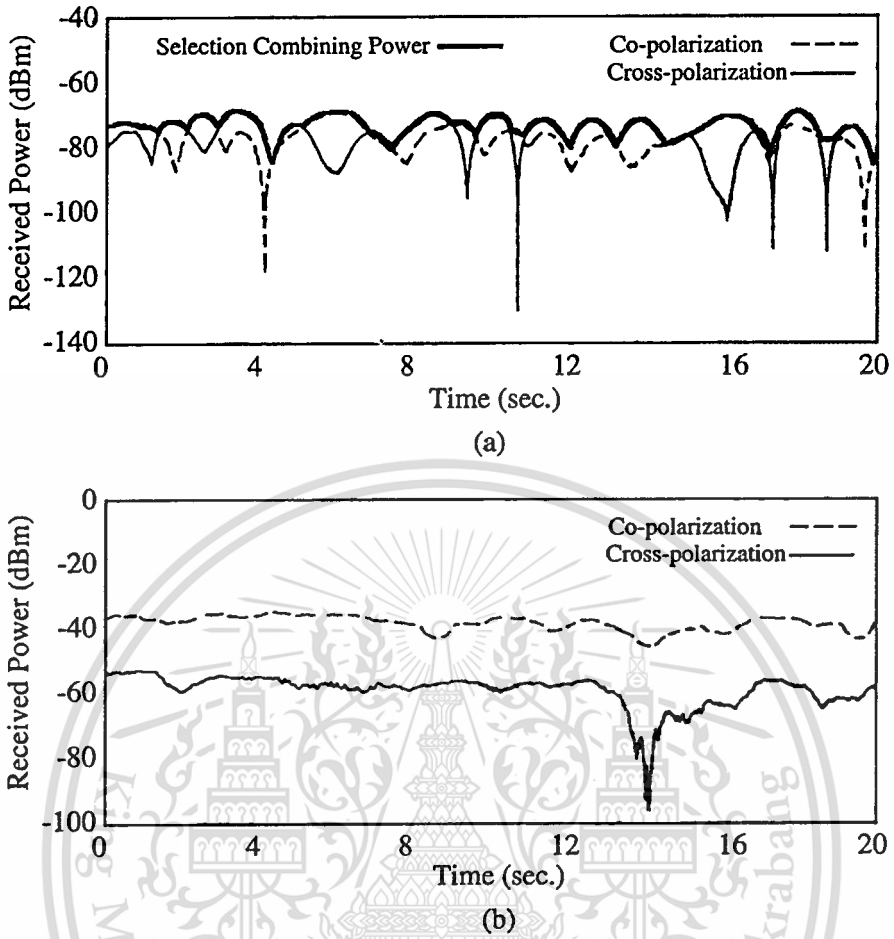

Figure 2.6 Co-polarization and cross-polarization of two received signal power in (a) non-line-of-sight (NLOS) environment (b) line-of-sight (LOS) environment [60].

2.4 Combining Methods

There are several diversity combining methods. This section will describe three main techniques: selection, maximum ratio, and equal gain, for the case that there is no correlation between each diversity branch (independent fading) and the mean received CNR of each branch is also equal. They can be used with each of the diversity techniques discussed in the preceding section.

Diversity receiver can be classified into two basic types—*predetection* and *postdetection*—each using either of three combining methods.

- **Predetection Combining:** each signal is cophased at the IF frequency and combined before detection.
- **Postdetection Combining:** each signal is combined with another signal after detection at the baseband level [64].

In predetection, because of the complexity of in-phase addition, the selection combining scheme which has no such complexity, is most preferable. While in postdetection, the selection combining scheme, which selects detected envelopes, is the simplest of all combining methods. Note that there is no essential difference between the two kinds of detection if a linear detector is used [65].

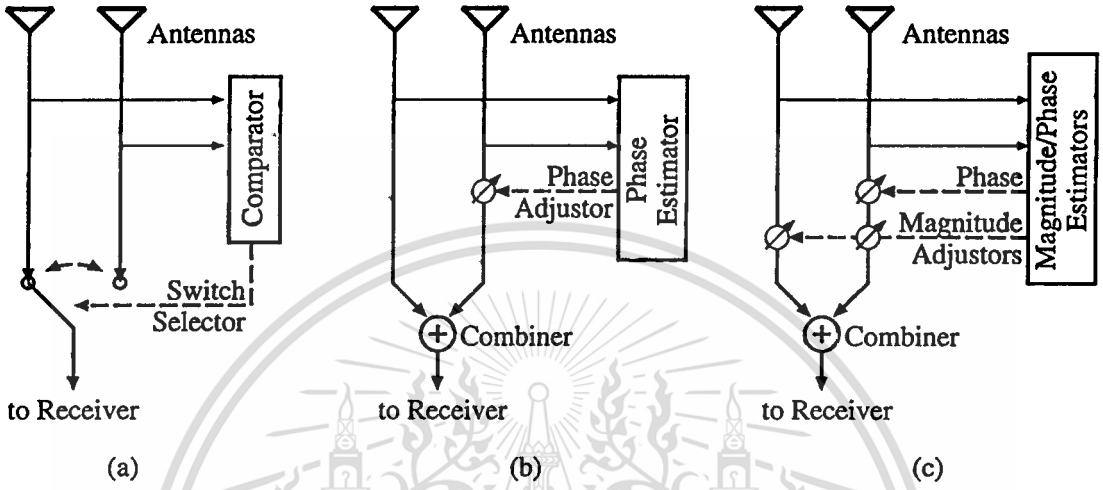

Figure 2.7 Diversity combining methods for two diversity branches (a) SC, (b) EGC, and (c) MRC.

2.4.1 Selection Combining

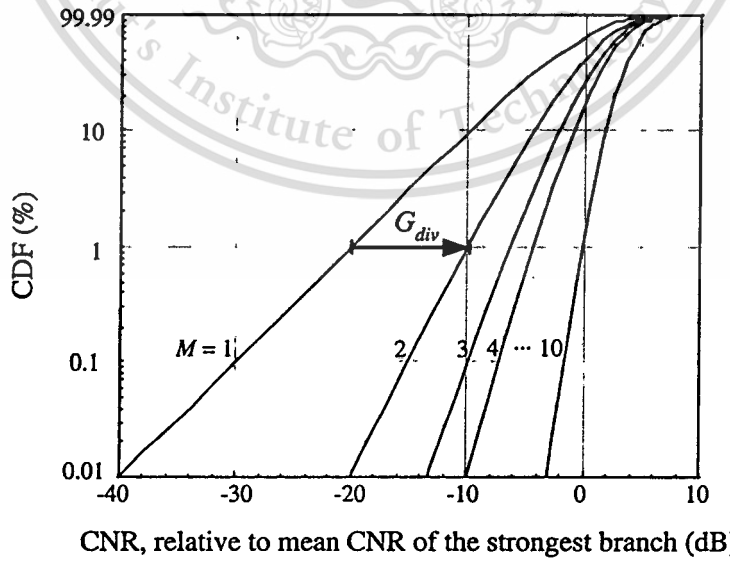

Figure 2.8 Cumulative distribution function of instantaneous CNR for SC.

Selection combining (SC) method is the simplest and perhaps the most frequently used form of diversity combining. In this technique, one of the two diversity branches with the highest CNR is connected to the output as shown in Fig. 2.6(a) with the circuit diagram shown in Fig. 2.7(a).

If we define instantaneous CNR (carrier-to-noise ratio), γ, and mean CNR, Γ, by

$$\gamma = \frac{\text{instantaneous received carrier power}}{\text{mean noise power}}, \tag{2.15}$$

$$\Gamma = \frac{\text{mean received carrier power}}{\text{mean noise power}}. \tag{2.16}$$

The probability that the CNR (γ_m, m is diversity branch number) is less than or equal to some specified value γ is

$$P(\gamma_m \leq \gamma) = 1 - e^{-(\frac{\gamma}{\Gamma})}. \tag{2.17}$$

The probability that γ_m in all branches with independent fading will be simultaneously less than or equal to γ is

$$P(\gamma_1, \gamma_2, ..., \gamma_M \leq \gamma) = \left(1 - e^{-(\frac{\gamma}{\Gamma})}\right)^M. \tag{2.18}$$

Selection combining also improves the mean CNR of the combiner output and can be shown [66] to be

$$E\{\gamma\} = \Gamma \sum_{m=1}^{M} \frac{1}{m}. \tag{2.19}$$

2.4.2 Equal Gain Combining

In equal gain combining (EGC) method, the signals from two branches are cophased and then summed up as shown in Fig. 2.7(b). The CDF of this combining method is quite complicated to find and it needs numerical technique. However, it is found that the CDF of this combining method is very close to MRC (less than a decibel) in all cases. The mean CNR can be [66] shown to be

$$E\{\gamma_e\} = \Gamma\left(1 + (M-1)\frac{\pi}{4}\right) \tag{2.20}$$

2.4.3 Maximum Ratio Combining

Maximum ratio combining (MRC) maximizes the signal-to-noise ratio (SNR) after combining. Two diversity branches are cophased, amplitudes adjusted, and then combined in this combining method as shown in Fig. 2.7(c). Among all combining methods, this method provides the highest performance at the expense of system complexity. The CDF of MRC has been shown [65] to be

$$P(\gamma_m \leq \gamma) = 1 - e^{-(\frac{\gamma}{\Gamma})} \sum_{m=1}^{M} \frac{(\frac{\gamma}{\Gamma})^{m-1}}{(m-1)!}. \tag{2.21}$$

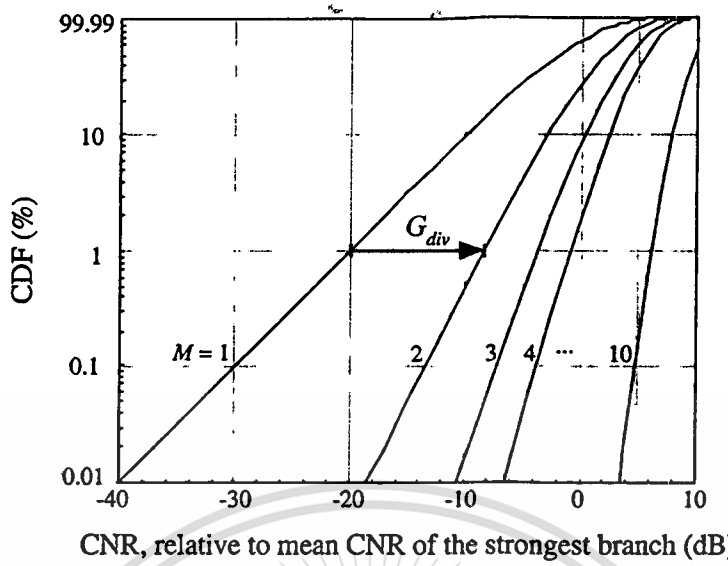

Figure 2.9 Cumulative distribution function of instantaneous CNR for MRC.

The mean CNR of the combined signal may be easily shown to be

$$E\{\gamma\} = M\Gamma. \tag{2.22}$$

Thus, the combiner output mean varies linearly with M. This combining method confirms the intuitive results that the output CNR average over fading should gain proportional to the number of diversity branches.

2.5 Concluding Remarks

As the coverage area of base stations at present is getting smaller, i.e., from the macrocell to microcell, nanocell, and even the picocell, the path loss becomes less dominant to the propagation problems. Whereas, the multipath fading appears to dominate among propagation problems. In this thesis, polarization diversity technique with selection combining method is chosen to apply for PIFA on a portable telephone, due to the compactness and the ease of implementation.

Chapter 3

Expressions of Mobile Antenna Performance

3.1 Introductory Remarks

This chapter deals with theoretical expressions of antenna performance in the mobile environment. Unlike static communications where environments and communication equipments are also static, mobile station is considered to have random movements around the spatio-temporal-variated environments. Hence, the traditional parameters, gain or directivity, are not appropriate to define mobile antennas that are not always at the same position as well as direction. Antenna gain has to be modified by including the statistical propagation characteristic that is angular distribution model of waves incident on the mobile stations. The *mean effective gain* (MEG) is used to define the mobile antenna characteristic instead.

When antenna diversity technique is applied, the *diversity gain* is the parameter for evaluating the diversity performance. Diversity gain is computed from the correlation and ratio of the median values between two diversity branches. *Diversity antenna gain* (DAG), product between MEG and diversity gain, is the parameter to evaluate the diversity antenna system.

3.2 Angular Distribution Model of Incident Waves

In general, multipath propagation in land mobile communication environment is caused by reflection, diffraction, and scattering from topology and buildings. Let us define the secondary wave source generically as the points at which the wave is reflected, diffracted, or scattered immediately before reaching the antenna as illustrated in Fig. 2.1.

There have been several multipath models suggested to explain the observed statistical nature of mobile channel. Ossana's model [67]—based on interference of waves incident and reflected from the flat sides of randomly located buildings—correctly predicts flat fading power spectra in suburban areas, it assumes the existence of a direct path between the transmitter and the receiver. Therefore, this model is inappropriate for urban areas where the direct path is almost always blocked by buildings and other obstacles. Clarke's model [68] is based on scattering and is widely used.

3.2.1 Simple Clarke's Model

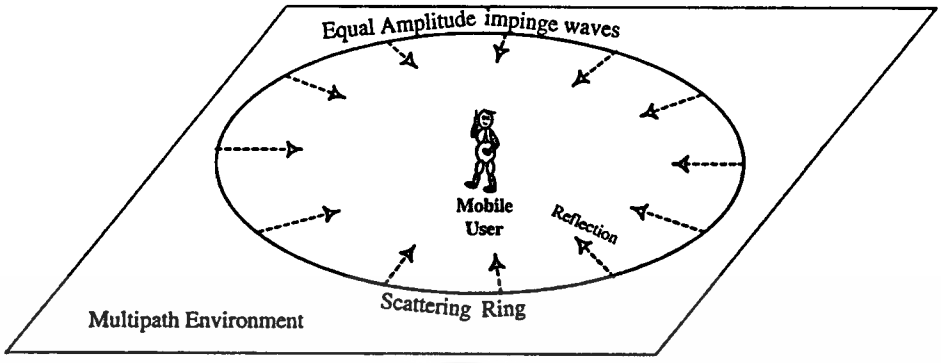

Figure 3.1 Angular power density function of waves incident on mobile antenna represented by simple Clarke's model.

Clarke [68] developed a model where the statistical characteristics of electromagnetic fields of the received signal at the mobile are deduced from scattering. The model assumes a fixed transmitter with a vertically polarized antenna. The field incident on the mobile antenna is assumed to be comprised of N *azimuthal plane waves* with *arbitrary carrier phase, arbitrary azimuthal angle of arrival,* and *each wave having equal average amplitude.* It should be noted that the equal average amplitude assumption is based in the fact that in the absence of a direct line-of-sight path, the scattered components arriving at a receiver will experience similar attenuation over small-scale distances.

Clarke's model is one of the most widely accepted model which is deduced from the statistic characteristics of electromagnetic field scatterings [68] and is subjected to Rayleigh fading.

To model the angular power density functions of incoming plane waves in multipath urban environment, it is reasonable to assume azimuthal distribution $P_{\theta,\phi}(\phi)$ to be uniform and elevational distribution $P_{\theta,\phi}(\theta)$ by the *Dirac delta function* as

$$P_{\theta,\phi}(\theta,\phi) = \frac{1}{2\pi}\delta(\theta - \frac{\pi}{2}). \tag{3.1}$$

3.2.2 Modified Clarke's Model

When the antenna moves randomly within a metropolitan area, the buildings heights and distances from the antenna are considered to be independent variables that are distributed around certain average values. Thus, the secondary wave sources can also be assumed to be distributed around the elevation direction. If it is assumed that an extremely large number of secondary wave sources are experienced during a random move, this elevation angle distribution can be assumed to be Gaussian distribution according to the central limit theorem.

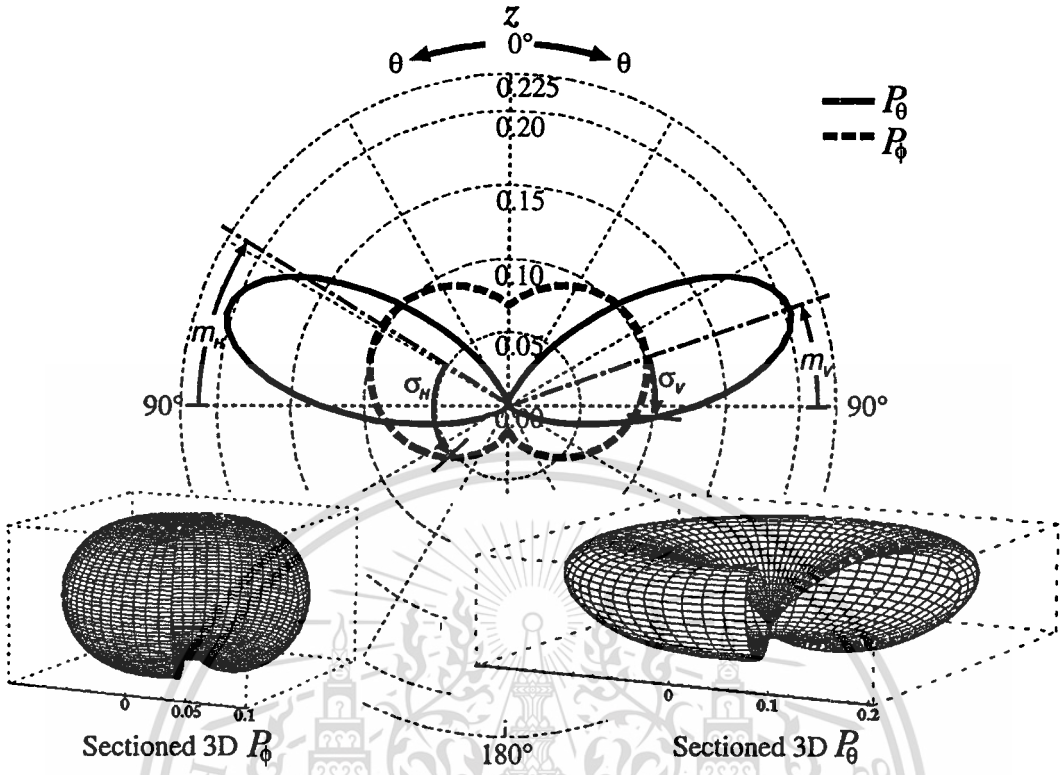

Figure 3.2 Angular power density function of waves incident on antenna in the urban environment [61].

To model the angular power density functions of incoming plane waves for modified Clarke's model, it is reasonable to assume azimuthal distribution $P_{\theta,\phi}(\phi)$ to be uniform and elevational distribution $P_{\theta,\phi}(\theta)$ by Gaussian distributions in the θ direction [61]. For $0 \leq \theta \leq \pi$

$$P_\theta(\theta,\phi) = A_\theta e^{-\left(\frac{\left(\theta-(\frac{\pi}{2}-m_V)\right)^2}{2\sigma_V^2}\right)} \tag{3.2}$$

$$P_\phi(\theta,\phi) = A_\phi e^{-\left(\frac{\left(\theta-(\frac{\pi}{2}-m_H)\right)^2}{2\sigma_H^2}\right)} \tag{3.3}$$

where m_V and σ_V are mean and standard deviation of incident angle of arrival of vertically polarized waves and m_H and σ_H are likewise for horizontally polarized waves (the mean angles are observed from the horizontal direction). If the mean power strengths of VP and HP waves in the directions of $\theta = \frac{\pi}{2} - m_V$ and $\theta = \frac{\pi}{2} - m_H$ are, respectively, P_{mV} and P_{mH}, then

$$P_{mV} = P_1 \cdot A_\theta \tag{3.4}$$

$$P_{mH} = P_2 \cdot A_\phi. \tag{3.5}$$

A_θ and A_ϕ are the amplitudes of P_θ and P_ϕ, respectively, which can be determined from the following condition. P_1 is the mean power that would be received by a θ-component-polarized isotropic antenna in the mobile radio environment. P_2 is likewise for ϕ-component-polarized.

$$\int_0^{2\pi}\int_0^{\pi} P_\theta(\theta,\phi)\sin\theta d\theta d\phi = \int_0^{2\pi}\int_0^{\pi} P_\phi(\theta,\phi)\sin\theta d\theta d\phi = 1 \tag{3.6}$$

The practical value of mean $m_{V,H}$ and standard deviation $\sigma_{V,H}$ of incident angle of arrival, have to be determined from the field measurement in mobile environment. One of the pioneers that measured the arrival direction of incident waves in urban by using 12-element Yagi-Uda antenna with 12 dBi gain in the 205 MHz band, noted that the elevation angles were spread over the range 0°–50° [69].

This thesis will use the urban outdoor environment model, corresponding to the values of $m_V = 19°, \sigma_V = 20°, m_H = 32°$, and $\sigma_H = 64°$ follow the measurement performed by Taga [61] using 0.9-m-diameter parabolic reflector antenna with a dipole element for the primary radiator in the 900 MHz band, as depicted in Fig. 3.2. These practical values are very useful for theoretical analysis of particular mobile communication performance.

3.3 Mean Effective Gain

The mean effective gain (MEG), denoted by G_e, is a statistical measure of the antenna gain in mobile environment. Figure 3.3 illustrates the notation where the signal transmitted from a base station antenna passes through a multipath environment and arrives at a mobile antenna. MEG is defined by the ratio of the mean received power of antenna P_{rec} to the total mean incident power over the random route $P_V + P_H$. It can be expressed by [61]

$$G_e = \frac{P_{\text{rec}}}{P_V + P_H} \tag{3.7}$$

The ratio of mean incident power P_V/P_H represents the *cross-polarization power ratio* (XPR) (in some particular cases it is referred as cross-polar discrimination, XPD), is determined by P_{mV} and P_{mH}, as shown in the following equation

$$\text{XPR} = \frac{P_V}{P_H} = \frac{P_1}{P_2} = \frac{P_mV}{P_mH} \cdot \frac{A_\theta}{A_\phi} \tag{3.8}$$

where P_V and P_H are mean incident power of vertically and horizontally polarized waves, respectively. In the suburban outdoor or indoor environment, where there is no line-of-sight signal, the XPR is close to 0 dB. However, in urban outdoor environments, the XPR varies considerably from 0 dB to +10 dB [61, 70].

The mean received power of a mobile antenna is expressed by [[66], p. 138]

$$P_{\text{rec}} = \int_0^{2\pi}\int_0^{\pi} \Big(P_1 G_\theta(\theta,\phi)P_\theta(\theta,\phi) + P_2 G_\phi(\theta,\phi)P_\phi(\theta,\phi)\Big)\sin\theta d\theta d\phi \tag{3.9}$$

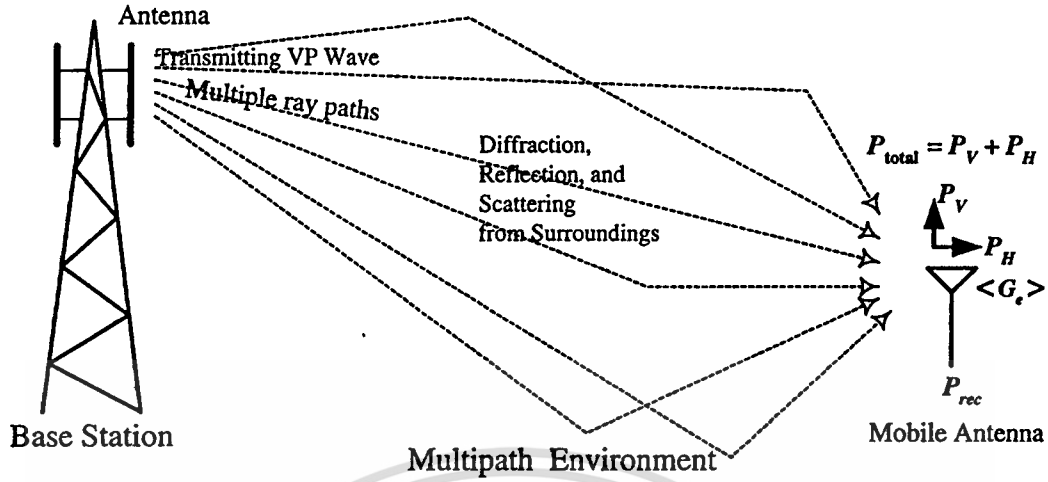

Figure 3.3 Average power arriving at receiving mobile antenna in multipath environment.

where $G_\theta(\theta,\phi)$ and $G_\phi(\theta,\phi)$ are the θ- and ϕ-components of the antenna power gain patterns, respectively, and $P_\theta(\theta,\phi)$ and $P_\phi(\theta,\phi)$ are the θ- and ϕ-components of the normalized angular power density functions of incoming plane waves, respectively. These functions satisfy (3.6) and the following condition

$$\int_0^{2\pi}\int_0^{\pi}\Big(G_\theta(\theta,\phi)+G_\phi(\theta,\phi)\Big)\sin\theta d\theta d\phi = 4\pi \tag{3.10}$$

By using (3.9) and the notation for the XPR, the expression for the MEG can be rearranged as the following equation

$$G_e = \int_0^{2\pi}\int_0^{\pi}\left(\frac{\mathrm{XPR}}{1+\mathrm{XPR}}G_\theta(\theta,\phi)P_\theta(\theta,\phi)+\frac{1}{1+\mathrm{XPR}}G_\phi(\theta,\phi)P_\phi(\theta,\phi)\right)\sin\theta d\theta d\phi. \tag{3.11}$$

When only a VP wave (XPR= 0) is incoming from a single (θ_s,ϕ_s) direction, with corresponds to line-of-sight propagation with VP wave transmission, the angular density functions in (3.11) are represented as

$$P_\theta(\theta,\phi) = \frac{\delta(\theta-\theta_s)\cdot\delta(\phi-\phi_s)}{\sin\theta_s} \tag{3.12}$$

and

$$P_\phi(\theta,\phi) = 0, \tag{3.13}$$

Then, it follows from (3.11)–(3.13) that the MEG becomes

$$G_e = G_\theta(\theta_s,\phi_s). \tag{3.14}$$

This means that the MEG corresponds to the antenna directive gain of the (θ_s,ϕ_s) direction when incoming signals are centered in the (θ_s,ϕ_s) direction.

If the characteristics of incoming signals in various environments can be represented as statistical distribution functions P_θ, P_ϕ, the MEG in (3.11) gives the mean power gain of the antenna in each of the environments.

3.4 Correlation Characteristics

The correlation coefficient is a commonly used gauge of diversity and has three different forms: *complex* (ρ_s), *envelope* (ρ_e), and *power* (ρ_p) correlation coefficients.

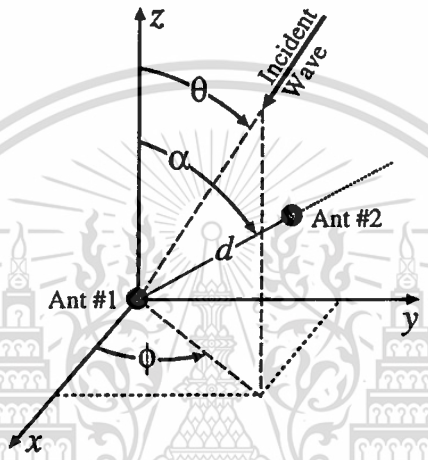

Figure 3.4 Antenna diversity and its coordinate system.

3.4.1 Complex Correlation Coefficient

To show the relation between the signal envelope correlation coefficient and the radiation pattern correlation coefficient. Let's assume the incident wave according to Fig. 3.4, it can be described by

$$\mathbf{F}(\theta,\phi) = F_\theta(\theta,\phi)\mathbf{i}_\theta + F_\phi(\theta,\phi)\mathbf{i}_\phi \tag{3.15}$$

where F_θ and F_ϕ indicate the random amplitude and phase of the incident electric field in $\mathbf{i}_\theta$ or $\mathbf{i}_\phi$ direction, respectively. Also, the complex electric field pattern of the antenna $n(n = 1, 2)$ can be given as follows.

$$\mathbf{E}_n(\theta,\phi) = E_{\theta n}(\theta,\phi)\mathbf{i}_\theta + E_{\phi n}(\theta,\phi)\mathbf{i}_\phi \tag{3.16}$$

where $E_{\theta n}$ and $E_{\phi n}$ are the complex expressions of the θ and ϕ components of the electric field pattern. Thus, the received voltages of the two antennas shown

in Fig. 3.4 are as follows.

$$V_1(t) = C_1 \int_0^{2\pi}\int_0^{\pi} \mathbf{E}_1(\theta,\phi)\cdot\mathbf{F}(\theta,\phi)e^{-jk\mathbf{u}\cdot\mathbf{r}t}\sin\theta d\theta d\phi \quad (3.17)$$

$$V_2(t) = C_2 \int_0^{2\pi}\int_0^{\pi} \mathbf{E}_2(\theta,\phi)\cdot\mathbf{F}(\theta,\phi)e^{-jk\mathbf{u}\cdot\mathbf{r}t}e^{jkx}\sin\theta d\theta d\phi \quad (3.18)$$

where $C_n(n=1,2)$ is the proportionality constant, $e^{-jk\mathbf{u}\cdot\mathbf{r}t}$ is the Doppler shift caused by the velocity $\mathbf{u}$ of the antenna, k is the wave number, $\mathbf{r}$ is the unit vector in the radiating direction, and x is the phase difference of the incident wave as seen at the two antennas. As shown in Fig. 3.4, $x = d(\sin\theta\sin\phi\sin\alpha+\cos\theta\cos\alpha)$ if the diversity antenna system lies on the yz-plane and the line the connects the antenna branches is tilted by the angle of α from the vertical axis. If it is assumed that there is no correlation between incident waves, then the following equations hold, since the phases of F_θ and F_ϕ are independent for incident waves from different directions $\Omega=(\theta,\phi)$ and $\Omega'=(\theta',\phi')$.

$$\langle F_\theta(\Omega)F_\theta^*(\Omega')\rangle = \langle F_\theta(\Omega)F_\theta^*(\Omega)\rangle\,\delta(\Omega-\Omega') \quad (3.19)$$

$$\langle F_\phi(\Omega)F_\phi^*(\Omega')\rangle = \langle F_\phi(\Omega)F_\phi^*(\Omega)\rangle\,\delta(\Omega-\Omega'). \quad (3.20)$$

Furthermore, since the phases of F_θ and F_ϕ are independent and uniformly distributed between 0 and 2π, the next relation is valid

$$\langle F_\theta(\Omega)F_\phi^*(\Omega')\rangle = 0 \quad (3.21)$$

where the brackets represent the *ensemble average*, the , and asterisk $(*)$ denotes complex conjugation. $V(t)$ is approximated by the *complex Gaussian process* with *average of zero* and satisfies

$$\langle V(t)\rangle = 0 \quad (3.22)$$

Hence, the cross-covariance (R_{mn} for $m \neq n$) of the two received voltages proportionally induced from $(E_{\theta m}, E_{\phi m})$ and $(E_{\theta n}, E_{\phi n})$ of the complex electric field patterns can be obtained as follows if (3.15) and (3.16) are substituted into (3.17) and (3.18), and the conditions of (3.19)–(3.21) are applied.

$$\begin{aligned} R_{mn} &= \langle V_m(t)V_n^*(t)\rangle \\ &= 2KP_H\int_0^{2\pi}\int_0^{\pi}\Big(XPR\cdot E_{\theta m}(\theta,\phi)E_{\theta n}^*(\theta,\phi)P_\theta(\theta,\phi) \\ &\quad + E_{\phi m}(\theta,\phi)E_{\phi n}^*(\theta,\phi)P_\phi(\theta,\phi)\Big)\sin\theta d\theta d\phi, \end{aligned} \quad (3.23)$$

where K is a proportionality constant. For

The complex correlation coefficient can be expressed as [65]

$$\rho_s = \frac{R_{12}}{\sqrt{R_{11}R_{22}}} \quad (3.24)$$

3.4.2 Envelope Correlation Coefficient

The envelope correlation coefficient ρ_e of the received signal between two antenna diversity branches in a Rayleigh fading environment can be approximated by the squared magnitude of complex correlation coefficient ρ_s as [68]

$$\rho_e \simeq |\rho_s|^2 = \frac{|R_{12}|^2}{R_{11}R_{22}}, \tag{3.25}$$

3.4.3 Power Correlation Coefficient

It has been shown that

$$\rho_p = \rho_e \tag{3.26}$$

for all practical proposes [71].

The most common reference to diversity performance is in terms of the envelope correlation although all three correlations are related. Therefore, when only correlation coefficient is mentioned, this thesis refers to the envelope correlation coefficient. It is preferable that $\rho_e \leq 0.7$ for practical use as will discuss in the next section and as suggested in [65, 66, 72] (ideally preferable, $\rho_e = 0$). Taga [73] has shown that the theoretical correlation properties of polarization diversity agreed very well to the measurement.

Equation 3.25 indicates that the correlation coefficient becomes zero regardless of XPR or the angular density function of the incident wave if the complex radiation patterns of the θ or ϕ components of the two antennas do not overlap.

3.5 Diversity Gain

In classical analog signal communication, the diversity gain G_{div} of the diversity antenna is defined as the difference of signal envelope at a certain CDF value (usually at 1%), between the CDF curve of the signal envelope of the diversity combiner output, and that of the single reference antenna output as shown in Fig. 2.8.

For modern digital signal communication, the diversity gain is defined as the difference of the average CNR at a certain value of the bit-error rate (BER) (usually at 10^{-3}), between the BER curve of the CNR envelope of the diversity combiner output, and that of the single reference antenna output under the Rayleigh fading environment.

The diversity gain with respect to BER is defined by [74]

$$G_{div} = \frac{\Gamma_{div}}{\Gamma_{non}}, \tag{3.27}$$

where Γ_{non} is the average carrier-to-noise power ratio (CNR) at the prescribed BER when the signals are received by the single branch non-diversity antenna which has the greater CNR of the two branches. Γ_{div} is the average CNR in case of diversity reception.

The average BER ($\overline{P}_e$) of the diversity antenna due to time varying attenuation can be obtained as

$$\overline{P}_e = \int_0^\infty p_e(\gamma)p(\gamma)d\gamma, \tag{3.28}$$

where $p_e(\gamma)$ is the conditional BER when the instantaneous CNR at the detector input is γ in the Rayleigh fading channel. $p(\gamma)$ is the PDF of the instantaneous CNR after combining. Two diversity schemes will be analyzed: MRC diversity provides the best diversity gain at the expense of receiver complexity, SC diversity which has the simplest structure. From (3.28), the average BER can be calculated as follows:

3.5.1 Maximum Ratio Combining

$p(\gamma)$ of the receiving signals for the two-branch MRC diversity under unequal median value and correlated signal can be expressed as [65]

$$p(\gamma) = \frac{e^{-(\frac{\gamma}{\lambda_1})} - e^{-(\frac{\gamma}{\lambda_2})}}{\lambda_1 - \lambda_2}, \tag{3.29}$$

where λ_1 and λ_2 are the eigen values for the covariance matrix of complex receiving signals and found from the following equations

$$\lambda_1 = \frac{1}{2}\left(\Gamma_1 + \Gamma_2 + \sqrt{(\Gamma_1+\Gamma_2)^2 - 4\Gamma_1\Gamma_2(1-|\rho_s|^2)}\right) \tag{3.30}$$

$$\lambda_2 = \frac{1}{2}\left(\Gamma_1 + \Gamma_2 - \sqrt{(\Gamma_1+\Gamma_2)^2 - 4\Gamma_1\Gamma_2(1-|\rho_s|^2)}\right) \tag{3.31}$$

where Γ_1 and Γ_2 are the average CNR of each branch and expressed as $\Gamma_2 = r\Gamma_1$.

$p_e(\gamma)$ of the $\pi/4$ *shifted quadrature phase shift keying* ($\pi/4$ QPSK) signals with delay detection in the *additive white gaussian noise* (AWGN) channel is obtained by the following equation [75].

$$P_e(\gamma) = \frac{1}{2}\text{erfc}\left(\sqrt{\frac{\gamma}{2}}\right) \tag{3.32}$$

where erfc($\cdot$) is a *complementary error function* and can be defined by

$$\text{erfc}(\alpha) = 1 - \text{erf}(\alpha) = \frac{2}{\sqrt{\pi}}\int_\alpha^\infty e^{-x^2}dx. \tag{3.33}$$

The complementary error function is related to Gaussian Q-function (often referred to as Gaussian probability integral) by

$$\text{erfc}(\alpha) = 2Q(\sqrt{2}\alpha) \tag{3.34}$$

By substituting (3.29) and (3.32) into (3.28), the average BER of MRC can be analytically integrated and expressed as

$$\overline{P}_e(\gamma) = \frac{1}{2} - \frac{1}{2(\lambda_1 - \lambda_2)}\left(\frac{\lambda_1}{\sqrt{\frac{2}{\lambda_1}}} - \frac{\lambda_2}{\sqrt{\frac{2}{\lambda_2}}}\right). \tag{3.35}$$

3.5.2 Selection Combining

$p(\gamma)$ of the receiving signals for the post-detection two-branch SC diversity under unequal median value and correlated signal condition is given as follows [76].

$$\begin{aligned} p(\gamma) &= \frac{d}{d\gamma}\Bigg(1 - e^{-\left(\frac{\gamma}{r\Gamma}\right)} Q_1\Big(\sqrt{\frac{2\gamma}{r\Gamma(1-\rho_e)}}, \sqrt{\frac{2\rho_e\gamma}{\Gamma(1-\rho_e)}}\Big) \\ &\quad - e^{-\left(\frac{\gamma}{r\Gamma}\right)}\Bigg(1 - Q_1\Big(\sqrt{\frac{2\rho_e\gamma}{r\Gamma(1-\rho_e)}}, \sqrt{\frac{2\gamma}{\Gamma(1-\rho_e)}}\Big)\Bigg)\Bigg), \end{aligned} \tag{3.36}$$

where Γ is the average CNR of branch A. r is the median value ratio defined by

$$r = \begin{cases} \frac{G_{eA}}{G_{eB}} & (G_{eA} \le G_{eB}), \\ \frac{G_{eB}}{G_{eA}} & (G_{eA} > G_{eB}), \end{cases} \tag{3.37}$$

where G_{eA} and G_{eB} are the MEG of diversity branches A and B, respectively. Q_1 is the first-order Marcum Q-function, whereas the mth order Marcum Q-function is defined by [77]

$$Q_m(\alpha, \beta) = \frac{1}{\alpha^{m-1}} \int_{\beta}^{\infty} x^m e^{-\left(\frac{x^2+\alpha^2}{2}\right)} I_{m-1}(\alpha x) dx, \tag{3.38}$$

where $I_m(\cdot)$ is the m-order modified Bessel function of the first kind defined by (2.10). It is noted that if $\beta \to \infty$, $Q_m(\alpha, \beta)$ can be related to the Gaussian Q-function as

$$Q_m(\alpha, \beta) \simeq \left(\frac{\beta}{\alpha}\right)^{m-\frac{1}{2}} Q(\beta - \alpha). \tag{3.39}$$

For the case $\alpha > \beta \ge 0$, which is satisfied by the arguments of the first-order Marcum Q function in (3.36), the appropriate form for numerical computation is

$$Q_1(\alpha, \beta) = 1 - \int_0^{\beta} x e^{-\left(\frac{x^2+\alpha^2}{2}\right)} I_0(\alpha x) dx. \tag{3.40}$$

$p_e(\gamma)$ of the $\pi/4$ QPSK signals with delay detection in the AWGN channel is calculated by the following equation [75].

$$p_e(\gamma) = \frac{1}{4\pi\sqrt{2}} \int_0^{2\pi} \frac{e^{-\gamma\left(1 - \frac{\cos t}{\sqrt{2}}\right)}}{1 - \frac{\cos t}{\sqrt{2}}} dt. \tag{3.41}$$

By substituting (3.36) and (3.41) into (3.28), the average BER can be calculated by numerical integration.

The diversity gain variation with respect to the correlation coefficient and the median ratio of 2-branch diversity are illustrated in Figs. 3.5 (a) and (b), respectively. It is noted that, from Fig. 3.5 (a), the considerable diversity gain (9.1 dB) can be achieved at $\rho_e \leq 0.7$ as suggested in [65, 66, 72] (ideally preferable, $\rho_e = 0$). It is also recommended that the median ratio should be greater than 0.5 (−3 dB) to achieve reasonable diversity gain (ideally preferable, $r = 1$).

3.6 Diversity Antenna Gain

The most effective parameter (figure-of-merit) to evaluate the performance of a diversity antenna is the diversity antenna gain (DAG) since it includes the correlation coefficient and the MEG characteristics. The DAG can be considered as the system gain when compared with the reference antenna under the same propagation environment. It is defined as a product of the MEG of the higher branch and the diversity gain as [74]

$$\mathrm{DAG} = \begin{cases} G_{eA} \cdot G_{div} & (G_{eA} > G_{eB}), \\ G_{eB} \cdot G_{div} & (G_{eA} \leq G_{eB}). \end{cases} \tag{3.42}$$

3.7 Concluding Remarks

It has been shown that the parameters for evaluation of mobile antenna are different from what antenna engineer is familiar. Since it has to consider the propagation, environment, and system in which the mobile antenna is supposed to be employed. By considering those factors, it leads to the antenna parameters including statistical information of the propagation and environment, and the transmission technique. The diversity antenna gain includes all mentioned parameters, it reveals the mobile antenna performance in system view-point.

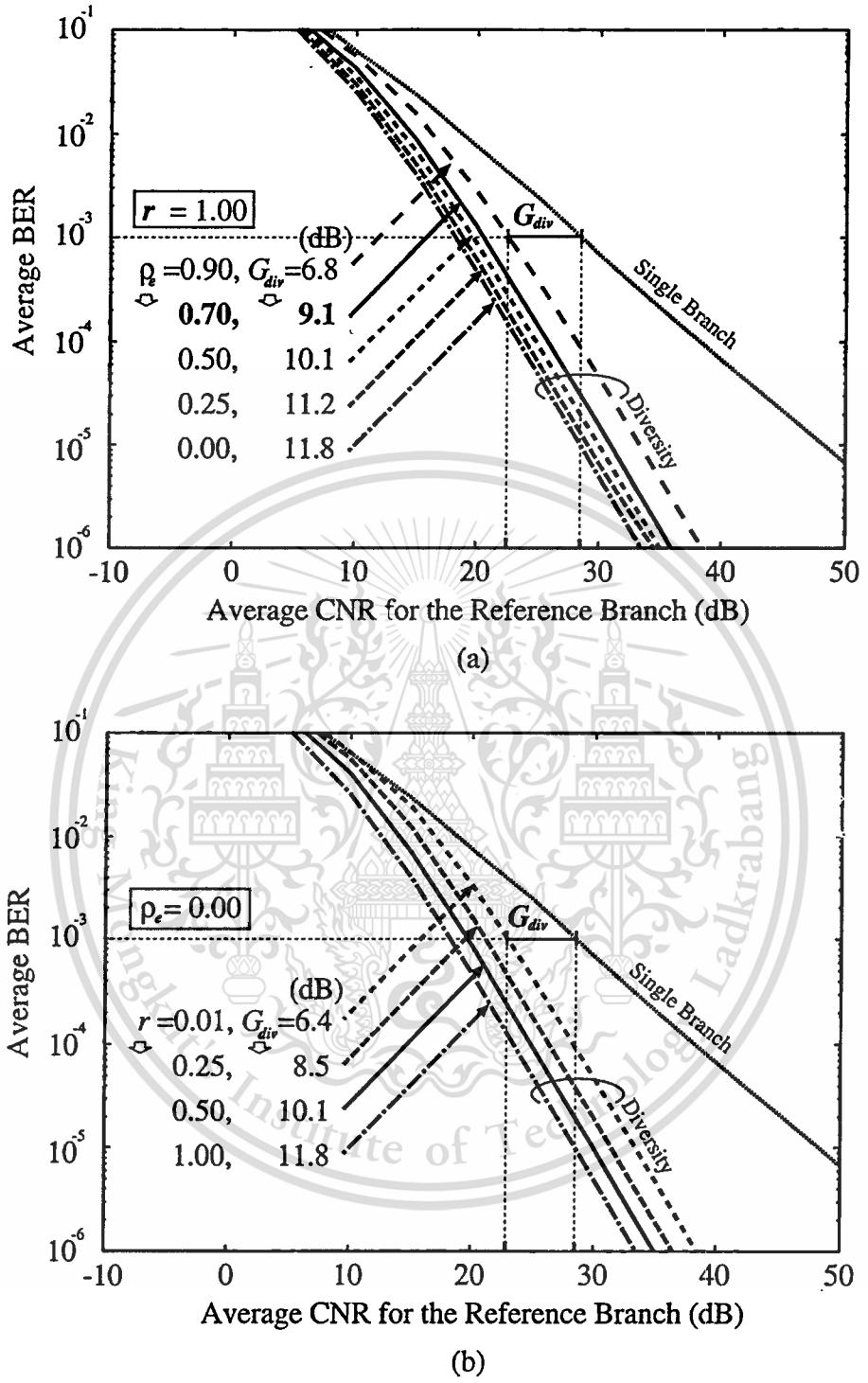

Figure 3.5 BER performance of $\pi/4$-QPSK of 2-branch SC diversity when:
(a) fix median ratio $r = 1$, vary correlation coefficient $0 \leq \rho_e \leq 1$,
(b) fix correlation coefficient $\rho_e = 0$, vary median ratio $0 \leq r \leq 1$.

Chapter 4

Electromagnetic Methodology

4.1 Introductory Remarks

Methods in computational electromagnetics may fall into two main categories: analytical and numerical methods. The numerical methods have been gained more attention due to the high degree of freedom in simulating various configurations of the structure and materials. Among numerical methods, the *finite-difference time-domain* (FDTD) method [17, 78, 79]—the space and time derivatives of *Maxwell's Equations* in *differential form*—is getting very popular as it can cope with very complicated material and structure. However, the computation time used in the simulation is extremely long when compares to other methods. And for the structure surface that does not place parallel to any coordinate axes, it is difficult to model the structure surface to conform to FDTD grid surface.

The *Method of Moments* (MoM)[80, 81, 82, 83], one of numerical methods, is interesting due to the ease of modeling, especially, for wire structure. The three dimensional structure can also be solved by MoM using wire-grid modeling [81, 82]. Surface patch modeling is an alternative for more accurate modeling [84, 85]. By introducing loaded surface impedance technique, MoM is applicable for homogeneous lossy dielectric object [50]. For heterogeneous dielectric material, it can be modeled by using volume integral of the dipole displacement.

Some other techniques, e.g., *generalized multipole technique* (GMT)—analytical multipole solutions of the *Helmholtz's equation* as basis functions whose origins are outside the region of interest to avoid singularity problems, and *finite integration technique* (FIT, is also identical to *finite volume method* (FVM))—the derivatives of *Maxwell's Equations* in *integral form*, are less popular, and are only sometimes employed. The comparison of four mentioned methods is available in [86].

As stated above, the NEC2 (the 2nd generation Numerical Electromagnetics Code) based on MoM is utilized in this work. To give the idea how NEC2 work, many canonical examples are illustrated. The accuracy of the simulations is also investigated in all possible aspects.

4.2 The Integral Equations

NEC2 is a user-oriented program developed at Lawrence Livermore Laboratory [87]. It is a Method of Moments code for analyzing the interaction of elec-

tromagnetic waves with arbitrary structures consisting of conducting wires and surfaces. It combines an integral equation for smoothing surface with one for wires to provide convenient and accurate modeling for a wide range of applications. The code can model nonradiating networks and transmission lines, perfect and imperfect conductors, lumped element loading, and perfect and imperfect conducting ground planes. It uses the electric field integral equation (EFIE) for thin wires and the magnetic field integral equation (MFIE) for surfaces.

4.2.1 The Electric Field Integral Equation

The form of EFIE used in wire-grid simulation follows from an integral representation for the electric field of a volume current distribution $\mathbf{J}$,

$$\mathbf{E}(\mathbf{r}) = -j\frac{\eta}{4\pi k}\int_V \mathbf{J}(\mathbf{r}')\cdot\overline{\mathbf{G}}(\mathbf{r},\mathbf{r}')dV', \tag{4.1}$$

where

$$\overline{\mathbf{G}}(\mathbf{r},\mathbf{r}') = \left(k^2\overline{\mathbf{I}} + \nabla\nabla\right)g(\mathbf{r},\mathbf{r}'), \tag{4.2}$$

$$g(\mathbf{r},\mathbf{r}') = \frac{e^{-jk|\mathbf{r}-\mathbf{r}'|}}{|\mathbf{r}-\mathbf{r}'|}, \tag{4.3}$$

and $k = \omega\sqrt{\mu_0\varepsilon_0}$, $\eta = \sqrt{\frac{\mu_0}{\varepsilon_0}}$, and the time convention is $e^{j\omega t}$. $\overline{(\cdot)}$ is the *dyadic* representation and $\overline{\mathbf{I}}$ is the *identity dyad* $(\hat{x}\hat{x} + \hat{y}\hat{y} + \hat{z}\hat{z})$. When the current distribution is limited to the surface of a perfectly conducting body, (4.1) becomes

$$\mathbf{E}(\mathbf{r}) = -j\frac{\eta}{4\pi k}\int_S \mathbf{J}_S(\mathbf{r}')\cdot\overline{\mathbf{G}}(\mathbf{r},\mathbf{r}')dA', \tag{4.4}$$

with $\mathbf{J}_S$ the surface current density. The observation point $\mathbf{r}$ is restricted to be off the surface S so that $\mathbf{r} \neq \mathbf{r}'$.

If $\mathbf{r}$ approaches S as a limit, (4.4) becomes

$$\mathbf{E}(\mathbf{r}) = -j\frac{\eta}{4\pi k}\oint_S \mathbf{J}_S(\mathbf{r}')\cdot\overline{\mathbf{G}}(\mathbf{r},\mathbf{r}')dA', \tag{4.5}$$

where the principal value integral, $\oint$, is indicated since $g(\mathbf{r},\mathbf{r}')$ is now unbounded.

An integral equation for the current induced on S by an incident field $\mathbf{E}^I$ can be obtained from (4.5) and the boundary condition for $\mathbf{r} \in S$,

$$\hat{n}(\mathbf{r}) \times \left(\mathbf{E}^S(\mathbf{r}) + \mathbf{E}^I(\mathbf{r})\right) = 0, \tag{4.6}$$

where $\hat{n}(\mathbf{r})$ is the unit normal vector of the surface at $\mathbf{r}$ and $\mathbf{E}^S$ is the field due to the induced current $\mathbf{J}_S$. Substituting (4.5) for $\mathbf{E}^S$ yields the integral equation,

$$-\hat{n}(\mathbf{r}) \times \mathbf{E}^I(\mathbf{r}) = -j\frac{\eta}{4\pi k}\hat{n}(\mathbf{r}) \times \oint_S \mathbf{J}_S(\mathbf{r}')\cdot\left(k^2\overline{\mathbf{I}} + \nabla\nabla\right)g(\mathbf{r},\mathbf{r}')dA'. \tag{4.7}$$

The vector integral in (4.7) can be reduced to a scalar integral equation when the conducting surface S is that of a cylindrical thin wire, thereby making the solution much easier.

The assumptions applied for a thin wire, known as the thin-wire approximation, are as follows:

I. Transverse currents can be neglected relative to axial currents on the wire.

II. The circumferential variation in the axial current can be neglected.

III. The current can be represented by a filament on the wire axis.

IV. The boundary condition on the electric field need be enforced in the axial direction only.

These widely used approximations are valid as long as the wire radius is much less than the wavelength and much less than the wire length. An alternate kernel for the EFIE, based on an extended thin-wire approximation in which condition III is relaxed, is also included for wires having too large a radius for the thin-wire approximation.

From assumption I, II and III, the surface current $\mathbf{J}_S(\mathbf{r})$ on a wire of radius a can be placed by a filamentary current I where

$$I(s)\hat{s} = 2\pi \mathbf{J}_S(\mathbf{r}), \tag{4.8}$$

s is a distance parameter along the wire axis at $\mathbf{r}$, and $\hat{s}$ is a unit vector tangent to the wire axis at $\mathbf{r}$.

Equation 4.7 then becomes

$$-\hat{n}(\mathbf{r}) \times \mathbf{E}^I(\mathbf{r}) = -j\frac{\eta}{4\pi k}\hat{n}(\mathbf{r}) \times \int_L I(s')\Big(k^2\hat{s}' - \nabla\frac{\partial}{\partial s'}g(\mathbf{r},\mathbf{r}')ds'\Big) \tag{4.9}$$

where the integration is over the length of the wire. Enforcing the boundary condition in the axial direction reduces (4.9) to the scalar equation,

$$-\hat{s}\cdot\mathbf{E}^I(\mathbf{r}) = -j\frac{\eta}{4\pi k}\int_L I(s')\Big(k^2\hat{s}\cdot\hat{s}' - \frac{\partial^2}{\partial s\partial s'}g(\mathbf{r},\mathbf{r}')ds'\Big). \tag{4.10}$$

Since $\mathbf{r}'$ is now the point at s' on the wire axis while $\mathbf{r}$ is a point at s on the wire surface $|\mathbf{r}-\mathbf{r}'| \geq a$ and the integrand is bounded.

4.2.2 The Magnetic Field Integral Equation

The MFIE is derived from the integral representation for the magnetic field of a surface current distribution $\mathbf{J}_S$,

$$\mathbf{H}^S(\mathbf{r}) = \frac{1}{4\pi}\int_S \mathbf{J}_S(\mathbf{r}')\times\nabla' g(\mathbf{r},\mathbf{r}')dA', \tag{4.11}$$

where the differentiation is with respect to the integration variable $\mathbf{r}'$. If the current $\mathbf{J}_S$ is induced by an internal incident field $\mathbf{H}^I$, then the total magnetic field inside the perfectly conducting surface must be zero. Hence, for $\mathbf{r}$ just inside the surface S,

$$\mathbf{H}^I(\mathbf{r}) + \mathbf{H}^S(\mathbf{r}) = 0, \tag{4.12}$$

where $\mathbf{H}^I$ is the incident field with the structure removed, and $\mathbf{H}^S$ is the scattered field given by (4.11). The integral equation for $\mathbf{J}_S$ may be obtained by letting $\mathbf{r}$ approach the surface point $\mathbf{r}_0$ from inside the surface along the normal $\hat{n}(\mathbf{r}_0)$. The surface component of (4.12) with (4.11) substituted for $\mathbf{H}^S$ is then

$$-\hat{n}(\mathbf{r}_0) \times \mathbf{H}^I(\mathbf{r}_0) = \hat{n}(\mathbf{r}_0) \times \frac{1}{4\pi} \lim_{\mathbf{r}\to\mathbf{r}_0} \int_S \mathbf{J}_S(\mathbf{r}') \times \nabla' g(\mathbf{r}, \mathbf{r}') dA', \tag{4.13}$$

where $\hat{n}(\mathbf{r}_0)$ is the outward directed normal vector at $\mathbf{r}_0$. The limit can be evaluated by using a result of potential theory to yield the integral equation

$$-\hat{n}(\mathbf{r}_0) \times \mathbf{H}^I(\mathbf{r}_0) = -\frac{1}{2}\mathbf{J}_S(\mathbf{r}_0) + \frac{1}{4\pi} \int\!\!\!\!\!\!- _S \hat{n}(\mathbf{r}_0) \times \Big(\mathbf{J}_S(\mathbf{r}') \times \nabla' g(\mathbf{r}, \mathbf{r}')\Big) dA', \tag{4.14}$$

This vector integral equation is resolved into two scalar equations along the orthogonal surface vectors $\mathbf{t}_1$ and $\mathbf{t}_2$ where

$$\mathbf{t}_1(\mathbf{r}_0) \times \mathbf{t}_2(\mathbf{r}_0) = \hat{n}(\mathbf{r}_0). \tag{4.15}$$

By using the identity $\mathbf{u} \cdot (\mathbf{v} \times \mathbf{w}) = (\mathbf{u} \times \mathbf{v}) \cdot \mathbf{w}$ and nothing that $\mathbf{t}_1 \times \hat{n} = -\mathbf{t}_2$ and $\mathbf{t}_2 \times \hat{n} = \mathbf{t}_1$, the scalar equations can be written,

$$\hat{t}_2(\mathbf{r}_0) \cdot \mathbf{H}^I(\mathbf{r}_0) = -\frac{1}{2}\hat{t}_1(\mathbf{r}_0) \cdot \mathbf{J}_S(\mathbf{r}_0) + \frac{1}{4\pi} \int\!\!\!\!\!\!- _S \hat{t}_2(\mathbf{r}_0) \cdot \Big(\mathbf{J}_S(\mathbf{r}') \times \nabla' g(\mathbf{r}, \mathbf{r}')\Big) dA'; \tag{4.16}$$

$$-\hat{t}_1(\mathbf{r}_0) \cdot \mathbf{H}^I(\mathbf{r}_0) = -\frac{1}{2}\hat{t}_2(\mathbf{r}_0) \cdot \mathbf{J}_S(\mathbf{r}_0) + \frac{1}{4\pi} \int\!\!\!\!\!\!- _S \hat{t}_1(\mathbf{r}_0) \cdot \Big(\mathbf{J}_S(\mathbf{r}') \times \nabla' g(\mathbf{r}, \mathbf{r}')\Big) dA'. \tag{4.17}$$

These two components suffice since there is no normal component of (4.14).

4.2.3 The EFIE-MFIE Hybrid Equation

The EFIE is used for thin wires and MFIE for surfaces. On wires the integral is simplified by the thin-wire approximation. The resulting coupled integral equations are, for $\mathbf{r}$ on wire surfaces,

$$\begin{aligned} -\hat{s} \cdot \mathbf{E}^I(\mathbf{r}) \;=\; & -j\frac{\eta}{4\pi k} \int_L I(s') \Big(k^2 \hat{s} \cdot \hat{s}' - \frac{\partial^2}{\partial s \partial s'}\Big) g(\mathbf{r}, \mathbf{r}') ds' \\ & -j\frac{\eta}{4\pi k} \int_{S1} \mathbf{J}_S(\mathbf{r}') \cdot \Big(k^2 \hat{s} - \nabla' \frac{\partial}{\partial s}\Big) g(\mathbf{r}, \mathbf{r}') dA', \end{aligned} \tag{4.18}$$

and for $\mathbf{r}$ on surfaces excluding wires

$$-\hat{t}_2(\mathbf{r})\cdot\mathbf{H}^I(\mathbf{r}) = \frac{1}{4\pi}\hat{t}_2(\mathbf{r})\cdot\int_L I(s')\Big(\hat{s}'\times\nabla' g(\mathbf{r},\mathbf{r}')\Big)ds' - \frac{1}{2}\hat{t}_1(\mathbf{r})\cdot\mathbf{J}_S(\mathbf{r}) - \frac{1}{4\pi}\oint_{S1}\hat{t}_2(\mathbf{r})\cdot\Big(\mathbf{J}_S\times\nabla' g(\mathbf{r},\mathbf{r}')\Big)dA', \quad (4.19)$$

and

$$-\hat{t}_1(\mathbf{r})\cdot\mathbf{H}^I(\mathbf{r}) = \frac{1}{4\pi}\hat{t}_1(\mathbf{r})\cdot\int_L I(s')\Big(\hat{s}'\times\nabla' g(\mathbf{r},\mathbf{r}')\Big)ds' - \frac{1}{2}\hat{t}_2(\mathbf{r})\cdot\mathbf{J}_S(\mathbf{r}) + \frac{1}{4\pi}\oint_{S1}\hat{t}_1(\mathbf{r})\cdot\Big(\mathbf{J}_S\times\nabla' g(\mathbf{r},\mathbf{r}')\Big)dA'. \quad (4.20)$$

The symbol $\int_L$ represents integration over wires while $\int_{S1}$ represents integration over surfaces excluding wires. The numerical method used to solve (4.18)–(4.20) is described in section 4.3.

4.3 Method of Moments

The integral equation (4.18), (4.19) and (4.20) can be solved by the Method of Moments (MoM) [88].

The MoM applies to a general linear-operator equation,

$$Lf = g \quad (4.21)$$

where L is a linear operator (an integral operator in the present case which corresponding to the *particular antenna structure*), f is an unknown response (corresponding to the *current distribution* on antenna), and g is a known excitation (corresponding to the *feed* position and applied voltage). The unknown function f may be expanded in a sum of basis function, f_i, as

$$f = \sum_{n=1}^{N}\alpha_n f_n. \quad (4.22)$$

A set of equations for the coefficients α_n are then obtained by taking the inner product of (4.21) with a set of weighting function $\{w_m\}$,

$$< w_m, Lf > = < w_m, g >, \qquad m = 1,\ldots,M. \quad (4.23)$$

Due to the linearity of L, (4.23) substituted for f yields,

$$\sum_{n=1}^{N}\alpha_n < w_m, Lf_n > = < w_m, g >, \qquad m = 1,\ldots,M. \quad (4.24)$$

This equation can be written in matrix notation as

$$[l_{mn}]\,[\alpha_n] = [g_m] \quad (4.25)$$

where

$$[l_{mn}] = \begin{bmatrix} <w_1, Lf_1> & <w_1, Lf_2> & \cdots \\ <w_2, Lf_1> & <w_2, Lf_2> & \cdots \\ \vdots & \vdots & \ddots \end{bmatrix}, \tag{4.26}$$

$$[\alpha_n] = \begin{bmatrix} \alpha_1 \\ \alpha_2 \\ \vdots \end{bmatrix}, \tag{4.27}$$

$$[g_m] = \begin{bmatrix} <w_1, g> \\ <w_2, g> \\ \vdots \end{bmatrix}. \tag{4.28}$$

If the matrix $[l_{mn}]$ is nonsingular, its inverse $[l_{mn}]^{-1}$ exists. The α_n are then given by

$$[\alpha_n] = [l_{mn}]^{-1} [g_m], \tag{4.29}$$

and the solution for f is given by (4.22). For concise expression of this results, define the matrix of functions

$$\left[\widetilde{f}_n\right] = [f_1 \quad f_2 \quad f_3 \quad \cdots], \tag{4.30}$$

and write

$$f = \left[\widetilde{f}_n\right] [\alpha_n] = \left[\widetilde{f}_n\right] [l_{mn}]^{-1} [g_m]. \tag{4.31}$$

For the solution of (4.18), (4.19), and (4.20), the inner product is defined as

$$<a, b> = \int_S a(\mathbf{r}) b(\mathbf{r}) dA, \tag{4.32}$$

where the integration is over the structure surface. Various choices are possible for the weighting functions w_m and basis function f_n. When $w_m = f_m$, the procedure is known as *Galerkin's method.* In this thesis, the basis and weighting functions are different, w_m being chosen as a set of delta functions

$$w_m(\mathbf{r}) = \delta(\mathbf{r} - \mathbf{r_m}), \tag{4.33}$$

with $\{\mathbf{r_m}\}$ a set of points on the conducting surface. The result is a point sampling of the integral equations known as the *point matching (collocation) method* of solution. Wires are divided into short straight segments with a sample point at the center of each segment.

4.3.1 Current Expansion on Wires

Wires are modeled by short straight segments with current on each segment represented by three terms—a constant, a sine, and a cosine function. This expansion provides rapid solution convergence [87]. It has the added advantage

that the fields of sinusoidal currents are easily evaluated in closed form. The amplitude of the constant, sine, and cosine terms are related such that their sum satisfies physical conditions on the local behavior of current and charge at the segment ends.

The total current on segment number n has the form

$$I_n(s) = A_n + B_n \sin k(s - s_n) + C_n \cos k(s - s_n), \qquad |s - s_n| < \frac{\Delta_n}{2}, \quad (4.34)$$

where s_n is the value of s at the center of segment n, and Δ_n is the length of segment n. Of the three unknown constants A_n, B_n, and C_n, two are eliminated but local conditions on the current leaving one constant, related to the current amplitude, to be determined by the matrix equation.

4.3.2 Evaluation of the Fields

The solution requires the evaluation of the electric field at each segment due to the current in (4.34). Three approximations of the integral equation kernel are used: a *thin-wire* form for most case, an *extended thin-wire* form for thick wire, and a *current element approximation* for large interaction distances. In each case the evaluation of the field is greatly simplified by the use of formulas for the fields of the constant and sinusoidal current components.

4.3.2.1 Thin-Wire

The accuracy of the thin-wire approximation for a wire of radius a and length Δ depends on ka and Δ/a. It has been shown from [87] that the thin-wire approximation leads to errors of less than 1% for Δ/a greater than 8. Furthermore, in the numerical solution of EFIE, the wire is divided into segments less than about 0.1λ in length to obtain an adequate representation of current distribution thus restricting ka to less than about 0.08. The extended thin-wire approximation is applicable to shorter and thicker segments, resulting in errors less than 1% for Δ/a greater than 2.

For the *thin-wire kernel*, the source current is approximated by a filament on the segment axis while the observation point is on the surface of the observation segment. The fields are evaluated with the source segment on the axis of a local cylindrical coordinate system as illustrated in Fig. 4.1(a)

Then with

$$G_0 = \frac{e^{-jkr_0}}{r_0}, \quad (4.35)$$

$$r_0 = \sqrt{\rho^2 + (z - z')^2}. \quad (4.36)$$

The ρ- and z-components of the electric field at point P due to sinusoidal current filament of sine and cosine functions

$$I = I_0 \begin{pmatrix} \sin kz' \\ \cos kz' \end{pmatrix}, \quad (4.37)$$

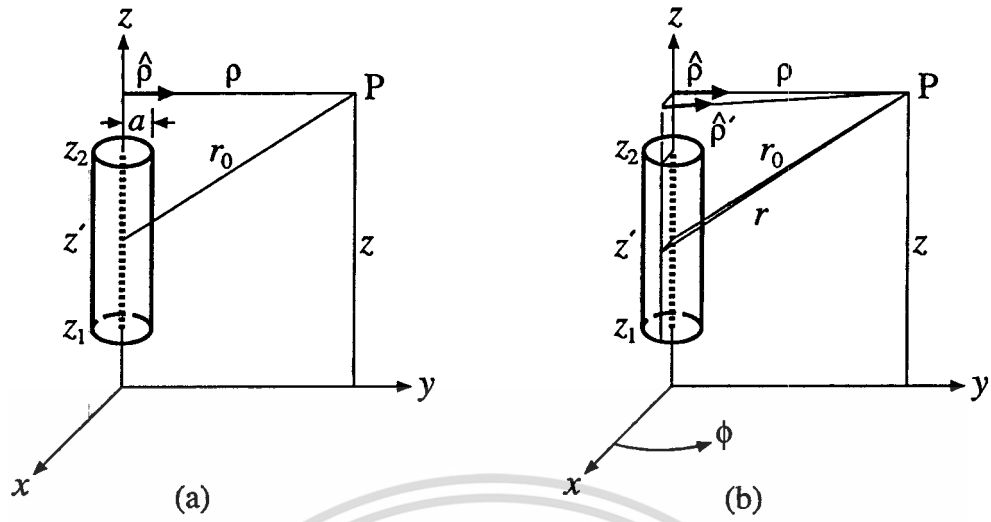

Figure 4.1 Current along wire segment geometry for: (a) thin-wire kernel, and (b) extended thin-wire kernel.

are

$$E_\rho(\rho,z) = -G_0\frac{I_0}{\lambda}\frac{j\eta}{2k^2\rho}\left(k(z-z')\begin{pmatrix}\cos kz'\\-\sin kz'\end{pmatrix} + \left(1-(z-z')^2\frac{(1+jkr_0)}{r_0^2}\right)\begin{pmatrix}\sin kz'\\\cos kz'\end{pmatrix}\right)\Bigg|_{z_1}^{z_2}, \tag{4.38}$$

$$E_z(\rho,z) = G_0\frac{I_0}{\lambda}\frac{j\eta}{2k^2}\left(k\begin{pmatrix}\cos kz'\\-\sin kz'\end{pmatrix} - (z-z')\frac{(1+jkr_0)}{r_0^2}\begin{pmatrix}\sin kz'\\\cos kz'\end{pmatrix}\right)\Bigg|_{z_1}^{z_2} \tag{4.39}$$

For a constant current of strength I_0,

$$E_\rho(\rho,z) = -\frac{I_0}{\lambda}\frac{j\eta\rho}{2k^2}\left((1+jkr_0)\frac{G_0}{r_0^2}\right)\Bigg|_{z_1}^{z_2}, \tag{4.40}$$

$$E_z(\rho,z) = -\frac{I_0}{\lambda}\frac{j\eta}{2k^2}\left(\left((z-z')(1+jkr_0)\frac{G_0}{r_0^2}\right)\Bigg|_{z_1}^{z_2} + k^2\int_{z_1}^{z_2}G_0\,dz'\right). \tag{4.41}$$

4.3.2.2 Extended Thin-Wire

Despite the seemingly crude approximation, the thin-wire kernel does accurately represent the effect of wire radius for wires that are sufficiently thin. For wires that are too thick for the thin-wire approximation, an *extended thin-wire kernel* has been developed.

The derivation of the extended thin-wire kernel starts with the current on the surface of the source segment with surface density,

$$J(z') = \frac{I(z')}{2\pi a}, \tag{4.42}$$

where a is the radius of the source segment. The geometry for evaluation of the fields is shown in Fig. 4.1(b). A current filament of strength $Id\phi/2\pi$ is integrated over ϕ with

$$\rho' = \sqrt{\rho^2 + a^2 - 2a\rho\cos\phi}, \tag{4.43}$$

$$r = \sqrt{\rho'^2 + (z - z')^2}. \tag{4.44}$$

The field equations with extended thin-wire approximation are given below. For a sinusoidal (only sine function) current of (4.37).

$$E_\rho(\rho, z) = -\frac{j\eta}{2k^2\lambda}\left((z' - z)I\frac{\partial G_2}{\partial z'} + IG_2 - (z' - z)G_2\frac{\partial I}{\partial z'}\right)\Bigg|_{z_1}^{z_2}, \tag{4.45}$$

$$E_z(\rho, z) = \frac{j\eta}{2k^2\lambda}\left(G_1\frac{\partial I}{\partial z'} - I\frac{\partial G_1}{\partial z'}\right)\Bigg|_{z_1}^{z_2}. \tag{4.46}$$

For a constant current of strength I_0,

$$E_\rho(\rho, z) = \frac{j\eta I_0}{2k^2\lambda}\left(\frac{\partial G_1}{\partial \rho}\right)\Bigg|_{z_1}^{z_2}, \tag{4.47}$$

$$E_z(\rho, z) = -\frac{j\eta I_0}{2k^2\lambda}\left(\left(\frac{\partial G_1}{\partial z'}\right)\Bigg|_{z_1}^{z_2} + k^2\left(1 - \frac{(ka)^2}{4}\right)\int_{z_1}^{z_2} G_0 dz' - \frac{(ka)^2}{4}\left(\frac{\partial G_0}{\partial z'}\right)\Bigg|_{z_1}^{z_2}\right). \tag{4.48}$$

For the observation point within a wire ($\rho < a$), with

$$r_a = \sqrt{a^2 + (z - z')^2}, \tag{4.49}$$

$$G_a = \frac{e^{-jkr_a}}{r_a}, \tag{4.50}$$

and the expression of G_1, G_2 and their derivatives are

$$G_1 = G_a\left(1 - \frac{\rho^2}{2r_a^2}(1+jkr_a) + \frac{a^2\rho^2}{4r_a^4}\Big(3(1+jkr_a) - k^2r_a^2\Big)\right), \quad (4.51)$$

$$\frac{\partial G_1}{\partial z'} = G_a\frac{(z-z')}{r_a^2}\left((1+jkr_a) - \frac{\rho^2}{2r_a^2}\Big(3(1+jkr_a) - k^2r_a^2\Big) - \frac{a^2\rho^2}{4r_a^4}\Big(jk^3r_a^3 + 6k^2r_a^2 - 15(1+jkr_a)\Big)\right), \quad (4.52)$$

$$\frac{\partial G_1}{\partial \rho} = -G_a\frac{\rho}{r_a^2}\left((1+jkr_a) - \frac{a^2}{2r_a^2}\Big(3(1+jkr_a) - k^2r_a^2\Big)\right), \quad (4.53)$$

$$G_2 = -G_a\frac{\rho}{2r_a^2}(1+jkr_a), \quad (4.54)$$

$$\frac{\partial G_2}{\partial z'} = -G_a\frac{(z-z')\rho}{2r_a^4}\Big(3(1+jkr_a) - k^2r_a^2\Big). \quad (4.55)$$

4.3.2.3 Current Approximation for Large Distance

When segments are separated by a large distance, the interaction may be computed with sufficient accuracy by treating the segment current as an infinitesimal current element at the segment center. In spherical coordinates, with the segment at the origin along the $\theta = 0°$ axis, the electric field is

$$E_r(r,\theta) = \frac{M\eta}{2\pi r^2}e^{-jkr}\left(1 - \frac{j}{kr}\right)\cos\theta, \quad (4.56)$$

$$E_\theta(r,\theta) = \frac{M\eta}{4\pi r^2}e^{-jkr}\left(1 + jkr - \frac{j}{kr}\right)\sin\theta. \quad (4.57)$$

The dipole moment M for a constant current I on a segment of length Δ_m is

$$M = I\Delta_m. \quad (4.58)$$

For current $I\cos k(s - s_m)$ with $|s - s_m| < \Delta_m/2$,

$$M = \frac{2I}{k}\sin\frac{k\Delta_m}{2}, \quad (4.59)$$

while for a current $I\sin k(s - s_m)$,

$$M = 0. \quad (4.60)$$

The use of this approximation saves a significant amount of time in evaluating the interaction matrix elements for large structure. A minimum distance of *one wavelength* is set for this approximation.

For each of the three methods of computing the field at a segment due to the current on another segment, the field is evaluated on the surface of the observation segment.

4.4 Wire-Grid Modeling

A wire segment is defined by the coordinates of two end points and its radius. Modeling a wire structure with segments involves both geometrical and electrical factors. Geometrically, the segments should follow the paths of conductors as closely as possible, using a piece-wise linear fit on curves. Wire segments can be used to model wire structure, conductor plate, and even the lossy dielectric object, by properly choosing the length, radius and conductivity loaded of the wire. The guidelines for wire-grid modeling of three types of structures are described below.

4.4.1 Conducting Wire

The main electrical consideration is segment length Δ relative to the wavelength λ. Δ should be less than about 0.1λ at the desired frequency. Somewhat longer segments may be acceptable on long wires with no abrupt changes while shorter segments, 0.05λ or less, may be needed in modeling critical regions of an antenna. The size of the segments determines the resolution in solving for the current on the model since the current is computed at the center of each segment. Extremely short segments, less than about $10^{-3}\lambda$, should also be avoided since the similarity of the constant and cosine components of the current expansion leads to numerical inaccuracy.

The wire radius, a, relative to λ is limited by the approximations used in the kernel of electric field integral equation. The field of the current is approximated by the first two terms in a series expansion of the exact field in powers of a^2. The first term in the series, which is independent of a, is identical to the thin-wire kernel while the second term (extended thin-wire kernel) extends the accuracy for larger values of a.

In either of these approximations, only currents in the axial direction on a segment are considered, and there is no allowance for variation of the current around the wire circumference. The acceptability of these approximations depends on both the value of a/λ and the tendency of the excitation to produce circumferential current or current variation. Unless $2\pi a/\lambda$ is much less than 1, the validity of these approximations should be considered.

Use of a small Δ/a at a bend, which results in the center of one segment falling within the radius of the other segment, generally leads to severe error.

The current expansion used in (4.34) enforces conditions on the current and charge density along wires, at junctions, and at wire ends. For these conditions to be applied properly, segments that are electrically connected must have coincident end points. If segments intersect other than at their ends, current will not be allowed to flow from one segment to the other.

The angle of the intersection of wire segments should be large enough to prevent overlaps. The acute angle may be so small as to place the observation point on one wire segment within volume of another wire segment, however, such overlapping may lead to meaningless results. The details of the current

distribution near the intersection may not be reliable even though the results for the current may be accurate at distances from this region.

Other rules for the segment model follow:

- Segments may not overlap since the division of current between two overlapping segments is indeterminate. Overlapping may result in a singular matrix equation.
- A large radius change between connected segments may decrease accuracy; particularly, with small Δ/a. The problem may be reduced by making the radius change in steps over several segments.
- A segment is required at each point where a voltage source will be located. A continuous wire across the gap is needed, so that the required voltage drop can be specified as a boundary condition.
- When wires are parallel and very close together, the segments should be aligned to avoid incorrect current perturbation from offset match point and segment junctions.

4.4.2 Conducting Plate

Wire-grid modeling of conducting surfaces has been used with varying success [80, 81, 82]. The earliest applications to the computation of radar cross sections (RCS) and radiation patterns provided reasonably accurate results. Even computation for the input impedance of antennas driven against grid models of surfaces have often exhibited good agreement with experiments. However, broad and generalized guidelines for near-field quantities have not been developed, and the use of wire-grid modeling for near-field parameters should be approached with caution. A single wire grid, however, may represent both surfaces of a thin conducting plate. The current on the grid will be the sum of the currents that would flow on opposite sides of the plate. While information on the currents on the individual surfaces is lost, the grid will yield the correct radiated fields.

The choice of the grid-wire radius is based on the equivalent surface area assumption [81, 89]. One specific reason is the accurate modeling of surface current loss. Generally, there are two forms of solid surface which will be discussed:

I. For *free-edged plate* as shown in Fig. 4.2(a), the total circumference of the N grid wires is equal to the 2-sided circumference of the plate (at the same length),

$$2\pi aN = 2A. \tag{4.61}$$

II. For *enclosed box* as shown in Fig. 4.2(b), the total circumference of the N grid wires is equal to the external circumference of the plate (at the same length),

$$2\pi aN = 2(A + B). \tag{4.62}$$

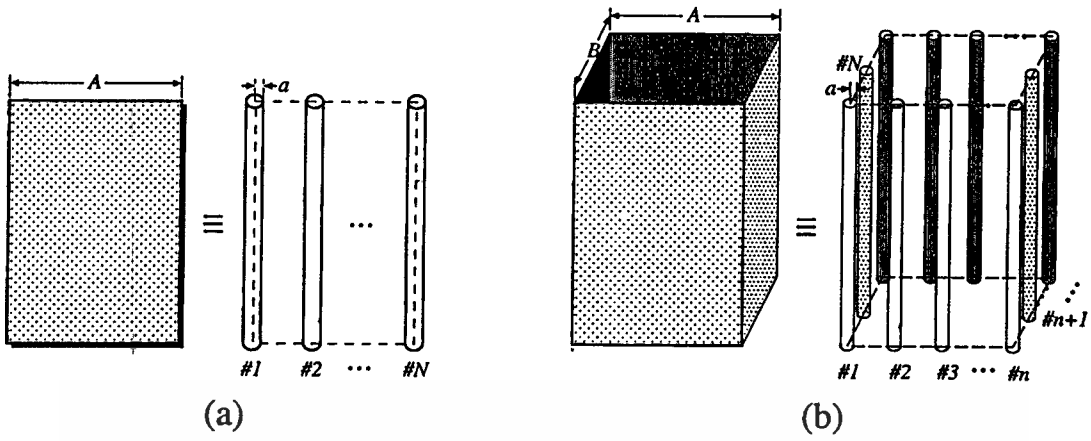

Figure 4.2 Geometry of wires needed to approximate a solid surface in the form of: (a) free-edged plate, and (b) enclosed box.

4.4.3 Lossy Dielectric

To obtain the scattered field of a lossy dielectric object, the advanced wire-grid model has been proposed [50]. This model has concentrated impedances, which are equivalent to the surface impedance, loaded into each wire junction, and thus is called a *loaded wire-grid model*. The calculation time using this model is almost the same as that when using ordinary wire-grid model. This technique can also be used to calculate the power absorbed by the lossy dielectric object.

A lossy dielectric material can be modeled by conductive wire-grid loaded with the surface impedance

$$Z_s = \sqrt{\frac{j\omega\mu}{\sigma + j\omega\varepsilon}}, \tag{4.63}$$

where σ is conductivity (in S/m), μ is permeability, and $\varepsilon = \varepsilon_0(\varepsilon_r' + j\varepsilon_r'')$ is complex permittivity of the dielectric material at particular frequency $\omega = 2\pi f$.

The radius of each wire to model surface of the dielectric object should be determined using the similar guidelines provided in the previous section.

4.5 Canonical Examples

To avoid the error that may occur in the simulation begun with very complicated structure and to assimilate know-how for investigation the results, the preliminary study of the effect of simple human head model to the most fundamental antenna element ($\lambda/2$-dipole antenna) is selected to investigate. it may be also regarded as the reference case.

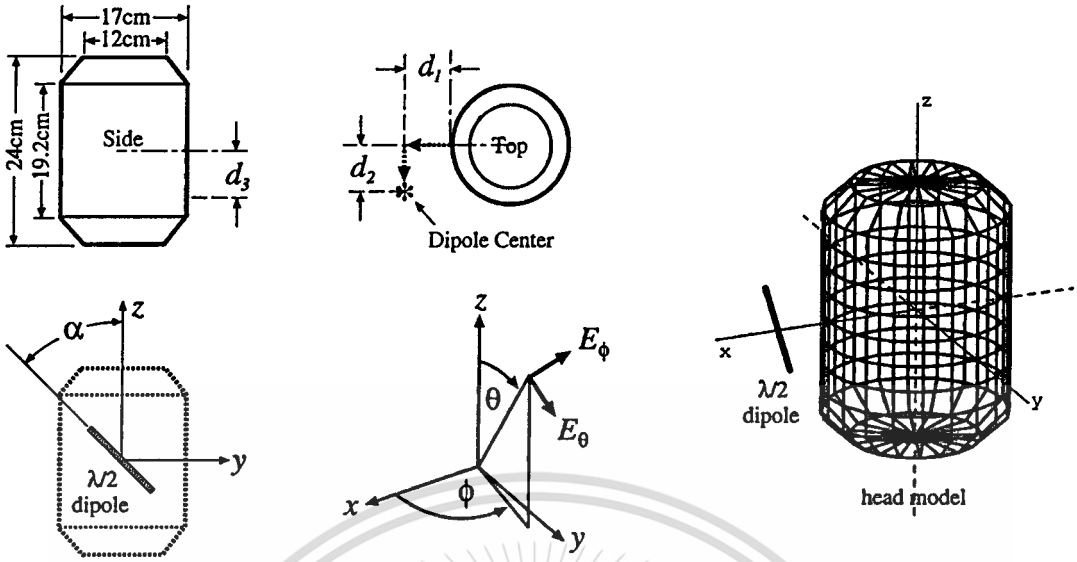

Figure 4.3 Coordinate and dimension of head model with $\lambda/2$-dipole antenna.

4.5.1 Dipole Near Head Model

To show the interaction of head model to a $\lambda/2$-dipole antenna with respect to various parameters—tilted angle α, separation distance d, and frequency f_r—as depicted in Fig. 4.3, the simulation results are shown in 5 cases as:

I. Varying dipole tilted angle α from 0°–90°
Results illustrated in Figs. 4.4(a)–(l); it is observed that the dominant polarization of this structure is the same to that of the dipole antenna in free space.

II. Varying dipole separation distance d_1 from 1.0–10 cm
Results illustrated in Figs. 4.5(a)–(l); it is observed that the absorption drastically decreases with the increasing radial separation distance.

III. Varying dipole separation distance d_2 from 0.0–10 cm
Results illustrated in Figs. 4.6(a)–(l); it has moderate effect to the reduction rate of the absorption as the separation distance increases.

IV. Varying dipole separation distance d_3 from 0.0–10 cm
Results illustrated in Figs. 4.7(a)–(l); it has least effect to the reduction rate of the absorption as the separation distance increases.

V. Varying frequency f_r from 850–5,500 MHz
Results illustrated in Figs. 4.8(a)–(l); it is observed that as the frequency increases the effective separation distance between dipole and head also increases, leads to lower absorption and head may act as the reflector.

4.5.2 Accuracy Analysis

To validate the modeling of the structure and the simulation, five aspects are investigated as follows:

4.5.2.1 Shape of Head Model

Different shapes of head model result to different radiation patterns, i.e., the significant difference of radiation occurs on the half-space behind the dipole as illustrated in Fig. 4.9. The cubic head model (Figs. 4.9 (a)–(c)) absorbs more radiation than cylindrical head model (Figs. 4.9 (d)–(f)), while tapered-end cylindrical head model (Figs. 4.9 (g)–(h)) shows minor improvement over the simple cylindrical model. However, the difference of the radiation patterns in vertical-cut planes are observable, it is therefore desirable to choose the tapered-end cylindrical head model.

4.5.2.2 Grid Size

Grid size drastically effects to the radiation. To investigate the effects, the grid size is varied for the head model while the segment length is fixed at 0.025λ for dipole. Figures 4.10 (a)–(c) show the results for the average grid size in the order of 0.5λ, it is far from the correct results. Smaller grid size in the order of 0.25λ gives somewhat better results as illustrated in Figs. 4.10 (d)–(f). The optimum grid size in the order of 0.1λ gives reasonable results (Figs. 4.10 (g)–(i)) while saving the computational time. It is, however, noted that the wire radius is kept constant to the optimum value a when grid size is varied (while the radius should be varied with respect to the grid size to satisfy (4.63)).

4.5.2.3 Wire Radius

The optimum wire radius a for head model is calculated from (4.62). Even the choice of different wire radii does not reveal the significant effects on the radiation patterns as shown in Figs. 4.11 (a)–(i), it greatly affects to the absorption loss L_a. It is noted that for the case of optimum wire radius (Figs. 4.11 (e) and (f)), the back-lobe is minimized. This result corresponds to the simulation performed by Miller [81] where $\lambda/2$-dipole is surrounded with a number of 2λ-wires and the radiation from the dipole is minimized when the radius of surrounded wires meets the condition of (4.62).

4.5.2.4 Current Flow Model on Wire

When comparing the results between using filament current model (thin-wire kernel) and cylindrical current sheet model (extended thin-wire kernel), the radiation patterns are identical. However, the extended thin-wire kernel provides slightly more absorption loss to the thin-wire kernel for 0.5%.

4.5.2.5 Surface Impedance Model

Figures 4.12 (a)–(c) show the radiation patterns for perfect conducting wire modeling of head, lossless absorption is observed. To model dielectric property of the head tissue, the surface impedance $Z_s = 45.31 + j15.92\,\Omega$—calculated from (4.63) with $\varepsilon_r = 45.31 + j15.92$, $\sigma = 0.85\,\mathrm{S/m}$ at 1,800 MHz [50]—is loaded to each grid, and the results are illustrated in Figs. 4.12 (d)–(f).

4.6 Concluding Remarks

The integral equations, Method of Moments, and wire-grid modeling are described as the means for simulation procedures. The canonical examples pertinent to the interested problems in the next chapter are thoroughly investigated. The obtained results will be used as the guidelines for the further simulations.

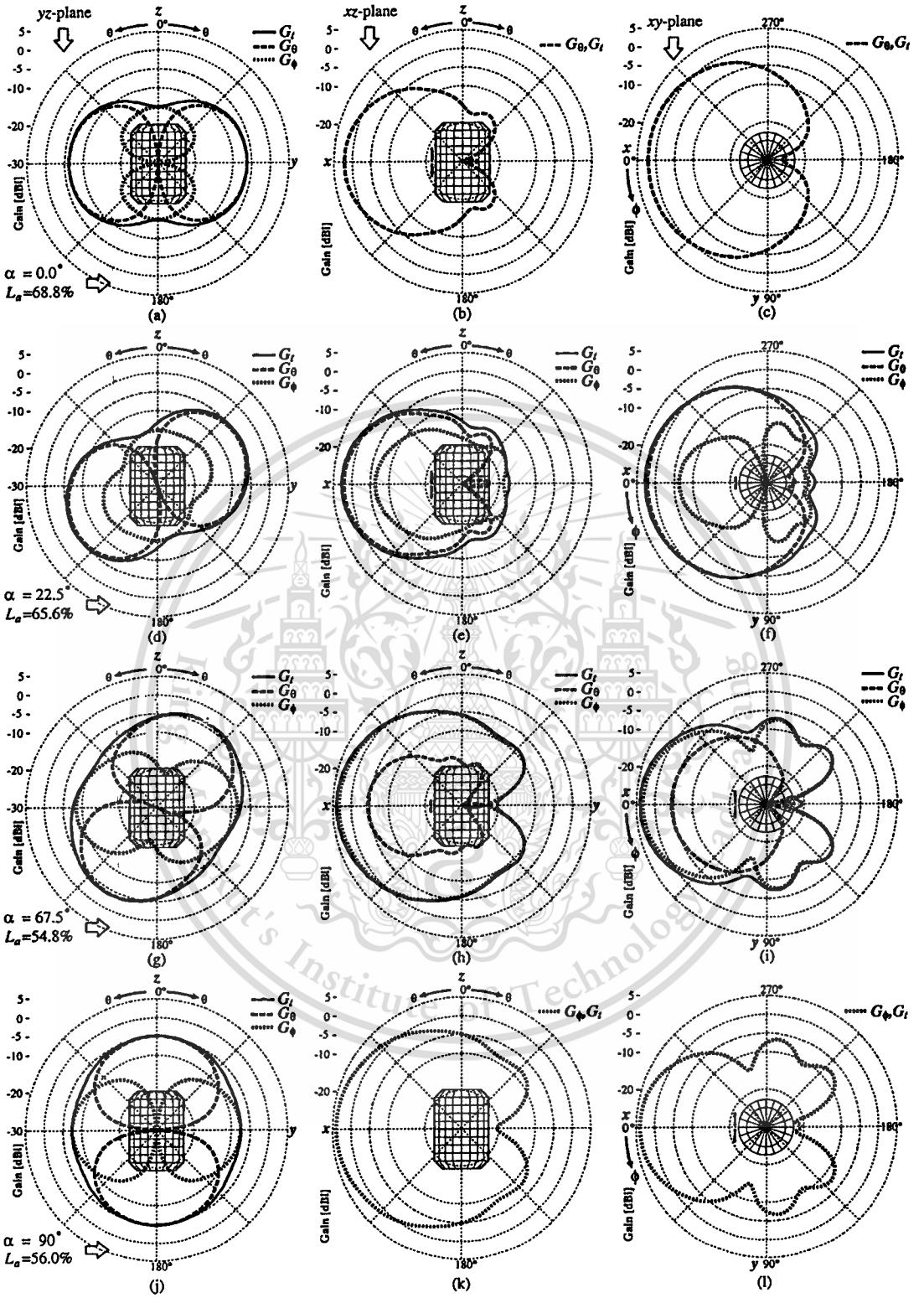

Figure 4.4 Component-gain patterns of $\lambda/2$-dipole separated from head model by the distance $d_1 = 1\,\text{cm}$, $d_2 = d_3 = 0\,\text{cm}$, vary tilted angle α: (a)–(c) $\alpha = 0°$, (d)–(f) $\alpha = 22.5°$, (g)–(i) $\alpha = 67.5°$, and (j)–(l) $\alpha = 90°$ (for $\alpha = 45°$, please see Figs. 4.5 (a)–(c)), L_a is the absorption loss.

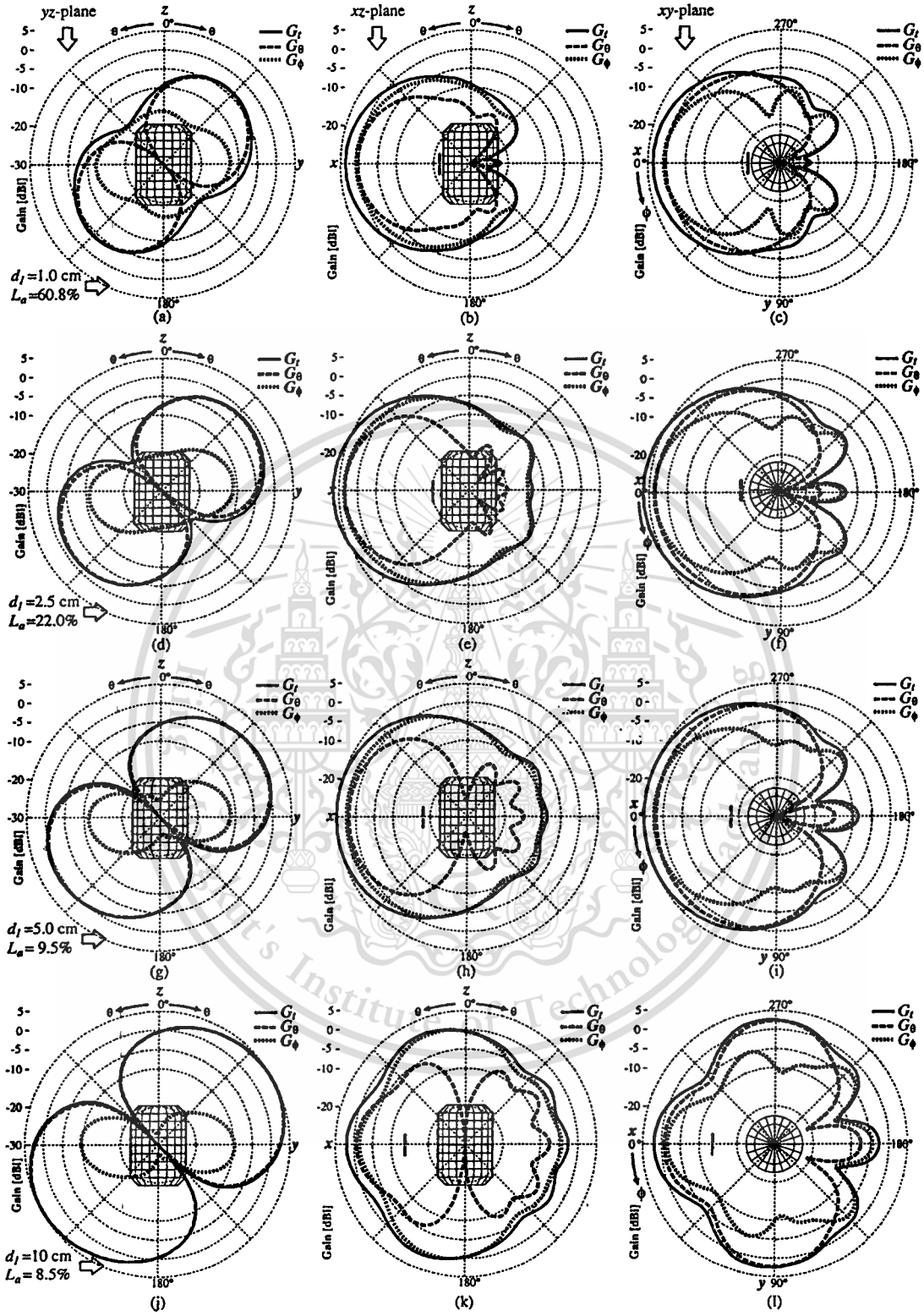

Figure 4.5 Component-gain patterns of 45°-tilted-$\lambda/2$-dipole separated from head model by the distance $d_2 = d_3 = 0\,\text{cm}$, vary d_1: (a)–(c) $d_1 = 1.0\,\text{cm}$, (d)–(f) $d_1 = 2.5\,\text{cm}$, (g)–(i) $d_1 = 5.0\,\text{cm}$, and (j)–(l) $d_1 = 10.0\,\text{cm}$.

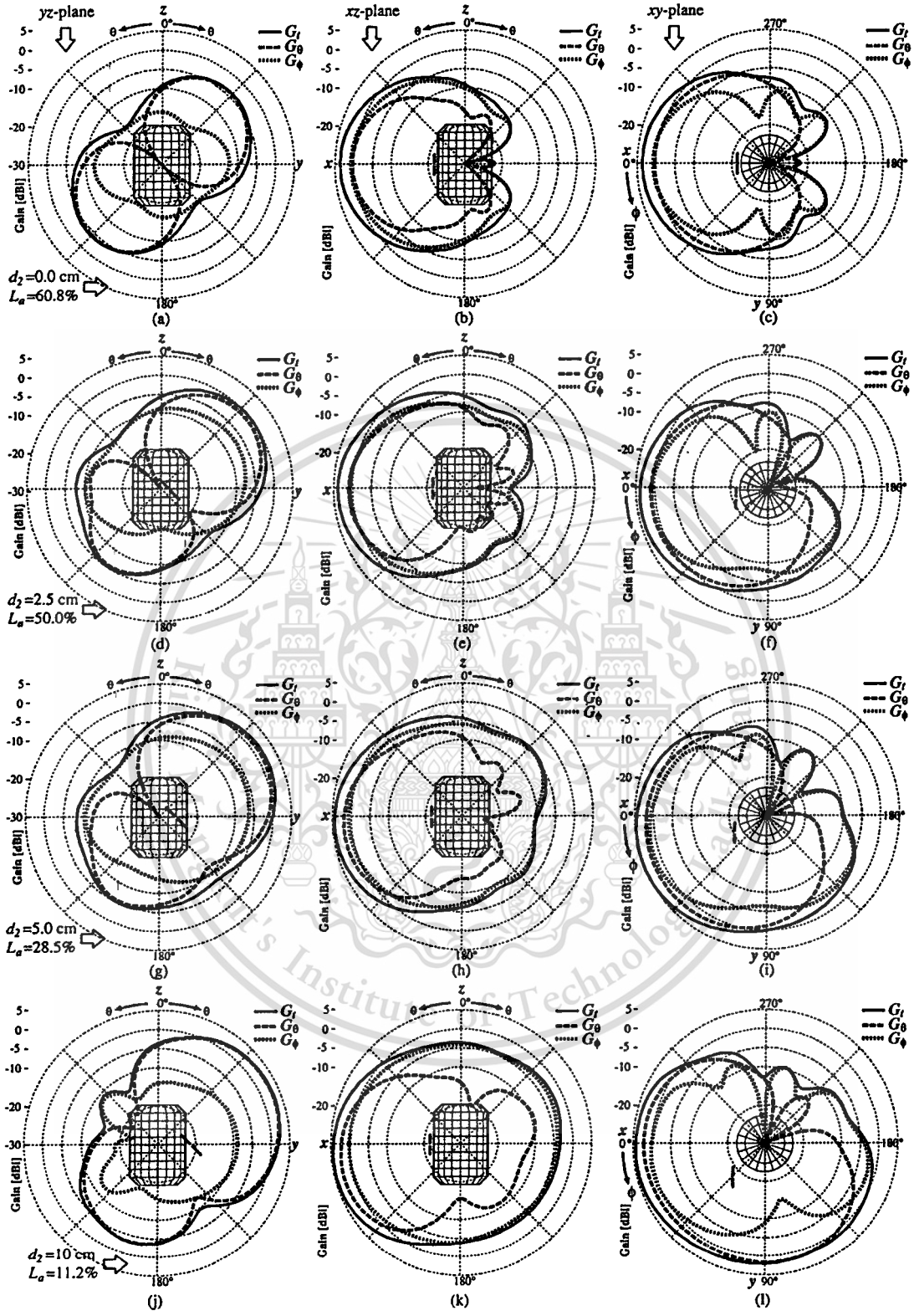

Figure 4.6 Component-gain patterns of 45°-tilted-$\lambda/2$-dipole separated from head model by the distance $d_1 = 1\,\text{cm}$, $d_3 = 0\,\text{cm}$, vary d_2: (a)–(c) $d_2 = 0.0\,\text{cm}$, (d)–(f) $d_2 = 2.5\,\text{cm}$, (g)–(i) $d_2 = 5.0\,\text{cm}$, and (j)–(l) $d_2 = 10.0\,\text{cm}$.

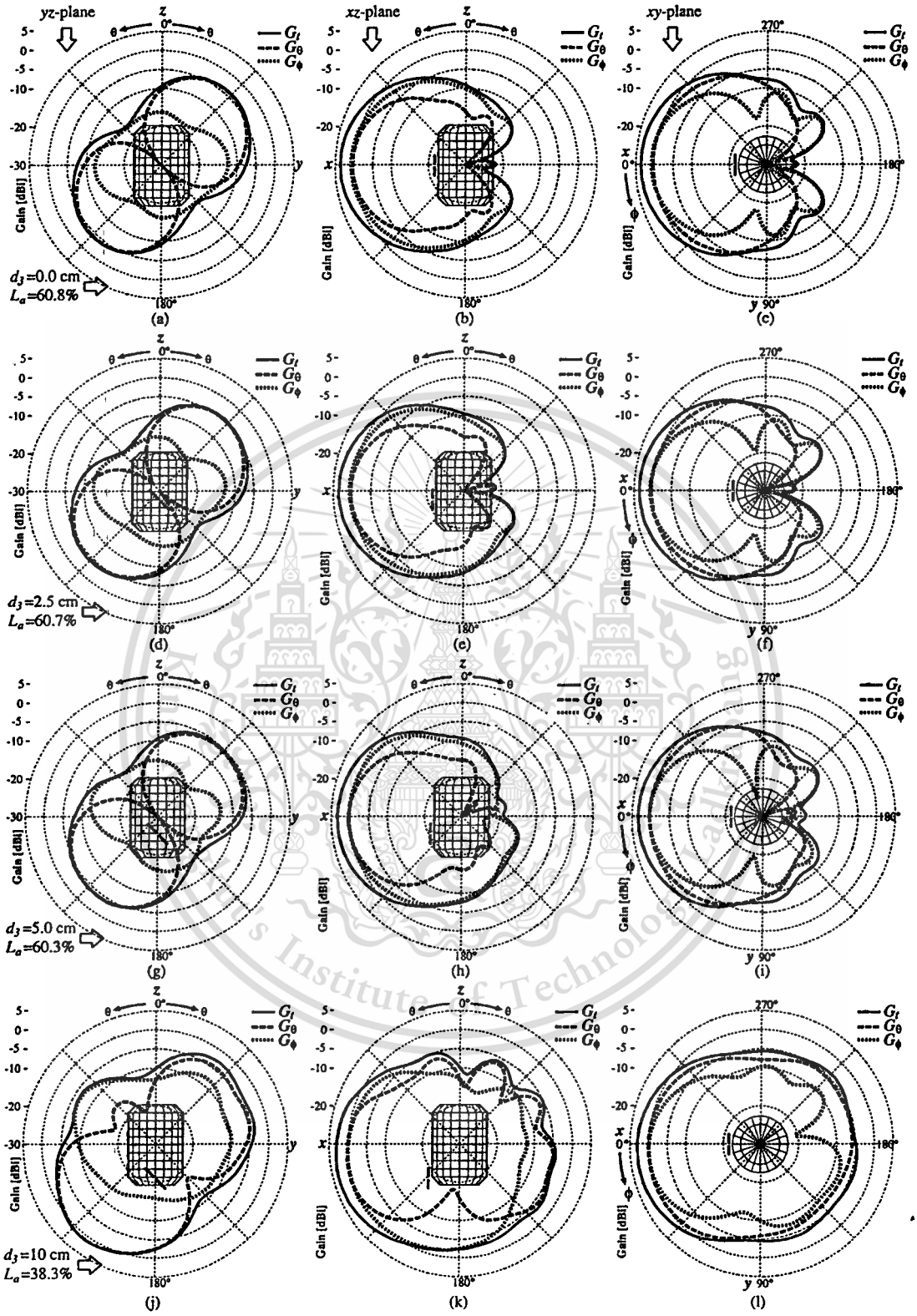

Figure 4.7 Component-gain patterns of 45°-tilted-$\lambda/2$-dipole separated from head model by the distance $d_1 = 1\,\text{cm}$, $d_2 = 0\,\text{cm}$, vary d_3: (a)–(c) $d_3 = 0.0\,\text{cm}$, (d)–(f) $d_3 = 2.5\,\text{cm}$, (g)–(i) $d_3 = 5.0\,\text{cm}$, and (j)–(l) $d_3 = 10.0\,\text{cm}$.

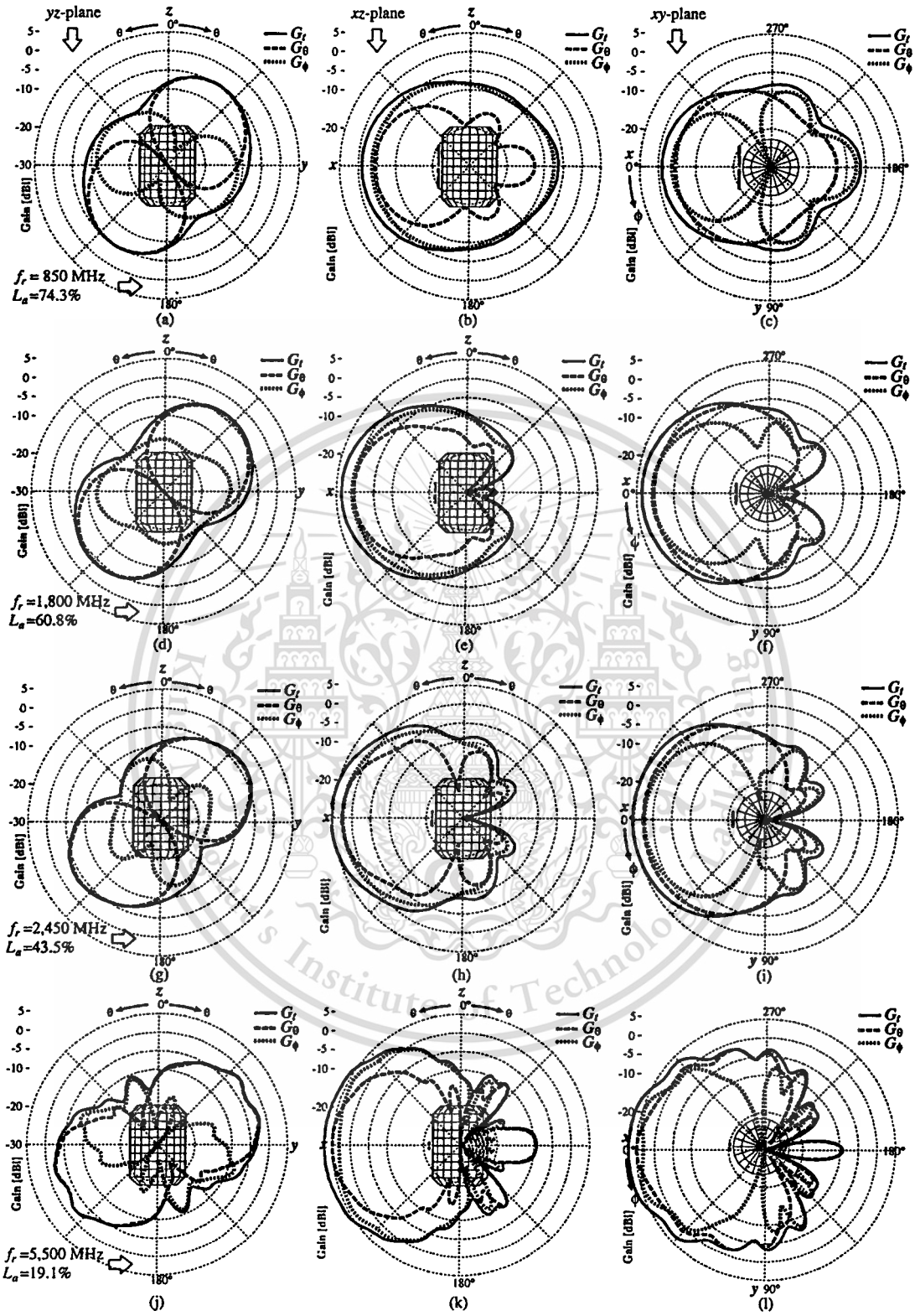

Figure 4.8 Component-gain patterns of 45°-tilted-$\lambda/2$-dipole separated from head model by the distance $d_1 = 1\,\text{cm}$, $d_2 = d_3 = 0\,\text{cm}$, vary frequency f_r: (a)–(c) $f_r = 850\,\text{MHz}$, (d)–(f) $f_r = 1,800\,\text{MHz}$, (g)–(i) $f_r = 2,450\,\text{MHz}$, and (j)–(l) $f_r = 5,500\,\text{MHz}$.

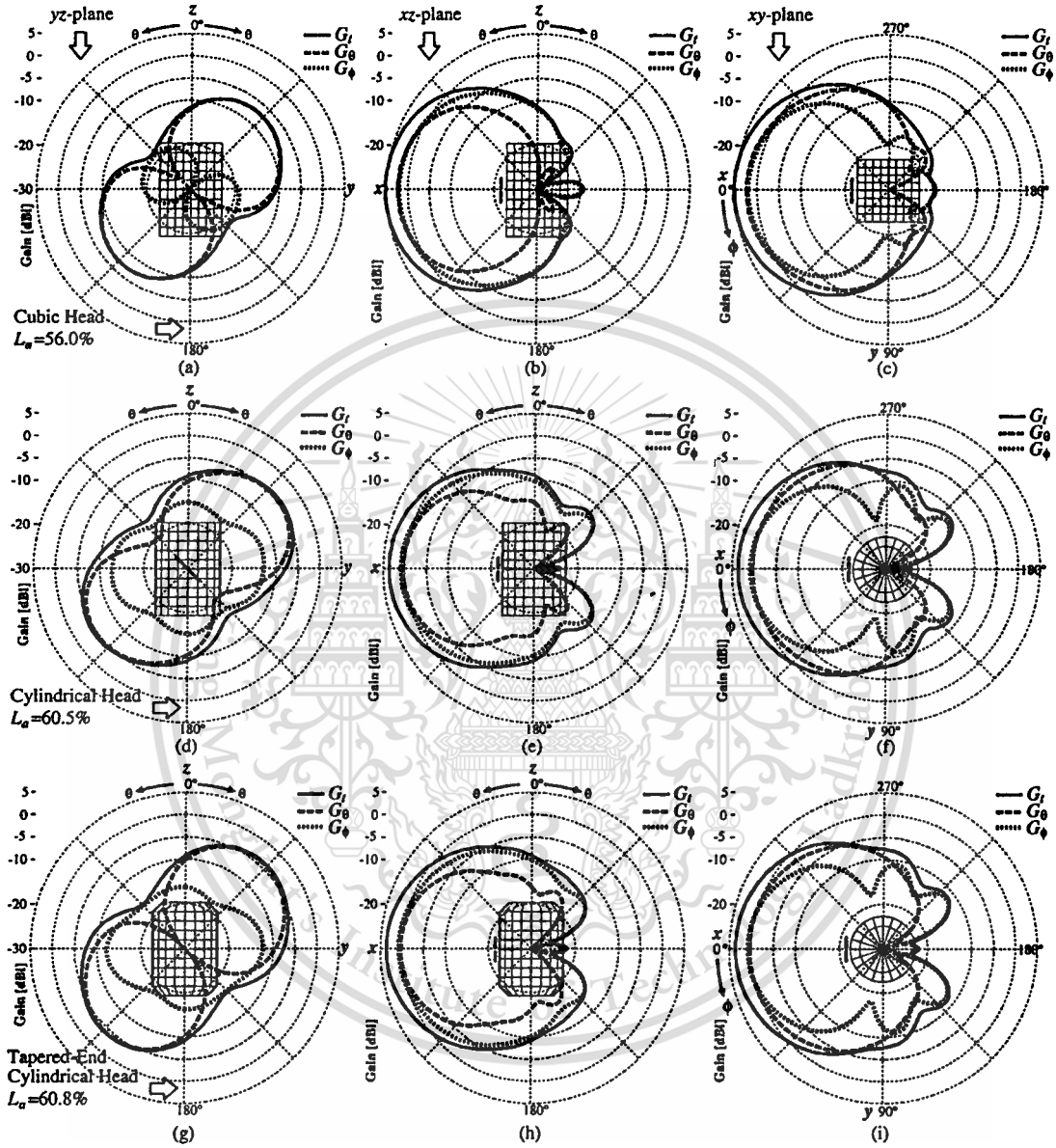

Figure 4.9 Component-gain patterns of 45°-tilted-$\lambda/2$-dipole separated from head model by the distance $d_1 = 1\,\text{cm}$, $d_2 = d_3 = 0\,\text{cm}$, vary configuration of head model: (a)–(c) cubic head model, (d)–(f) cylindrical head model, (g)–(i) tapered-end cylindrical head model.

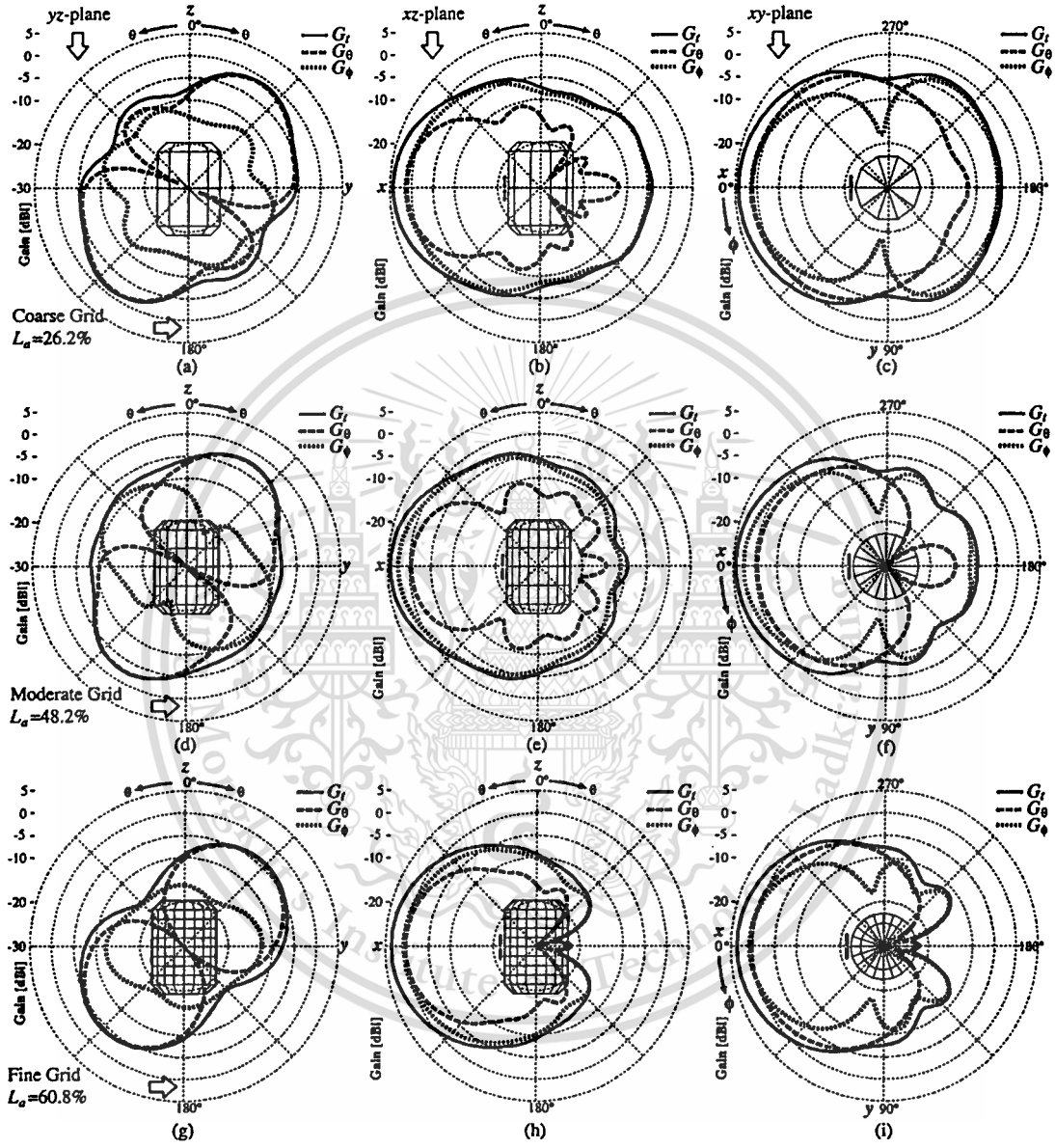

Figure 4.10 Component-gain patterns of 45°-tilted-$\lambda/2$-dipole separated from head model by the distance $d_1 = 1\,\text{cm}$, $d_2 = d_3 = 0\,\text{cm}$, vary grid size: (a)–(c) coarse grid, (d)–(f) moderate grid, (g)–(i) fine grid.

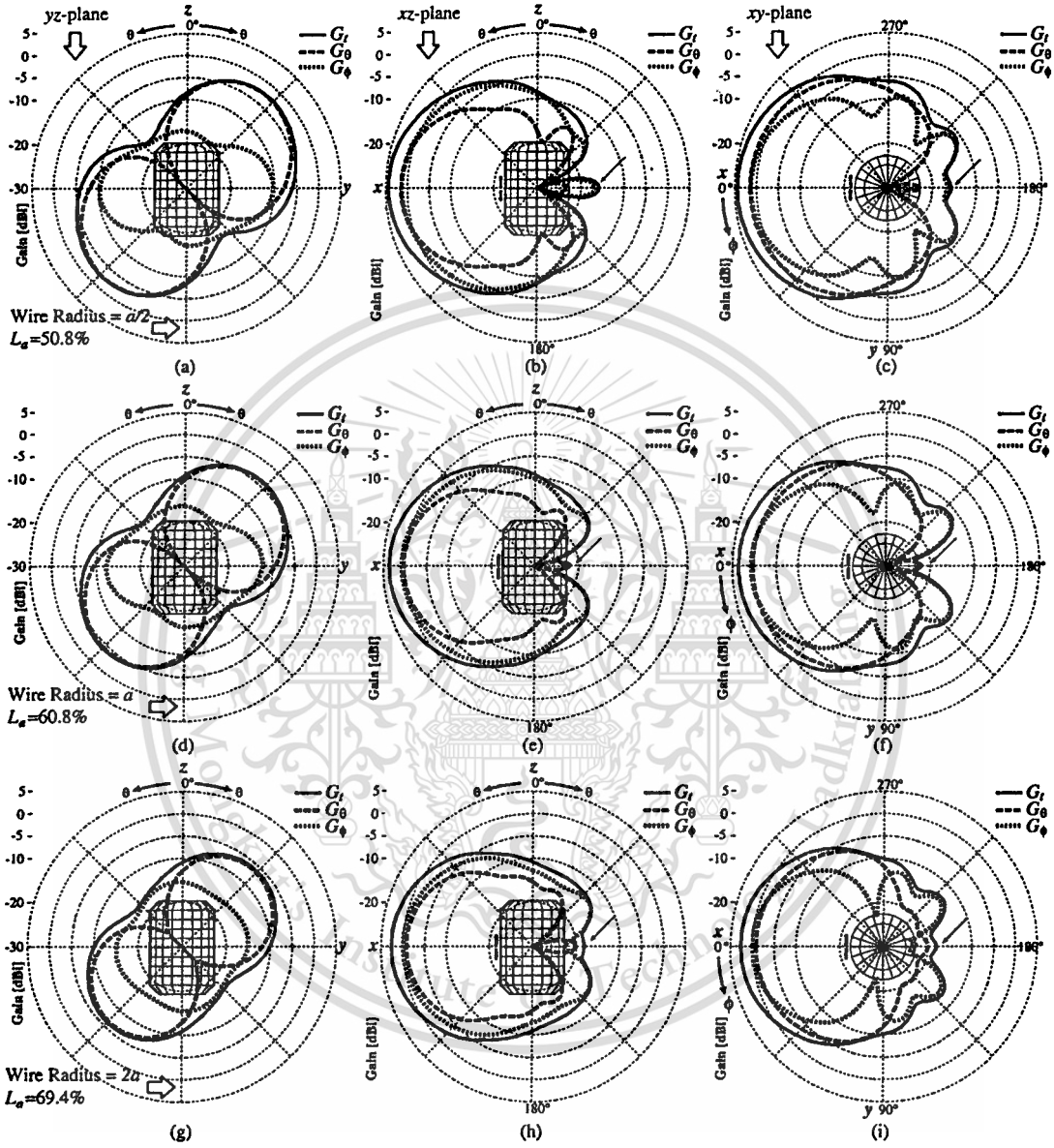

Figure 4.11 Component-gain patterns of 45°-tilted-$\lambda/2$-dipole separated from head model by the distance $d_1 = 1\,\text{cm}$, $d_2 = d_3 = 0\,\text{cm}$, vary wire radius: (a)–(c) wire radius $= a/2$, (d)–(f) wire radius $= a$ (optimum), (g)–(i) wire radius $= 2a$.

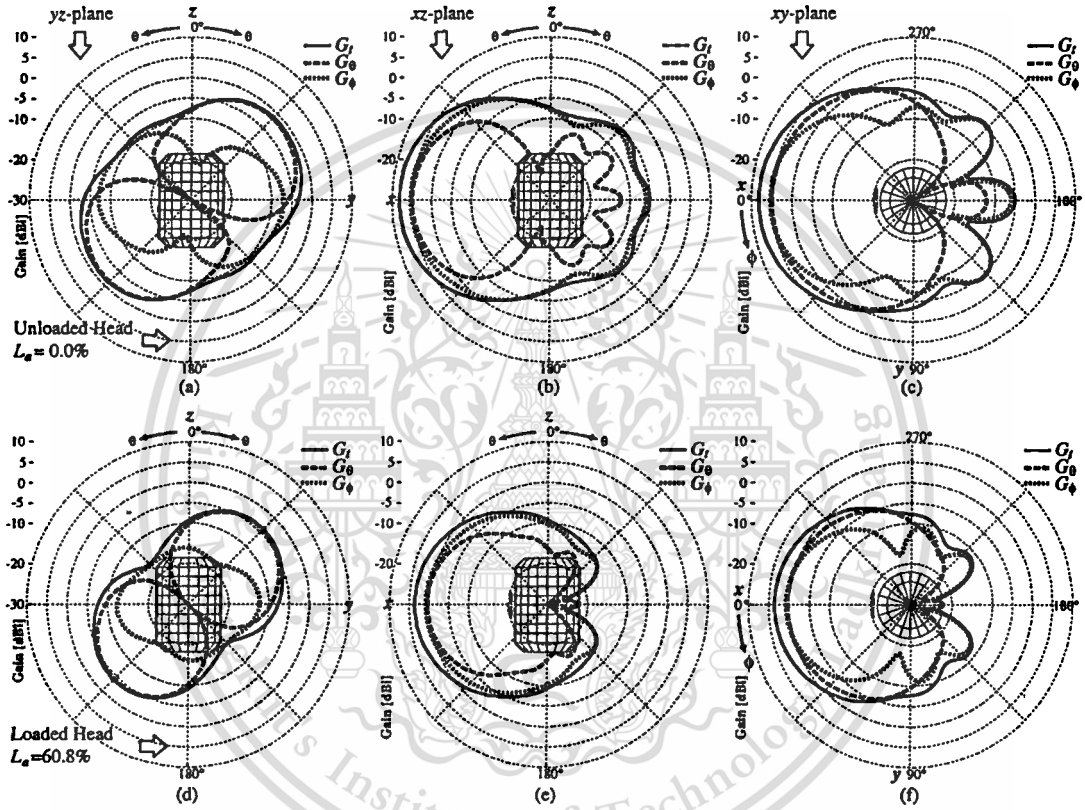

Figure 4.12 Component-gain patterns of $\lambda/2$-dipole separated from head model by the distance $d_1 = 1\,\text{cm}$, $d_2 = d_3 = 0\,\text{cm}$, with: (a)–(c) unloaded (conductive) head model, and (d)–(f) loaded head model.

Chapter 5

Polarization Diversity PIFA

5.1 Introductory Remarks

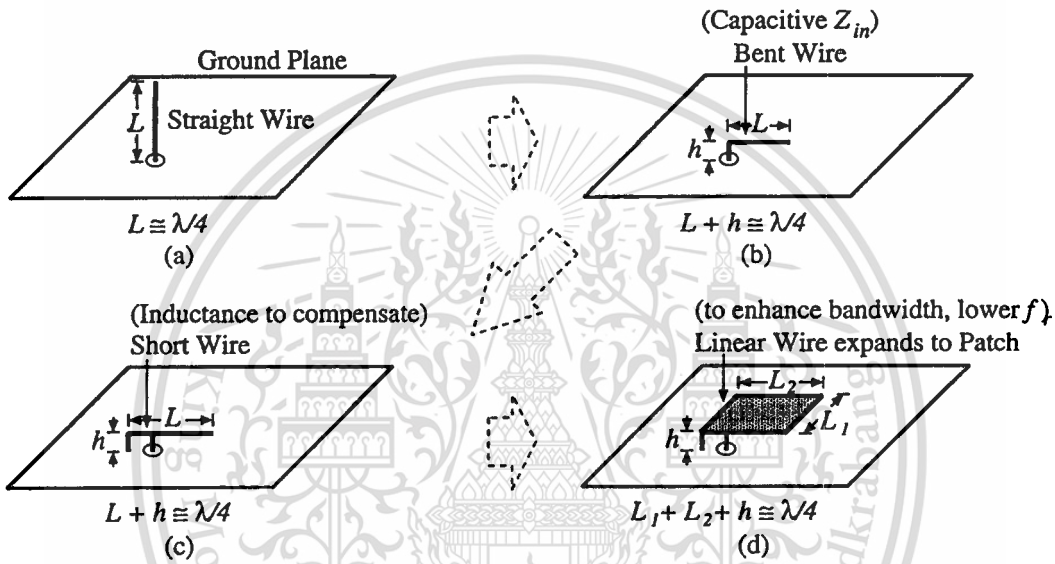

Figure 5.1 Evolution of PIFA from $\lambda/4$-monopole antenna: (a) monopole, (b) ILA, (c) IFA, and (d) PIFA.

One of the most fundamental antenna elements is a $\lambda/4$-monopole on ground plane as shown in Fig. 5.1(a). For the applications that the low profile structure is physical constraint, the $\lambda/4$-monopole can be bent parallel to the ground plane as shown in Fig. 5.1(b) and it is called inverted-L antenna (ILA). However, the input resistance is much reduced to be equal to that of vertical monopole with the same height h, furthermore, the input reactance becomes increasingly capacitive. To compensate this capacitance, a small I-L element is attached to the vertical section of ILA and the appearance is that of a *letter F* facing the ground plane—thus its name becomes the inverted-F antenna (IFA) as shown in Fig. 5.1(c). The IFA is also well known as a *shunt-driven inverted-L antenna-transmission line with an open end.* For the antenna with short-circuit stub, the structure has strong relation to the wavelength, therefore, the frequency bandwidth is always considerably narrow. To enhance the bandwidth and lower the resonant frequency, a rectangular plate is attached to the wire section parallel to the ground plane as shown in Fig. 5.1(d), and it is named a planar inverted-F

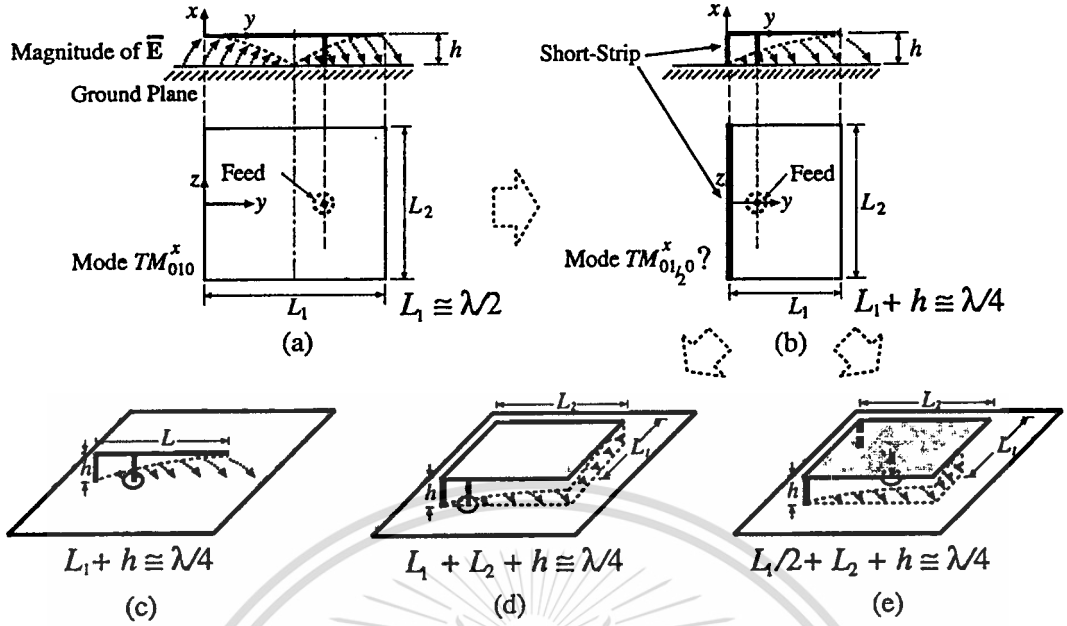

Figure 5.2 Evolution of PIFA from $\lambda/2$-microstrip antenna: (a) microstrip antenna, (b) PIFA with broad short-strip, (c) IFA, (d) PIFA with single short-pin, and (e) PIFA with dual short-pin.

antenna (PIFA). On the other hand, the PIFA can also be considered as a kind of short-circuit rectangular microstrip antenna [90] as shown in Fig. 5.1. The field distribution (resonant mode) beneath the patch of PIFA (Fig. 5.1(b)) is the same to that of a $\lambda/2$-microstrip antenna (Fig. 5.1(a)) cut by half. *Short* denotes *short-circuit*, hereafter.

From the basic idea of the PIFA, this chapter shows how to achieve the polarization diversity from the original PIFA. Firstly, the polarization diversity PIFA on a ground plane is investigated. Then, the ground plane is replaced by a portable telephone. The user's body is included in the investigation to take into account all possible interaction from the practical situation, finally. The results reveal in current distribution, input impedance, radiation patterns, and radiation efficiency. A polarization diversity PIFA is sometimes referred as a PDA (polarization diversity antenna) in the contexts for briefing, hereafter.

5.2 Wire-Grid Modeling

The wire-grid modeling is utilized for investigation of all focused structures, hereafter. The guidelines of how to properly model the antenna structure follow the Sec. 4.4.

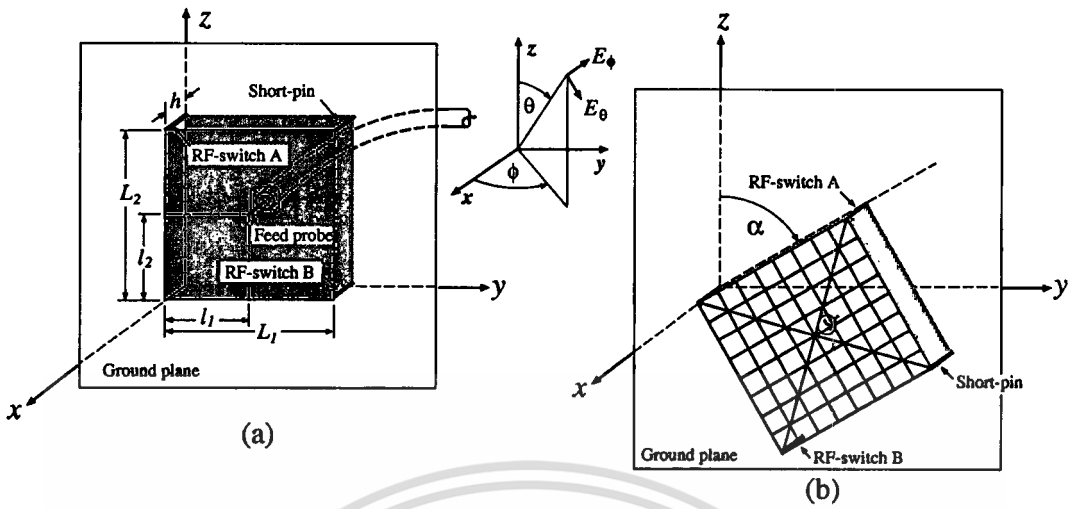

Figure 5.3 The PDA on a ground plane; (a) configuration, (b) wire-grid model.

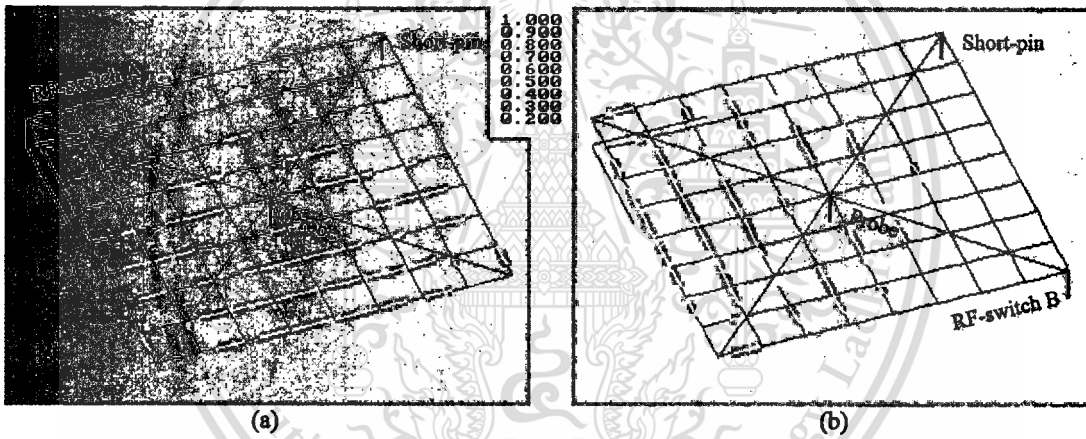

Figure 5.4 Current distribution on wire-grid model of PDA on ground plane (not shown in the figure) when: (a) RF-switch A operates (VP mode), and (b) RF-switch B operates (HP mode).

5.2.1 Polarization Diversity PIFA

The PIFA in Fig. 5.1(d) can be modified to be polarization diversity by replacing the short-pin (short section) by an RF-switch, and adding another RF-switch to either of adjacent corners. And operate by turning on either of the switches for the desired polarization. However, by simply doing this, the input impedance matching can not be achieved since for matching condition the feed probe has to be located close to the short-pin. By contrast, the feed probe has to be located in symmetry with respect to either of short-pins to maximize the polarization diversity effect.

To solve this problem, the one permanent short-pin is introduced to attach

to one (top-right) corner as shown in Fig. 5.3(a), and two RF-switches are attached to two opposite corners perpendicular to each other with respect to the permanent short-pin position. The antenna is fed by the probe via the ground plane at the center of the patch.

To analyze the characteristics of the PDA at 1,800 MHz, the metallic patch is modeled by 8×8 wires with two wires in diagonal to support the current flow from the probe direction. The RF-switch is modeled by the conducting wire when turned on and nothing when turned off. The total segments of the wire-grid are 495 segments. The wire-grid structure is excited by the *delta gap feed* at the bottom of the probe. The dimension of the square patch is $L_1 = L_2 = 26\,\text{mm}$, $l_1 = l_2 = 13\,\text{mm}$, $h = 5\,\text{mm}$, and α is tilted angle from vertical axis.

- Current Distribution

When the RF-switch A operates, the current distribution on the wire-grid structure start flowing from the opposite (to the RF-switch and short-pin) edge of the patch and increasingly drifting parallel to the RF-switch and short-pin directions as shown in Fig. 5.4(a). As the RF-switch B operates, the pattern is that of the case of RF-switch A operates but rotate 90° clockwise as shown in Fig. 5.4(b). From the current flow in Fig. 5.4(a), it is understandable that the dominant polarization is *linear* along z-axis (and denotes as vertical polarization (VP) mode), while Fig. 5.4(b) renders the linear dominant polarization in y-axis (and denotes as horizontal polarization (HP) mode).

5.2.2 Polarization Diversity PIFA on Portable Telephone

Since this PDA is proposed for portable telephone, it is more reasonable to include the portable telephone structure into the analysis, as it should have the significant effect to the resonant and radiation mechanisms of the PDA. The PDA is attached to the portable telephone as depicted in Fig. 5.5(a). A $\lambda/4$ monopole is also model for the reference case. The wire-grid structure pertinent to the simulated model is depicted in Fig. 5.5(b). The number of wires modeled for PDA is reduced to 6×6 wires as the compensation for the increasing segments for the overall structure. The total segments of the wire-grid are 723 segments.

- Current Distribution

By comparing the current distribution pattern of the PDA on a ground plane (Figs. 5.4(a) and (b)) to that of the PDA on a portable telephone (Figs. 5.6(a) and (b)), the very similar patterns are observed. To briefly conclude the resonant mechanism of the PDA, it has the resonant length for the square patch as part of the periphery plus height is approximately equal to a quarter-wavelength

$$\frac{L}{2} + L + h \approx \frac{\lambda}{4}, \tag{5.1}$$

as also illustrated for easily understanding in Fig. 5.5(c).

It is seen from the current distribution in Fig. 5.7 that the $\lambda/4$ monopole induces large current flow on the portable telephone (Fig. 5.7(c)) while the PDA, for both VP and HP modes, has strong current confines to the antenna region.

5.2.3 Polarization Diversity PIFA on Portable Telephone with User's Body

The study of human interaction to portable radio equipment have been gained more attention since less than 10 years ago. At the beginning, the attention was focused on the portable radio for volunteer amateur radio (VR) [91] and the paging system [92]. As the mobile cellular was getting ubiquitous, the study has been orientated to the portable mobile telephone. Among the pioneer researches, there had been originally studied the human body interaction by modeling only head [93, 94] with the portable telephone which could provide the rough estimation. The more improvement by including hand model has later been investigated [18, 62, 95, 96], however the antenna tilted angle was set at only vertical orientation, which could not properly render the realistic RF-phenomenon.

As the upper-half part of the human body is considered to most contribute to the interaction with the mobile handheld antennas. To correctly model the portable telephone user's body, many samples have been observed as depicted in Fig. 5.8. This thesis will use the average tilted angle α of portable telephone at

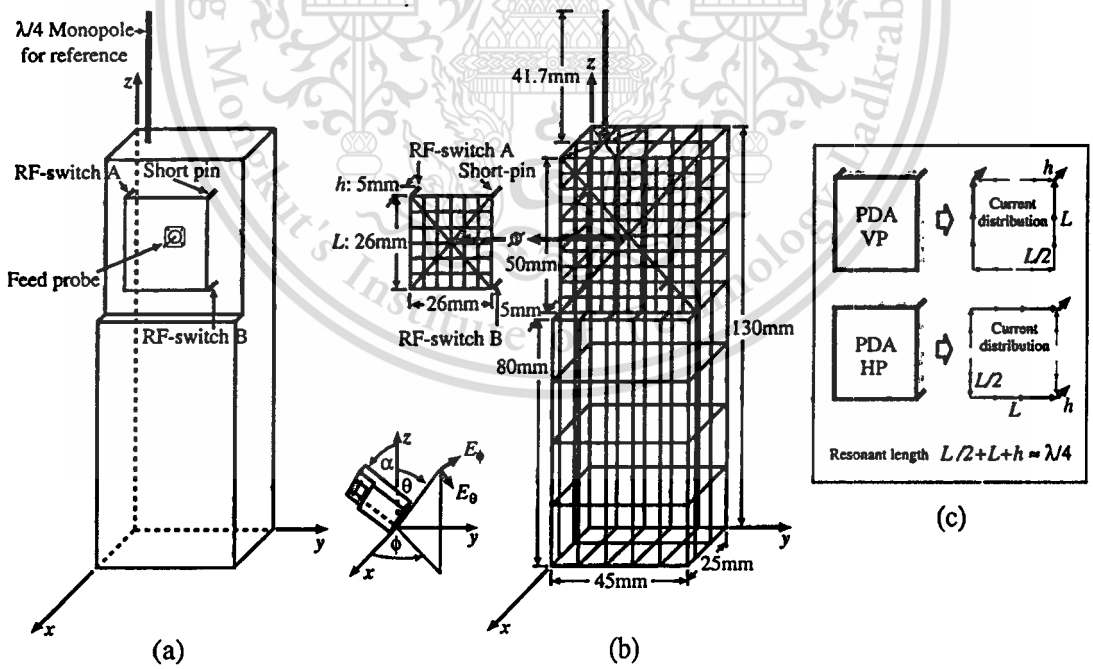

Figure 5.5 The PDA on portable telephone and the reference $\lambda/4$ monopole antenna (a) configuration, (b) wire-grid model, and (c) current distribution diagram on PDA.

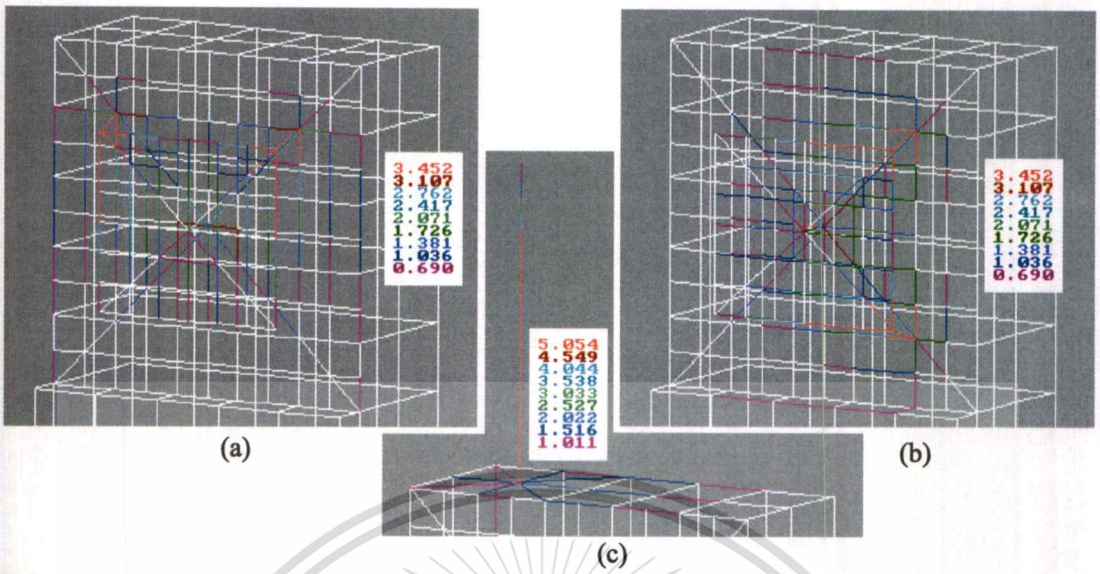

Figure 5.6 Enlargement of antenna portion illustrating current distribution on wire-grid model of portable telephone mounted with: PDA in (a) VP mode, (b) HP mode; and (c) $\lambda/4$ monopole.

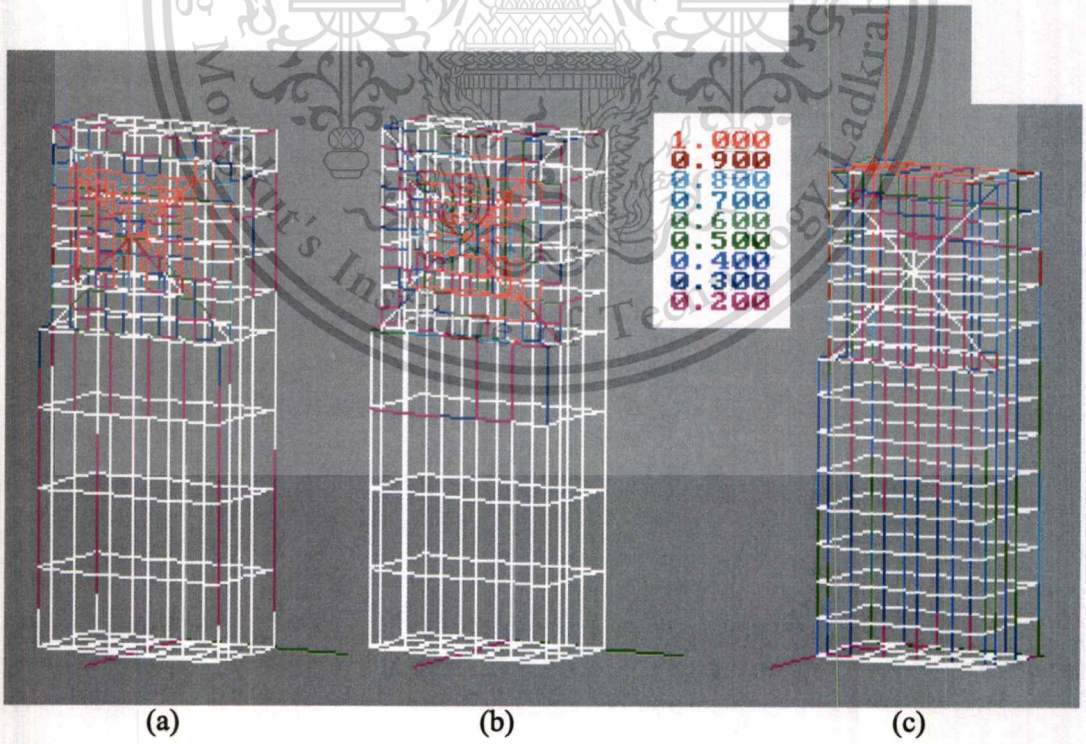

Figure 5.7 Current distribution on wire-grid model of portable telephone mounted with: PDA in (a) VP mode, (b) HP mode; and (c) $\lambda/4$ monopole.

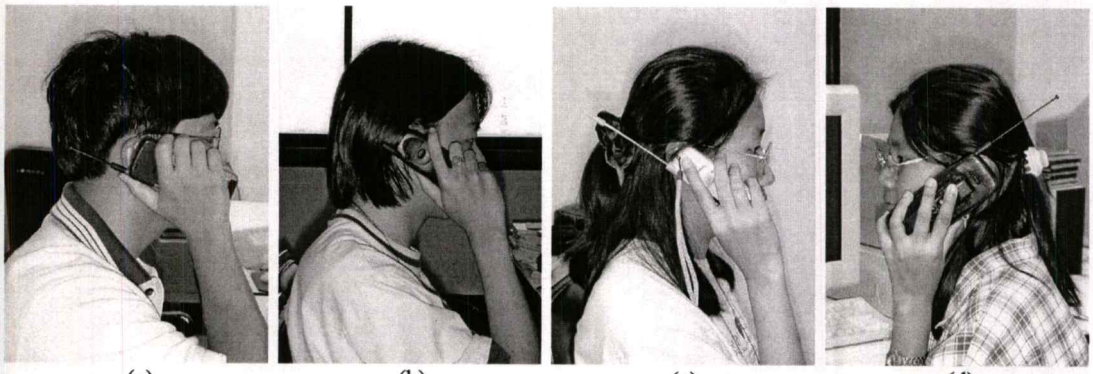

Figure 5.8 Samples of mobile users while operating portable telephone at tilted angle α: (a) $\alpha = 68°$ in right hand, (b) $\alpha = 56°$ in right hand, (c) $\alpha = 57°$ in right hand, (d) $\alpha = 55°$ in left hand.

60 degrees, and for *right-hand* operator. The configuration and dimension of a human body is: the phantom of the head is modeled by a tapered-end cylinder and placed on the center of the shoulder. The hand is positioned 5 mm apart from the right-hand side of the head with tilted angle $\alpha = 60°$, and the telephone is in the the hand with same orientation as shown in Fig. 5.9(a) and (b). The cylindrical model of head, parallelepiped model of hand and arm, and trapezoidal model of shoulder are assigned by the dimensions as depicted in Figs. 5.9(a)–(c).

The phantoms are modeled by conductive wire-grid loaded with the surface impedance as expressed in (4.63), where the conductivity $\sigma = 0.85$ S/m and the complex relative permittivity $\epsilon_r = 48 - j30$ averaged for a head [97], and $\sigma = 1.39$ S/m and $\epsilon_r = 54 - j14$ averaged for muscle from FCC (Federal Communication Commission, USA), to simulate the dielectric property of the human tissue as depicted in Fig. 5.9. The adaptive gridding is employed in the modeling. The grid-size is small for the antennas and nearby structures, e.g., the telephone box part beneath the PDA patch and at the base of a monopole antenna. The larger grid-size is assigned for the structures far from the primarily radiating structures. The segment-length of each wire-grid is assigned adaptively (1 mm–45 mm), likewise. The total segments of the wire-grid are 2174 segments. The wire-grid models that are illustrated in Fig. 5.5(b) and Fig. 5.9 relevant to the simulated model.

5.3 Input Impedance

Figure 5.10(a) shows the calculated input impedance of PDA on handset in VP and HP modes. The PDA resonates at the desired frequency with high input resistance, and the resonant frequency becomes increasing when the human body is included for both VP mode (Fig. 5.10(b)) and HP mode (Fig. 5.10(c)), while the calculated input impedance becomes decreasing. The measured input

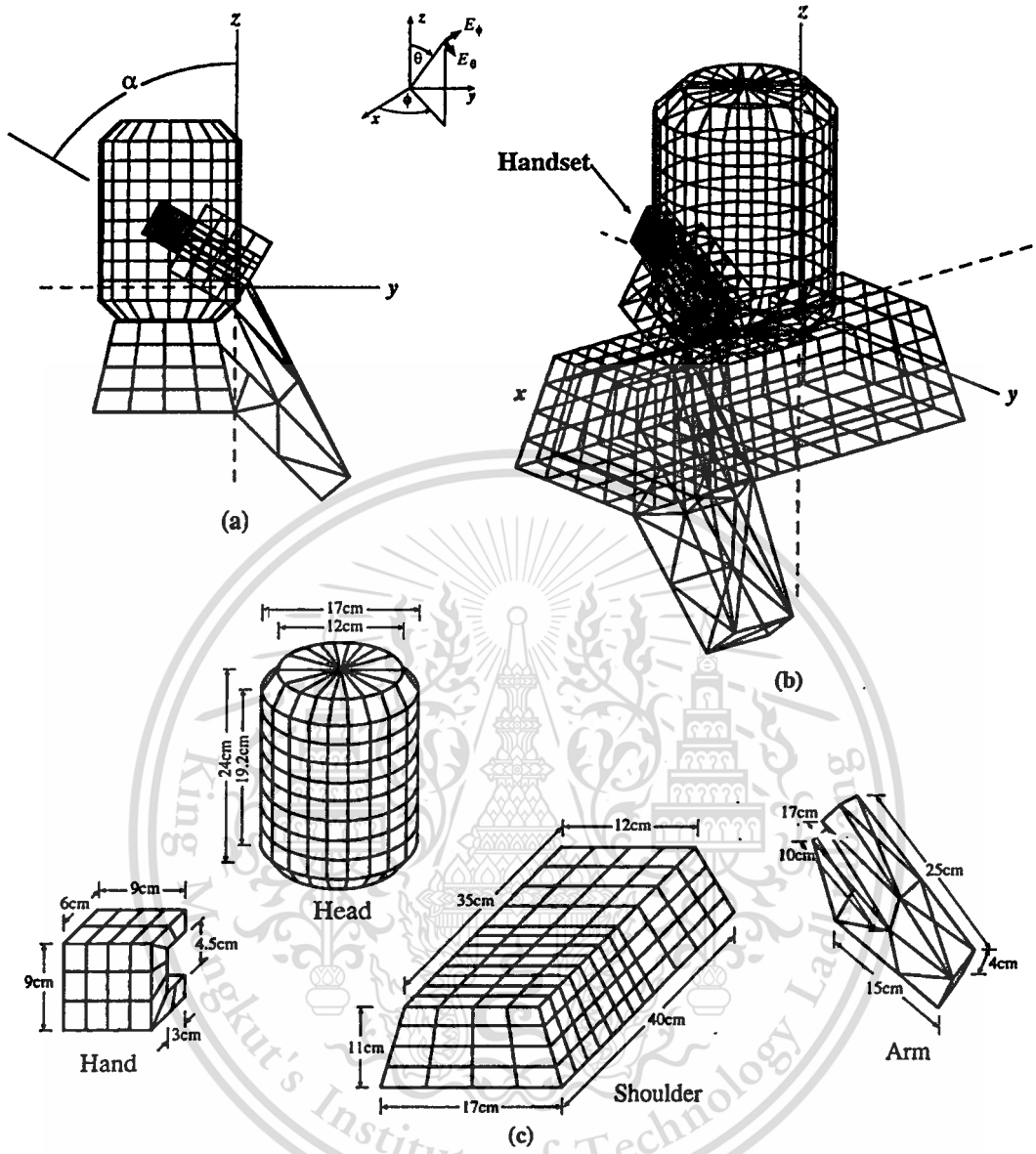

Figure 5.9 Wire-grid model of the antenna with human phantom (a) side-view (b) isometric view (c) phantom dimension.

impedance of PDA on handset with human body are in the same trend with the calculated ones (Figs. 5.10(b)–(c)), Especially for HP mode, both results are in good agreement.

Q-factor (quality factor) of this antenna can be determined from

$$Q = \frac{f_r}{f_h - f_l} \tag{5.2}$$

where f_r is the resonant frequency, f_l is the lower frequency where $R_l = X_l$, and f_h is the higher frequency where $R_h = X_h$. It is found that the Q-factor in VP

mode of PDA on handset is equal to 13.5 (bandwidth BW = 132 MHz) and it decreases to 6.2 (BW = 290 MHz) when the human body is included. For HP mode, the Q-factor is equal to 21.2 (BW = 85 MHz) and it decreases to 15.2 (BW = 119 MHz) for the same condition.

Even though the input impedance could be matched to 50Ω if the feed probe is moved along diagonal line ($l_1 = l_2$, always) toward the short-pin (by considering the current distribution on PDA as shown in Fig. 5.4), this paper fixed the feed point at the center to maintain the highest diversity characteristics. Therefore, the PDA in this configuration needs matching circuit beneath the feed probe. The resonant frequency of HP mode is slightly higher than VP mode, it can also be trimmed to obtain the same resonance by slightly lengthening the horizontal dimension (L_1) of the patch.

5.4 Radiation Patterns and Efficiency

To investigate the radiation characteristics of the PDA and a reference $\lambda/4$ monopole, it is considered into four cases: antenna on portable telephone, includes head, includes hand, and includes all upper parts of the user body. It is investigated for the case of antenna tilted angle $\alpha = 60°$ for practical situation and at $\alpha = 0°$ for reference case.

The far-field radiation patterns of the PDA and monopole are simulated by the Numerical Electromagnetic Code (NEC2) [87] based on the Method of Moments at the frequency of 1,800 MHz. The far-field distance is fixed at 5 m (the minimum required far-field distance of the overall structure is 2.43 m) to be feasible if experimentation is required to set up for some particular cases.

To find the radiation efficiency η, the conductor loss due to the wire-grid structure of the phantom model is first investigated. And it is found that the conductor loss is always less than 0.5%. Therefore, the absorbtion loss (L_a) due to the surface impedance modeling the lossy dielectric material is only significant.

5.4.1 Antenna Tilted Angle $\alpha = 0°$

Figures 5.11(a)–(f) illustrate the total-gain patterns of the PDA in VP and HP modes comparing to the $\lambda/4$ monopole in three principle planes (yz-, xz-, and xy-planes). These figures show the radiation of the antenna on portable telephone, and absorption from each part of the phantom model.

It is observed that the inclusion of head and hand models contributes to most of interaction in azimuthal (xy-) plane (Fig. 5.11(i)). Whereas, the interaction in the vertical (yz- and xz-) planes requires the shoulder model (Figs. 5.11(j) and (k)). The radiation efficiency of PDA and monopole on a portable telephone approaches 100%, and it decreases as the parts of phantom are gradually included (absorption increases). The efficiency of VP mode PDA is 56.7% while it is 53.1% for HP mode, and 42.4% for $\lambda/4$ monopole. The absorption from the phantom is approximated 3 dB degraded from the case without phantom.

The component-gain pattern of the $\lambda/4$ monopole for the dominant polarization is similar to the butterfly shape pattern in xz-plane [40] (relevant to Fig. 5.11(b)) as also noted in [17, 98].

To illustrate the polarization diversity effect (the changing of G_θ in VP mode to G_ϕ in HP mode), the total-gain patterns in Fig. 5.11 has to separate into the G_θ- and G_ϕ-component patterns as shown in Figs. 5.12(a)–(l). The strong polarization diversity effect is observed in $+x$-direction in both xz- and xy-planes. When compares the patterns in Fig. 5.12(c) to Fig. 5.12(l), it seems that the diversity effect degrades as the phantom is included. The quantitative evaluation of this diversity effect (diversity gain) will be discussed in Sec. 6.4.

5.4.2 Antenna Tilted Angle $\alpha = 60°$

To realize the realistic situation, the antenna on portable telephone is tilted to $\alpha = 60°$ and the results of total-component gain patterns are illustrated in Figs. 5.13(a)–(l). By comparing to Figs. 5.11 the similar trend of the pattern changing from without to with phantom is observed. There are some differences, the patterns are higher in $-y$-direction but more absorbed in $+y$-direction for xy-plane (Fig. 5.13(l)). For xz- and yz-planes (Figs. 5.13(j) and (k)), the patterns of the PDA decrease while they increase for $\lambda/4$ monopole to reach the similar level in $+z$-direction.

With the phantom, the efficiency of monopole is 52.3%, it is 58.2% for VP PDA, and 53.2% for HP PDA. The efficiency improvement of the $\lambda/4$ monopole up to 10% from tilted angle $\alpha = 0°$ to $\alpha = 60°$ is due to the increasing separation distance between the monopole and the head. When the antenna on portable telephone is tilted to $\alpha = 60°$, the polarization diversity effect can still be achieved as illustrated by the component-gain patterns in Figs. 5.14(a)–(l). It is noted that for this orientation, G_ϕ becomes dominant for VP mode while G_θ dominates for HP mode, in $+x$-direction (Figs. 5.14(k) and (l)).

To illustrate the radiation patterns other than only three principle planes, the three-dimensional radiation patterns of G_t in linear scale (as it is more suitable to realize the radiated and absorbed power) are shown in Figs. 5.15(a)–(f). It is obvious that the $\lambda/4$ monopole on portable telephone produces the umbrella-shape pattern (it is similar to butterfly-shape if sectioned in yz-plane, as noted in the previous section) as shown in Fig. 5.15(a). The pattern of VP PDA is similar to that of monopole in $+x$-direction, but it is much smaller in portable telephone ($-x$) direction (Fig. 5.15(c)). The HP PDA produces rather omni-pattern in $+x$-direction (Fig. 5.15(e)). When the phantom is included the radiated power is much absorbed in the phantom direction for all three cases (Figs. 5.15(b), (d), and (f)).

5.5 Experimental Results

To validate the simulation results, PDA on a ground plane, and PDA on conductive telephone box have been fabricated as shown in Fig. 5.16 according to the dimension specified in Fig. 5.5. The set up for input impedance measurement is shown in Fig. 5.18, where the input impedance was measured via S_{11}-parameter using HP8510C *vector network analyzer* (VNA).

The radiation patterns of this antenna were measured via S_{21}-parameter using the same VNA with *angle domain* option in the *opened area test site* (OATS) on the rooftop of the building, the antenna was installed at 2.5m high from the floor, an absorber was installed on the floor between the transmitting antenna (10-dBi-Gain 7-E Yagi-Uda antenna, regarded as quite high polarization purity in the somewhat simple structure) and the *antenna under test* (AUT) to suppress ground reflection as shown in Fig. 5.17. The test range is 5 m. To measure the G_θ, the Yagi-Uda antenna is set in the vertical orientation (the array-axis points to the AUT), whereas, it is set in the horizontal orientation for G_ϕ measurement.

Three cases are chosen to measure the radiation patterns. Firstly, PDA on a ground plane in vertical orientation $\alpha = 0°$, and the results for VP and HP modes are illustrated in Figs. 5.19(a) and (b), respectively. For VP mode (Fig. 5.19(a)), the dominant polarization in x-direction is a linearly vertical polarization, whereas linearly horizontal polarization dominates at $-y$ and $+y$-directions. When the PDA switches to HP mode (Fig. 5.19(b)), there is only one linearly horizontal polarization in all directions. Even though low level of measured G_θ (regarded as cross-polarization for HP mode) exists, it arises due to the spurious radiation from the cable connected between the AUT and the network analyzer.

Secondly, a PDA on portable telephone in vertical orientation $\alpha = 0°$, and the results for VP and HP modes are illustrated in Figs. 5.19(c) and (d), respectively (these results pertinent to Fig. 5.12(c)). The similarity to the previous case can be observed in x-direction, the radiation in $-x$-direction occurs with less than 5 dB to the x-direction. In HP mode (Fig. 5.19(d)), the G_θ significantly increases in with respect to Fig. 5.19(b)

Finally, a PDA on portable telephone at tilted angle $\alpha = 60°$, and the results for VP and HP modes are illustrated in Figs. 5.19(e) and (f), respectively (these results pertinent to Fig. 5.14(c)). By tilting the PDA to $\alpha = 60°$, the dominant polarization interchanges between G_θ and G_ϕ as seen in Fig. 5.19(e) for VP mode (compares with Fig. 5.19(c)), and G_ϕ to G_θ for HP mode (compares with Fig. 5.19(d)), in $+x$-direction. It is noted that other than $+x$-direction, the G_ϕ is always dominant. However, the radiations in these directions do not contribute to the diversity effect due to the absorption from the user's body.

5.6 Concluding Remarks

The wire-grid modeling of polarization diversity PIFA on portable telephone with user's body has been explained and shown the simulation results of current distribution on antenna structure, input impedance, radiation patterns in total- and single-component gain patterns, and the radiation efficiency (in other word, the absorption from user's body) at 1,800 MHz. A $\lambda/4$ monopole antenna under the same condition is set as a reference. Some experimental results of radiation patterns have been depicted to validate to simulation results, and they are in a very good agreement. It it found that the radiation efficiency of the polarization diversity PIFA in both VP and HP modes are higher than that of a $\lambda/4$ monopole antenna. The modeling of all upper parts of the user's body is necessary for the simulation if the three-dimensional pattern is desirable, especially, for further evaluation of diversity performance, or even the communication performance.

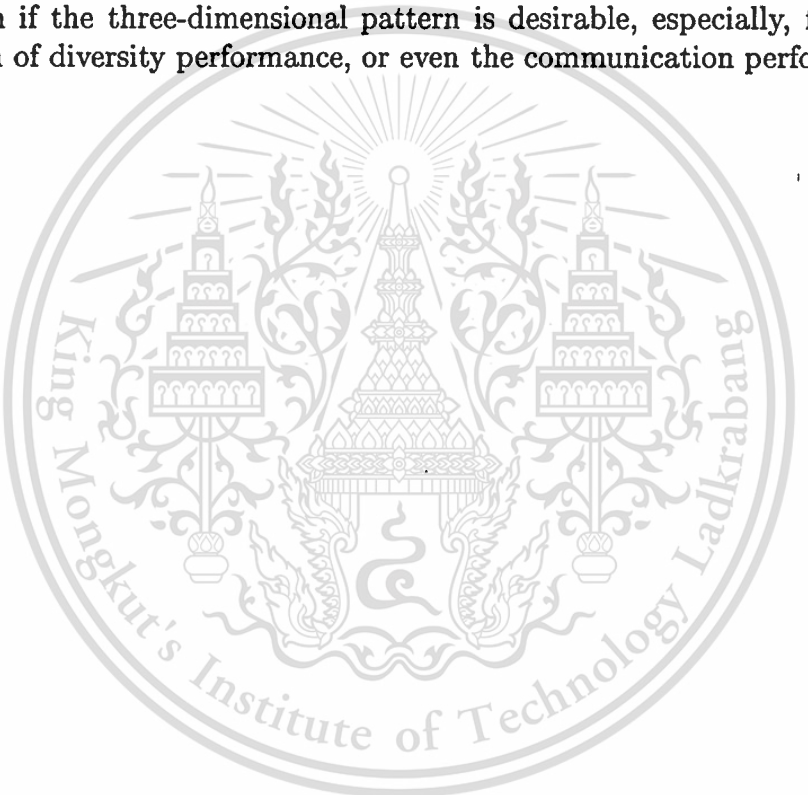

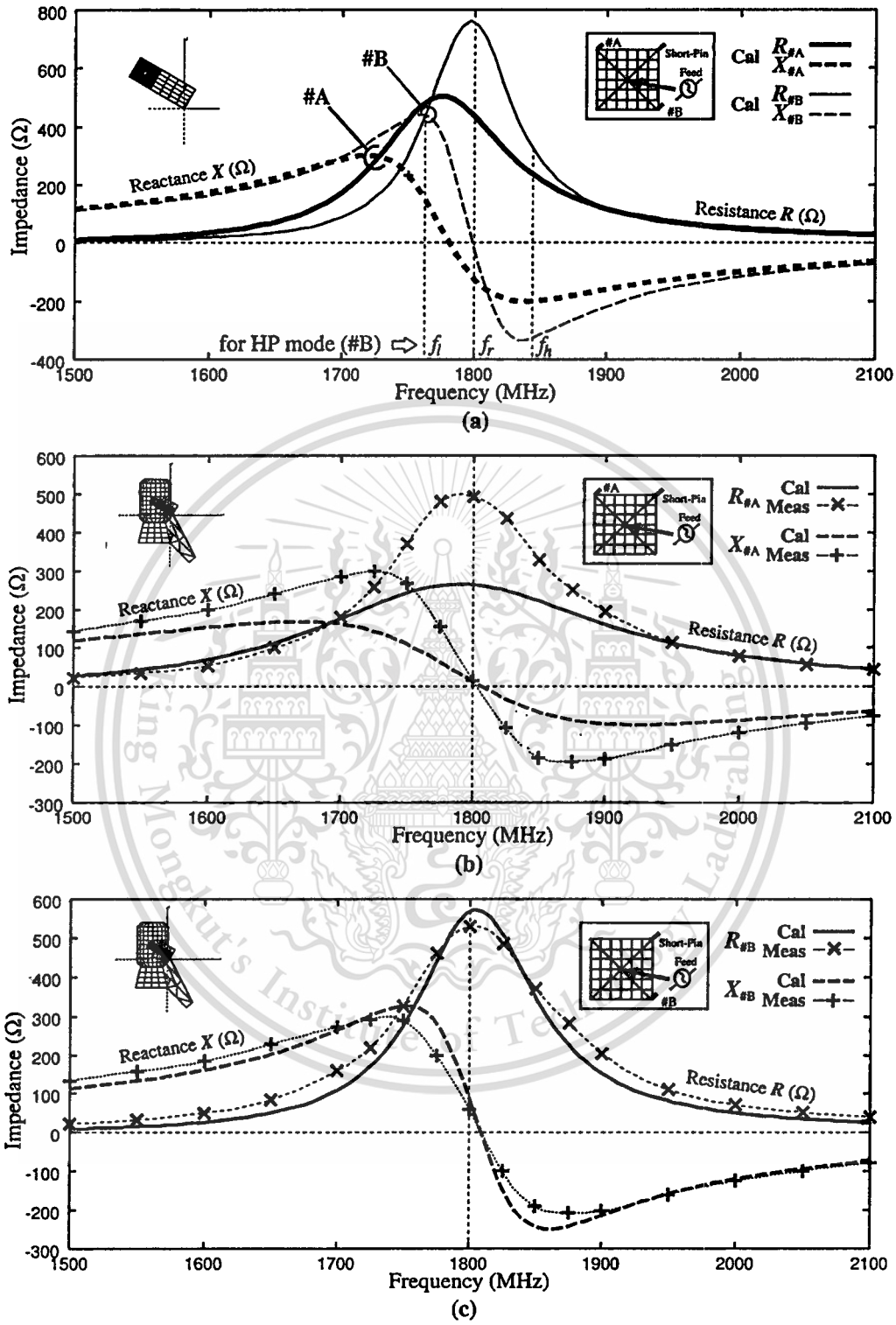

Figure 5.10 Input resistance (R) and reactance (X) of PDA: (a) on handset in VP and HP modes, (b) with human body in VP mode, and (c) with human body in HP mode.

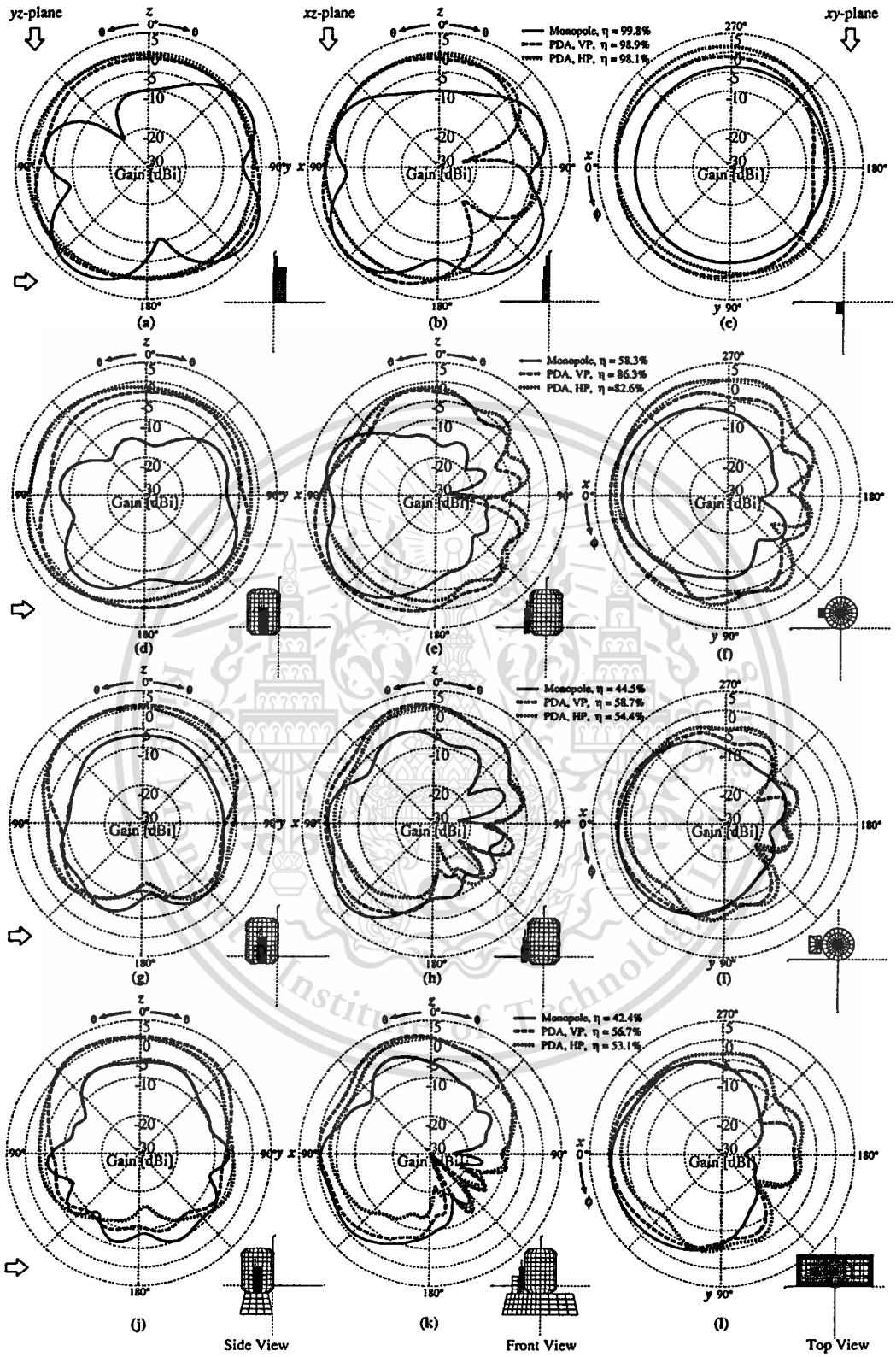

Figure 5.11 The total-gain (G_t) patterns of PDA and monopole at tilted angle $\alpha = 0°$; (a)–(c) on handset; (d)–(f) with head; (g)–(i) with hand and head; (j)–(l) with upper body. η is the radiation efficiency.

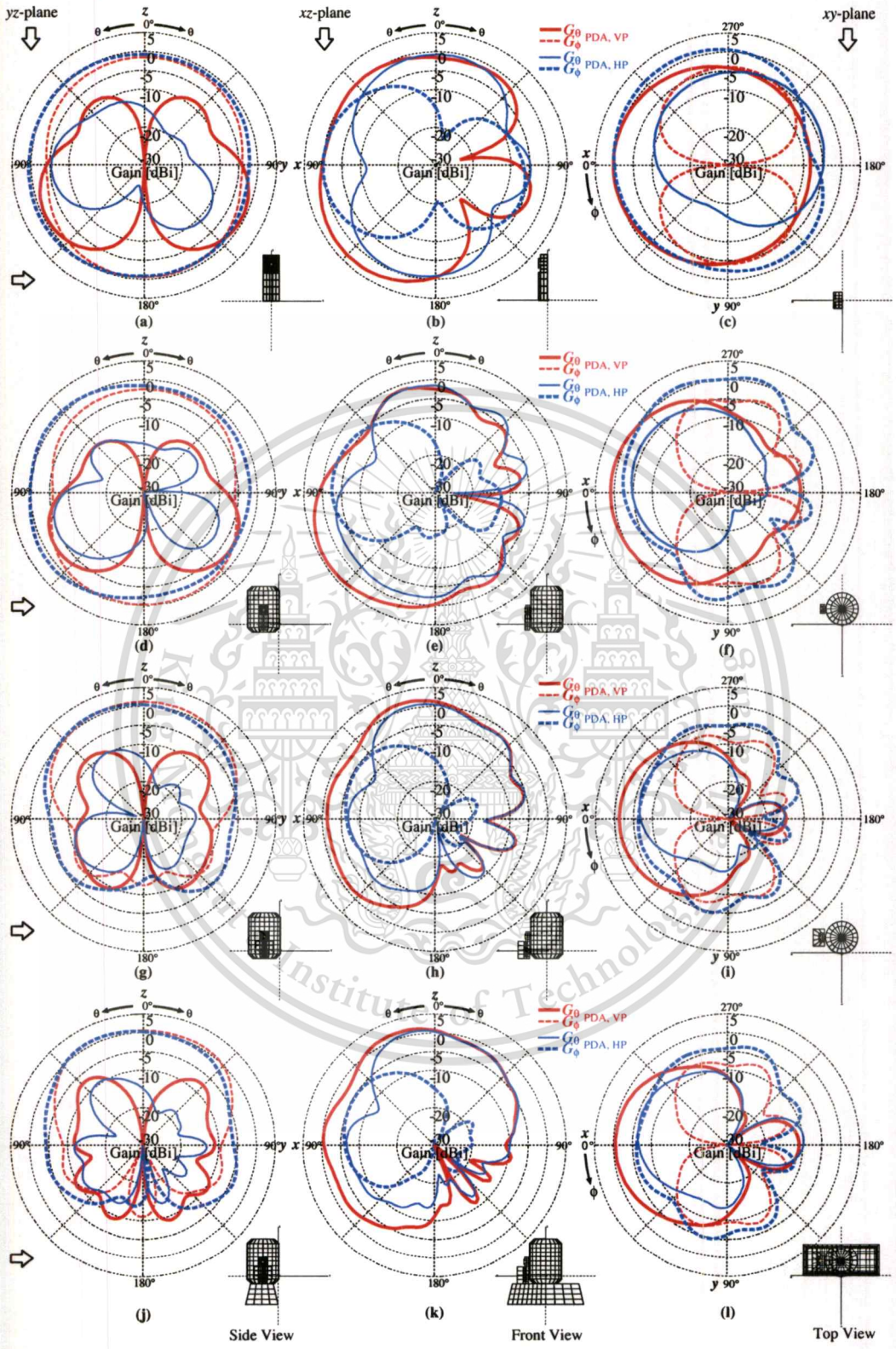

Figure 5.12 The G_θ and G_ϕ patterns of the PDA at tilted angle $\alpha = 0°$; (a)–(c) on handset; (d)–(f) with head; (g)–(i) with hand and head; (j)–(l) with upper body.

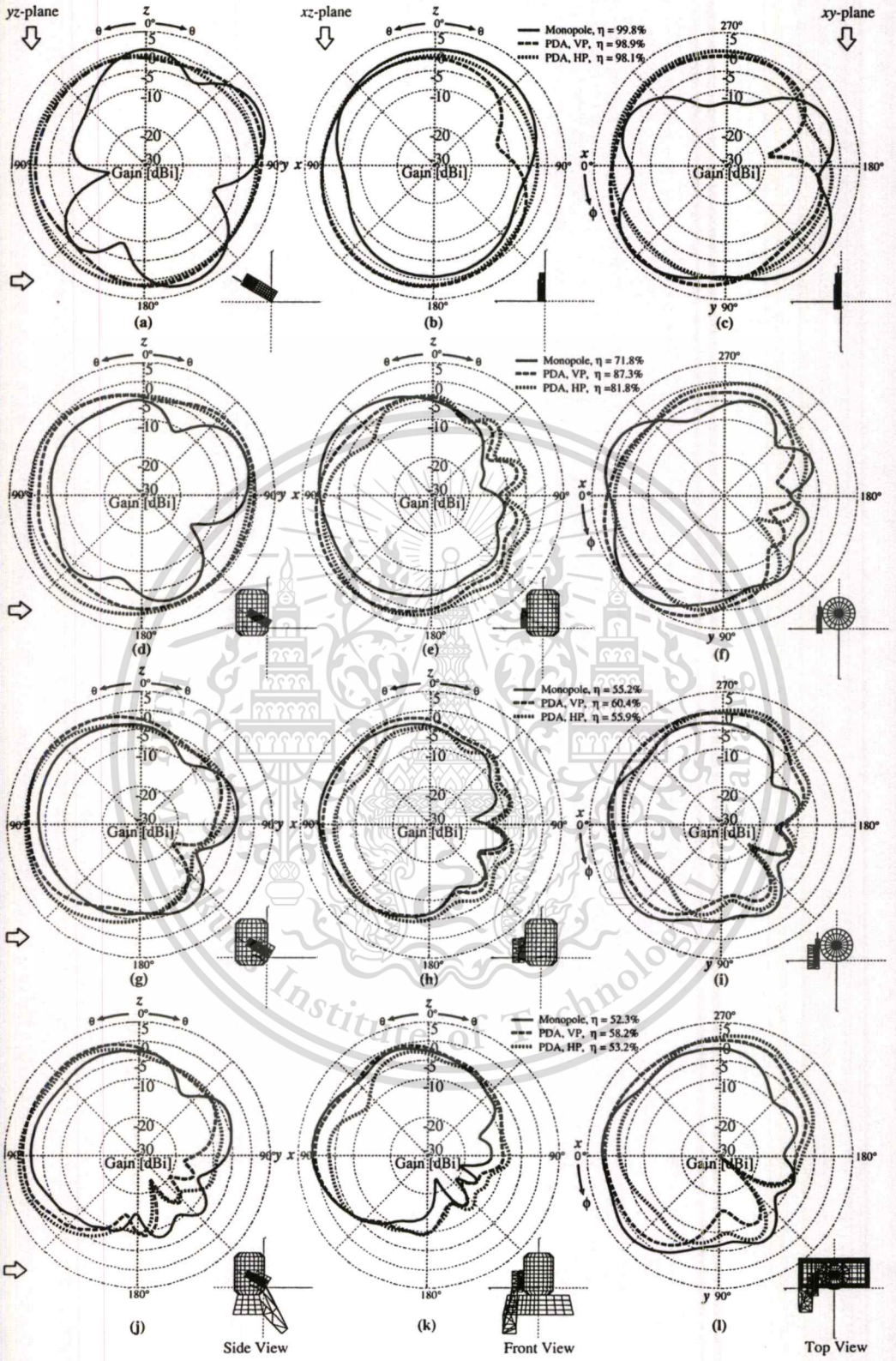

Figure 5.13 The total-gain (G_t) patterns of PDA and monopole at tilted angle $\alpha = 60°$; (a)–(c) on handset; (d)–(f) with head; (g)–(i) with hand and head; (j)–(l) with upper body. η is the radiation efficiency.

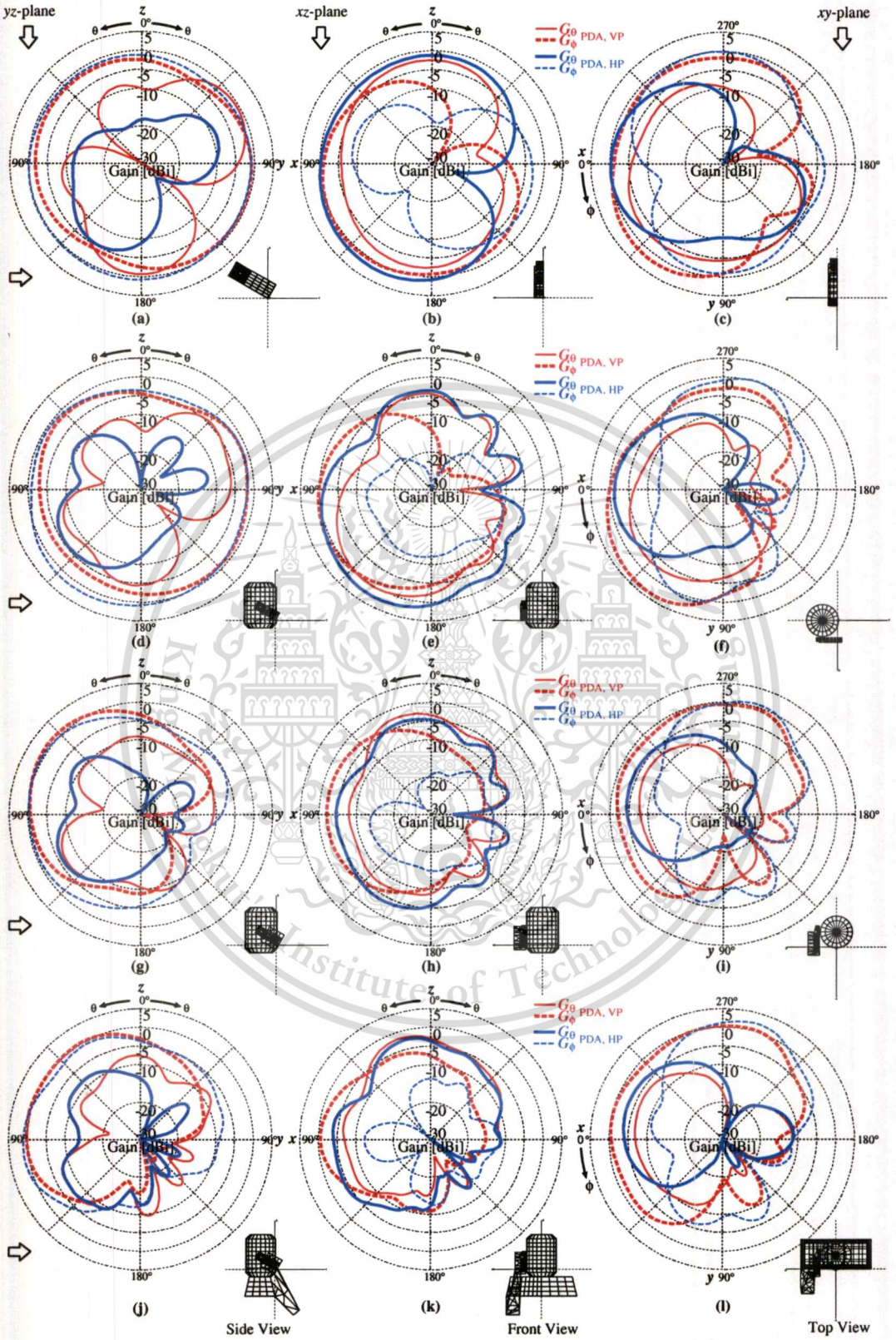

Figure 5.14 The G_θ and G_ϕ patterns of the PDA at tilted angle $\alpha = 60°$; (a)–(c) on handset; (d)–(f) with head; (g)–(i) with hand and head; (j)–(l) with upper body.

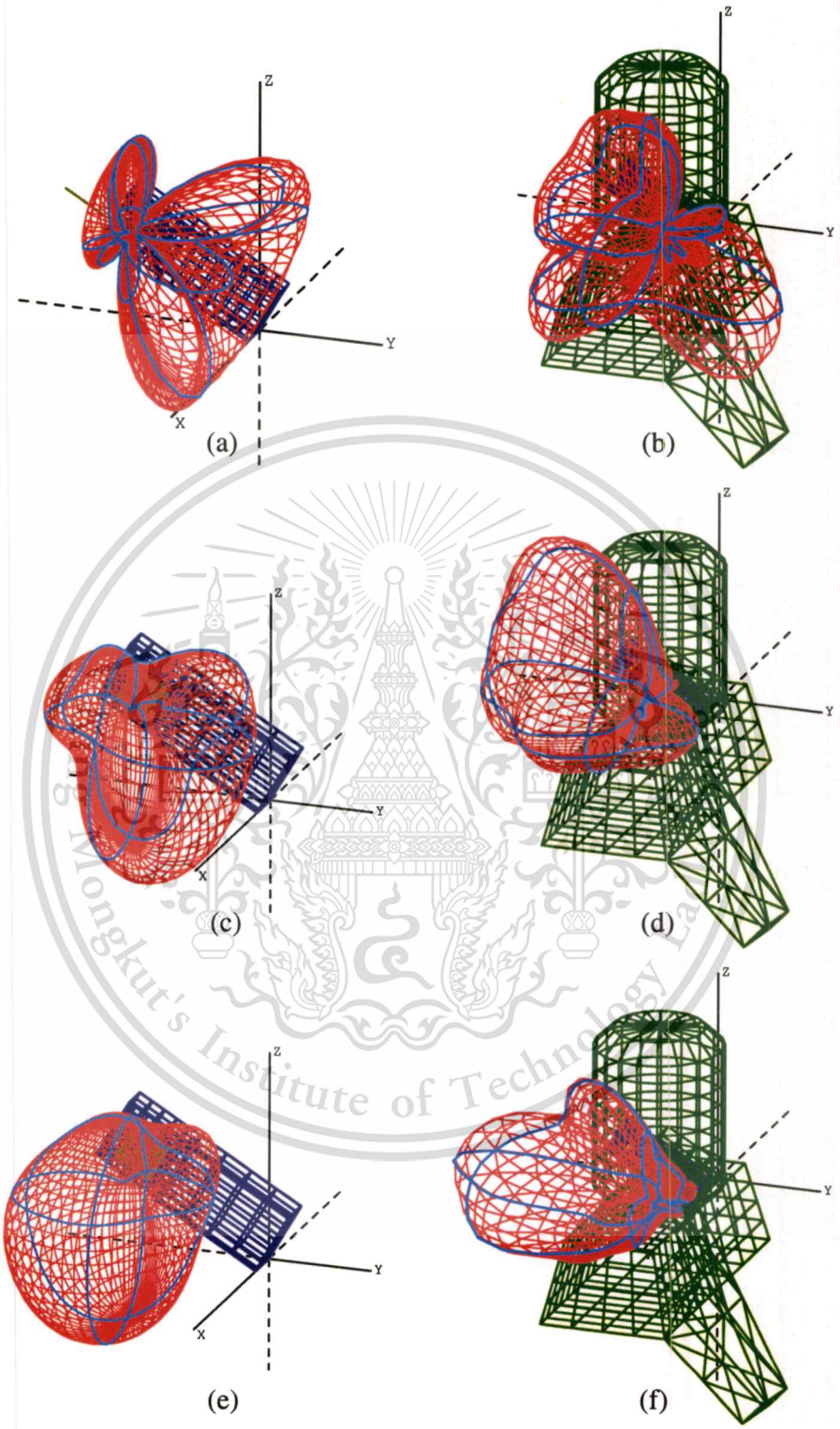

Figure 5.15 The 3D-total-gain (G_t) patterns (*red*, patterns in principle planes shown in *blue*) at antenna tilted angle $\alpha = 60°$ of ; (a) $\lambda/4$ monopole, (b) with upper body; (c) PDA-VP, (d) with upper body; (e) PDA-HP, (f) with upper body (in linear scale).

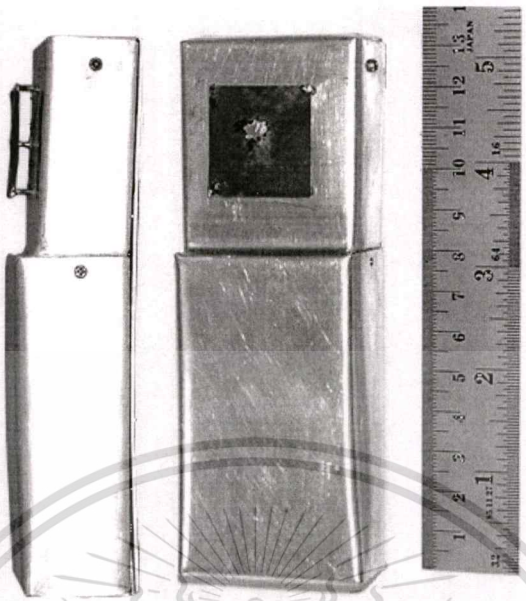

Figure 5.16 Prototype of PDA on handset: (a) side-view, (b) front-view.

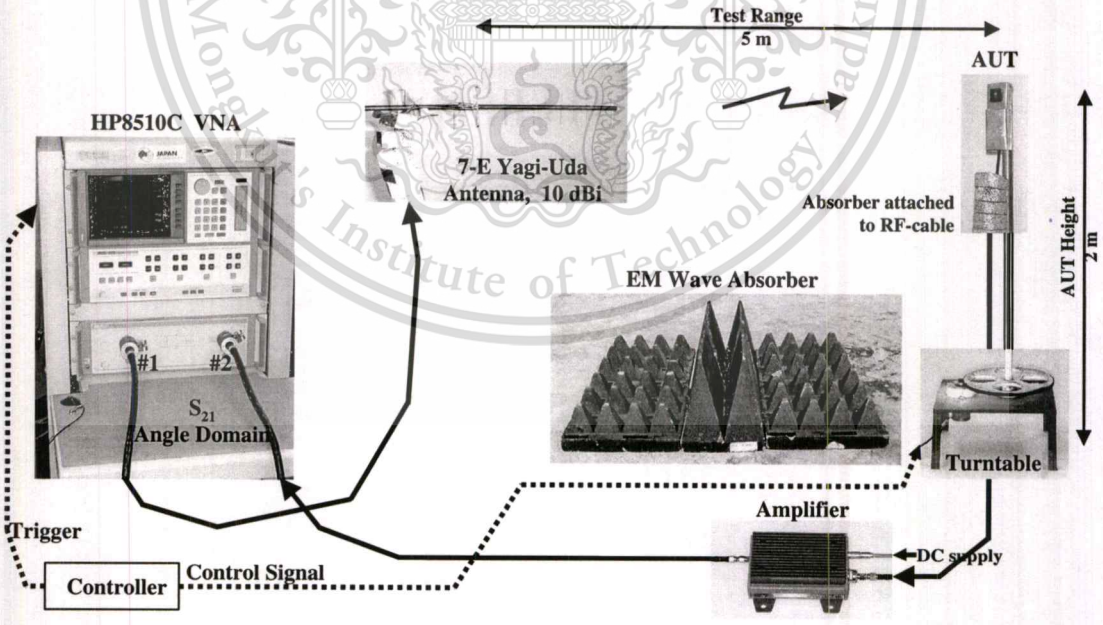

Figure 5.17 Radiation pattern measurement setup on the rooftop of the building.

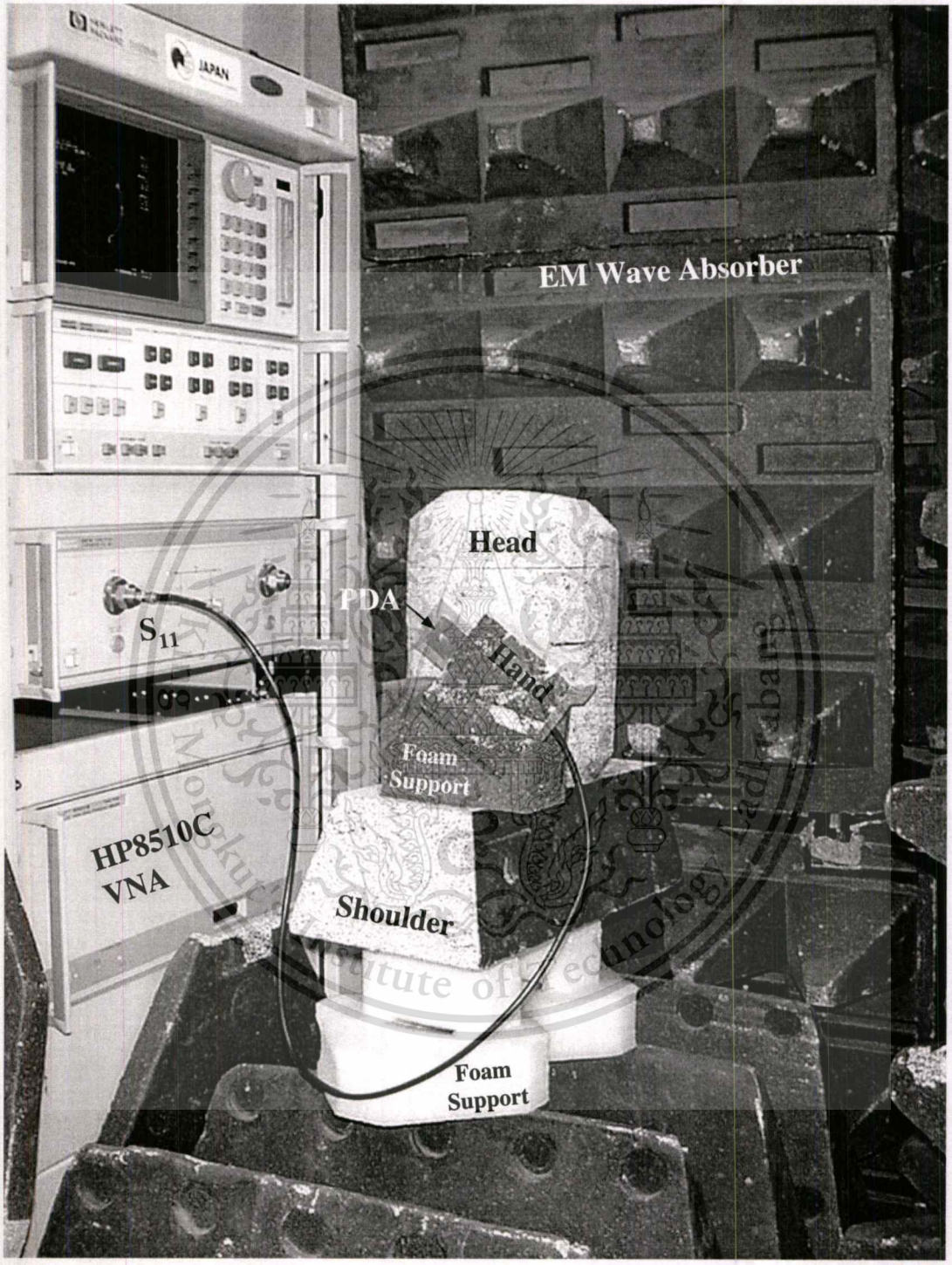

Figure 5.18 Input impedance measurement setup of PDA on handset with human phantom.

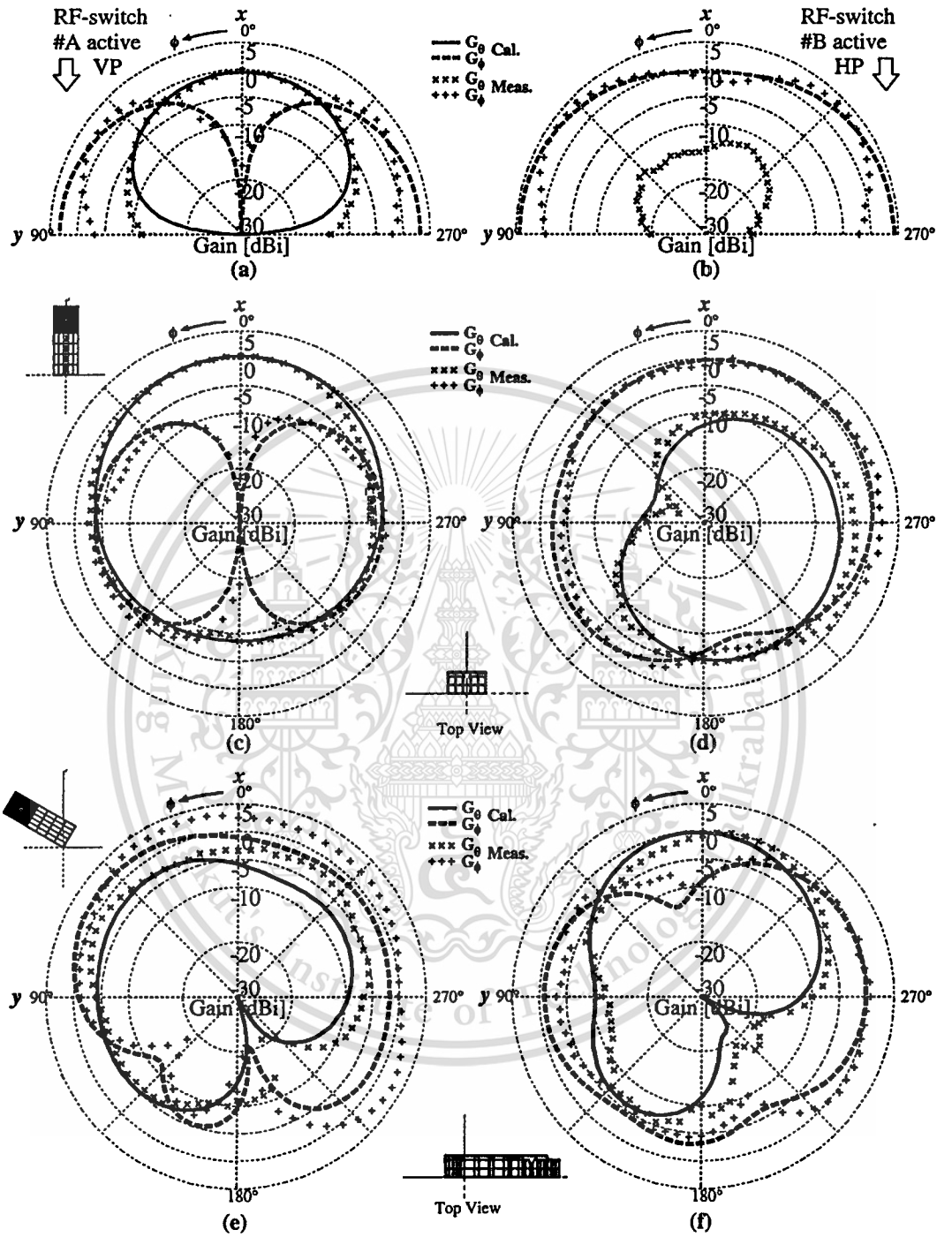

Figure 5.19 The G_θ and G_ϕ patterns, in xy-plane of; the PDA on ground plane at $\alpha = 0°$ (a) VP mode, and (b) HP mode; PDA on handset at $\alpha = 0°$ (c) VP mode, and (d) HP mode; PDA on handset at $\alpha = 60°$ (e) VP mode, and (f) HP mode.

Chapter 6

Antenna Characteristics in Mobile Environment

6.1 Introductory Remarks

As stated in the Introduction that the mobile antennas closely relates with the propagation, system, and environment. Therefore, the results of the PDA in Chap. 5, which consider only the antenna with the user's body, can not be used to judge the performance in mobile environment/system. In practice, the mobile users are not static, they move randomly. However, for the certain mobile environment, it is possible to statistically predicted the propagation characteristics. This thesis adopts the angular probability distribution of incident waves from Taga [61], as explained in Sec. 3.2. This chapter focuses on *macro-cellular* environment in dense urban area where there is NLOS (non line-of-sight). The probability distribution of amplitude of the incident waves are subjected to Rayleigh fading. This propagation model is recognized as the extended-Clarke model.

To combine the signal from two polarization diversity branches, the selection combining scheme is selected to investigate due to the simplicity from the view point of the circuit implementation, however, at the expense of difficulty for the BER evaluation. As the diversity gain is evaluated based on BER, the signal transmission using $\pi/4$-QPSK is chosen. The $\pi/4$-QPSK modulation scheme is one promising candidate for mobile communication due to its tolerance and robustness to the impairment of the signal quality in mobile propagation channel.

The evaluations of the mean effective gain (MEG), correlation coefficient (ρ_e), diversity gain (G_e), and diversity antenna gain (DAG) are based on the expressions explained in Chap. 3. However, the 3D-radiation patterns in Chap. 5 are needed as the fundamental parameters to calculate all of diversity parameters.

6.2 Mean Effective Gain

The XPR range is chosen to cover all possible value from $-10\cdots+10$ dB [61, 70] as a variable parameter for the MEG. The MEG is determined from (3.11). Figure 6.1 illustrates the MEG at antenna tilted angle $\alpha = 0°$, the MEG of PDA for VP mode and a $\lambda/4$ monopole are in the same trend, they increase with respect to the increasing XPR value. Whereas, the MEG is vice versa for the HP PDA. For the case of antenna on handset, it is interesting that at XPR= 2.2 dB the MEG of the PDA both VP and HP modes, and the monopole

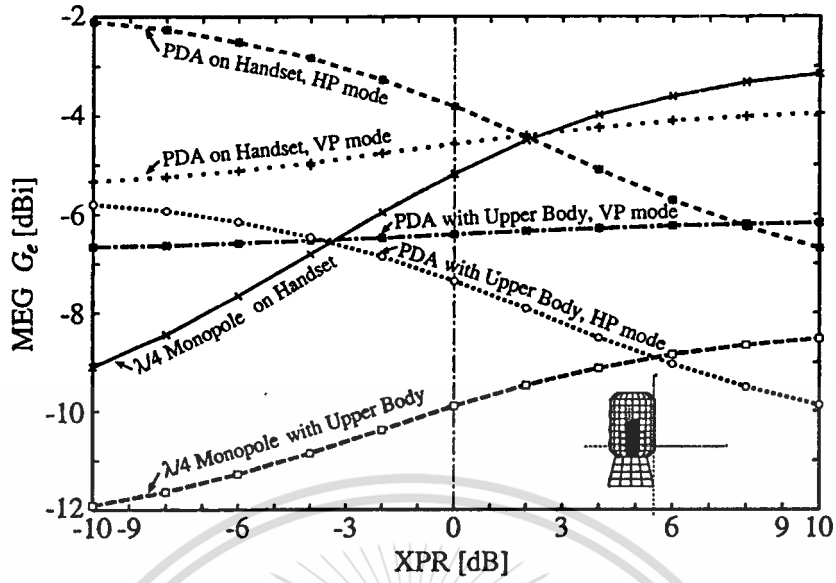

Figure 6.1 The differences of MEG of PDA in VP and HP modes, and $\lambda/4$ monopole vs. XPR, $\alpha = 0°$.

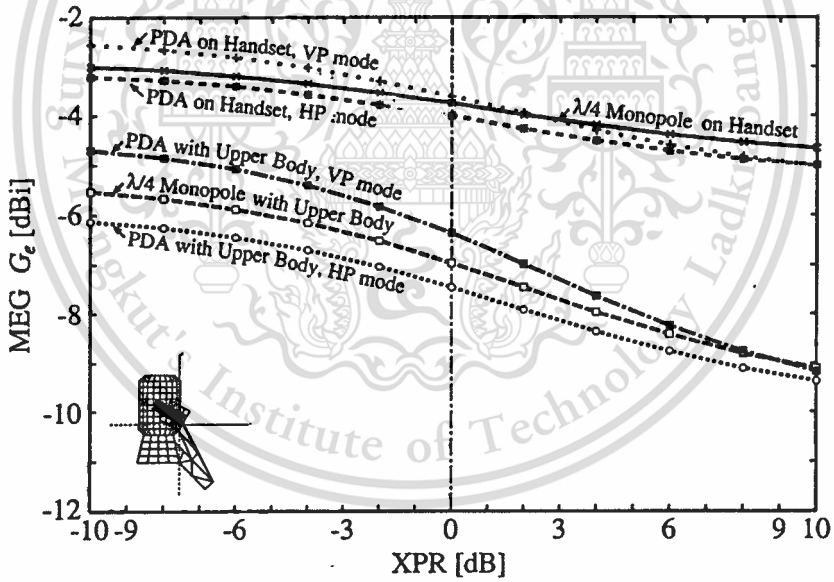

Figure 6.2 The differences of MEG of PDA in VP and HP modes, and $\lambda/4$ monopole vs. XPR, $\alpha = 60°$.

are equal to each other and are equal to -4.5 dBi. At this point, these antenna can receive the same power level. When the user's body is included, the MEG degrade 3 dB on average. The MEG for PDA in VP and HP modes have the cross-point at XPR= -3.5 dB with MEG equals -6.5 dBi. It is found that the MEG of monopole degrades 6.5 dB at XPR= 10 dB, its MEG has the cross-point

with HP PDA at XPR= 5.5 dB with the MEG equals −8.8 dBi.

From Fig. 6.2, the MEG of PDA for both VP and HP modes and monopole on handset are similar and monotonously decrease from $-3\cdots-2.5$ dBi to $-6\cdots-5.6$ dBi with respect to the increasing XPR. When the upper body is included, the MEG of PDA and monopole decrease by 3–4 dB from the previous case and are still in the same trend. The MEG that is degraded by a half is due to the user's body absorption of the radiation patterns in almost half space.

6.3 Correlation Coefficient

Two diversity branches are considered to be uncorrelated if the correlation coefficient is less than 0.5. However, the reasonable improvement for diversity reception (diversity gain) can be achieved with the correlation coefficient of 0.7 [65].

The correlation coefficient is determined from (3.25). For both the case of antenna tilted angle $\alpha = 0°$ and the $\alpha = 60°$ case, as illustrated in Fig. 6.3 and Fig. 6.4, respectively, the correlation coefficient has the very similar trend that it increases to 0.68 if the human body is included. The ρ_e for every case, through all the XPR range, is rather constant and is between 0.32 and 0.66 which is sufficient for practical use. The value of ρ_e in this simulation corresponds to the measurement for the similar structure by Pedersen and Skjaerris [99]. It may be concluded that the correlation coefficient is almost independent to the antenna tilted angle as well as the XPR value. And the existence of the user's body raise the correlation coefficient for 0.2, approximately.

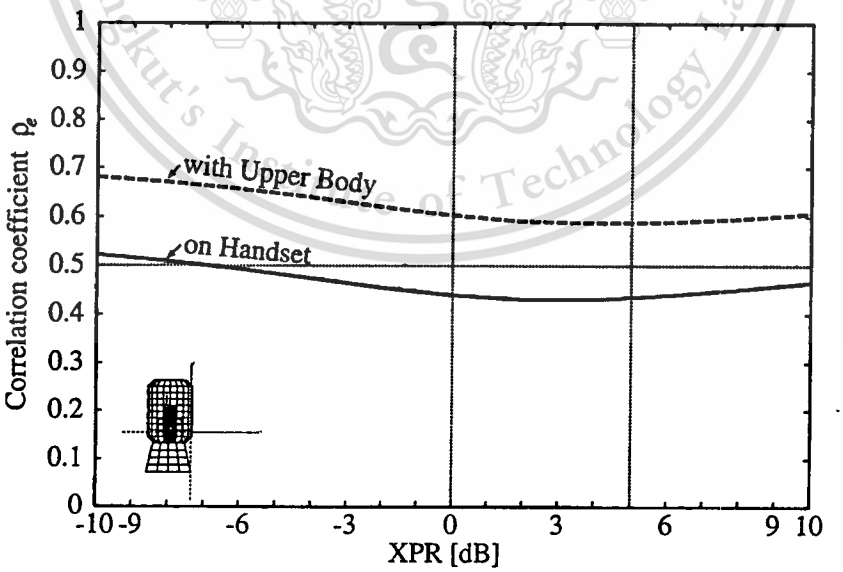

Figure 6.3 The differences of correlation coefficient ρ_e of PDA vs. XPR, $\alpha = 0°$.

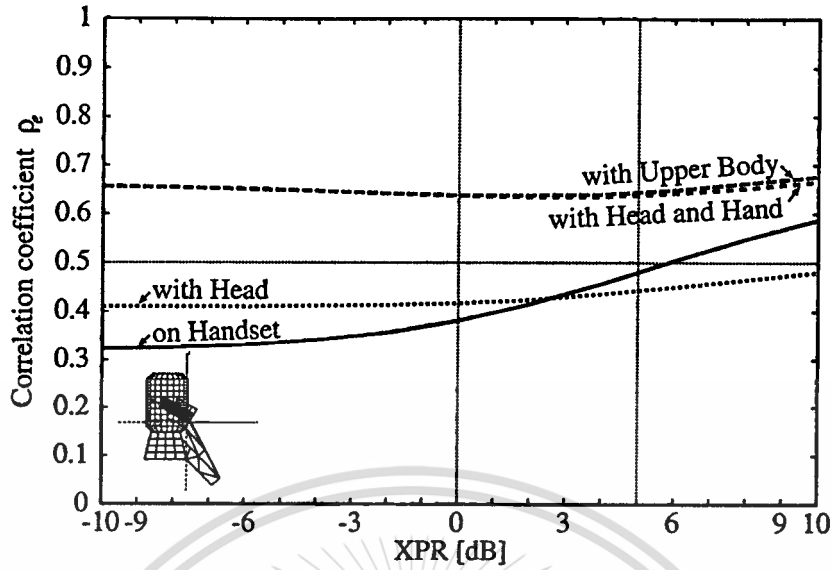

Figure 6.4 The differences of correlation coefficient ρ_e of PDA vs. XPR, $\alpha = 60°$.

6.4 Diversity Gain

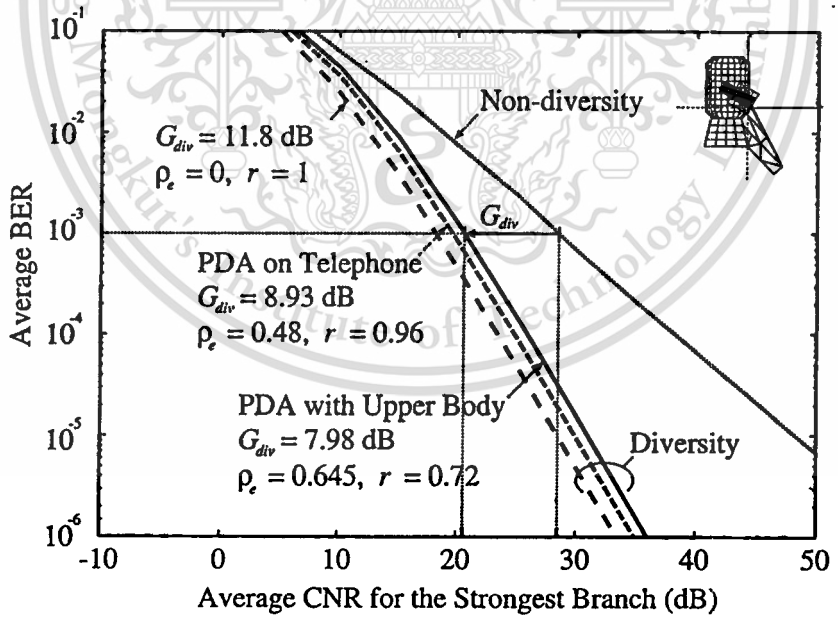

Figure 6.5 Diversity gain differences of PDA due to ρ_e and r at XPR = 5 dB, $\alpha = 60°$.

The diversity gain of PDA is determined from the MEG differences between VP and HP modes and the correlation coefficient. Quantitatively, the diversity

gain is determined from (3.27) and (3.28). To show the received average BER improvement from the non-diversity (single antenna) reception, Fig. 6.5 depicts diversity gain at 10^{-3} BER. The maximum diversity gain for two uncorrelated channels ($\rho_e = 0$) and equal MEG ($r = 1$) is 11.8 dB. The diversity gain with respect to the XPR is rather constant for both cases ($\alpha = 0°, 60°$) as shown in Fig. 6.6 and Fig. 6.7. When including the human body, the diversity gain is approximately 1 dB degraded to about 6.6–8.0 dB.

6.5 Diversity Antenna Gain

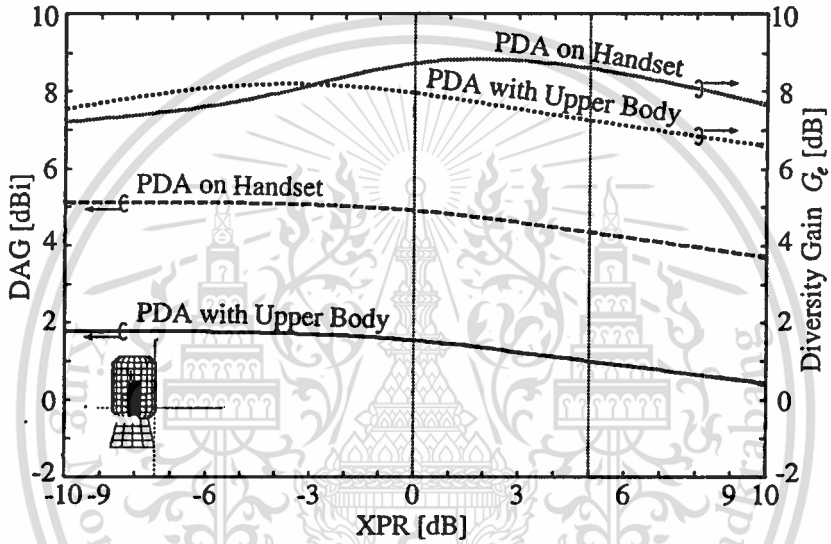

Figure 6.6 Diversity antenna gain and diversity gain of PDA vs. XPR, $\alpha = 0°$.

The DAG of PDA including human body at $\alpha = 0°$ is degraded 3.3 dB below the PDA on handset case. It is 1.8–0.4 dBi with respect to the increasing XPR from −10 dB as shown in Fig. 6.6.

For $\alpha = 60°$, the DAG of PDA including human body is approximately degraded 3.8–4.7 dB below the PDA on handset case. It is $2.8 \cdots -1.2$ dBi with respect to the increasing XPR from −10 dB as shown in Fig. 6.7. Ogawa [74] investigated the selection combining diversity between PIFA and $\lambda/4$ monopole branches at 900 MHz under the similar condition, the DAG of 3 dBi was achieved.

6.6 Concluding Remarks

To conclude about the results of each diversity parameter, the MEG for $\alpha = 0°$ of the PDA in VP and HP modes is similar to the $\lambda/4$ monopole and it is sensitive to the antenna tilted angle. However, the MEG always degrades 3 dB when the user's body is included. The correlation coefficient is almost independent to

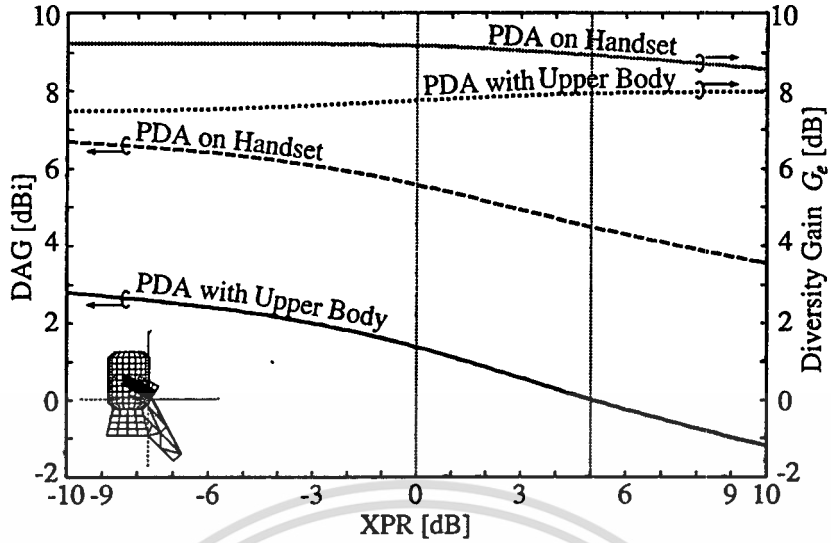

Figure 6.7 Diversity antenna gain and diversity gain of PDA vs. XPR, $\alpha = 60°$.

XPR value as well as antenna tilted angle. The inclusion of the user's body raise the correlation coefficient for 0.2 to approximately 0.7, it is still in the acceptable value to produce the meaningful diversity effect.

The diversity gain is also almost independent to XPR value and antenna tilted angle, as the correlation coefficient is. The average diversity gain for all cases is approximately 7.0 dB. The DAG has the similar characteristics to the MEG for $\alpha = 60°$. It degrades approximately 3–4 dB when the human body is included.

Chapter 7

Conclusions

This thesis reports the intensive investigation of the polarization diversity planar inverted-F antenna on portable telephone including the user's body interaction. The diversity performance is revealed via diversity antenna gain. It is found that the diversity antenna gain degrades for 4 dB when user's body is taken into account. The handset orientation effects to the diversity antenna gain at a certain degree (1.5 dB maximum difference).

This chapter gives brief synopses of all preceding chapters, as well as the remarks for the further research work on the context of polarization diversity planar inverted-F antenna or related.

7.1 Summary of Preceding Chapters

The necessity of antennas in wireless communications, especially, land mobile cellular systems, is stated in Chap. 1. Mobile antennas are considered closely related to system and propagation environment, it is hence impractical to solely design and analyze the antenna in isolation. As the mobile terminal equipment has been gradually miniaturized since the invention of the mobile system, the antenna attached to this equipment has to also be developed to fit with.

Chapter 2 describes the fundamental of the mobile propagation, the inherent problems, e.g., multipath fading and time-delay spread. And the polarization diversity techniques with selection combining scheme is suggested to combat the multipath fading. To correctly investigate the diversity effect of diversity antenna, expressions of mobile antenna performance, i.e., angular distribution model of incident waves, mean effective gain, correlation characteristics, diversity gain, and diversity antenna gain are explained in Chap. 3.

The methodology for the simulation are outlined in Chap. 4. The canonical examples relevant to the problem of interest are scrutinized. The know-how obtained in this chapter is effectively utilized as the guidelines for the simulation in Chap. 5. As the results of radiation patterns of the polarization diversity PIFA on portable telephone with user's body are obtained, the polarization diversity effect can be observed, it is nevertheless unable to indicate the quantity of the diversity effect. From the results in Chap. 5, they are manipulated to render the diversity parameters, i.e., mean effective gain, correlation coefficient, diversity gain, and diversity antenna gain. The diversity performance is self-compared for the different antenna tilted angles or for the inclusion of different parts of user's body.

7.2 Remarks for Future Studies

The design optimization of the antenna dimension on portable telephone with user's body has not been studied, since this thesis mainly focuses on the method to evaluate the diversity antenna performance. This method can be applied to any sorts of portable mobile diversity antenna. Therefore, the antenna dimension optimization as well as feed-position optimization for input impedance matching is left opened for the further research work on the context of polarization diversity PIFA. The excellent guidelines for small antenna optimization can be found in [90, 100].

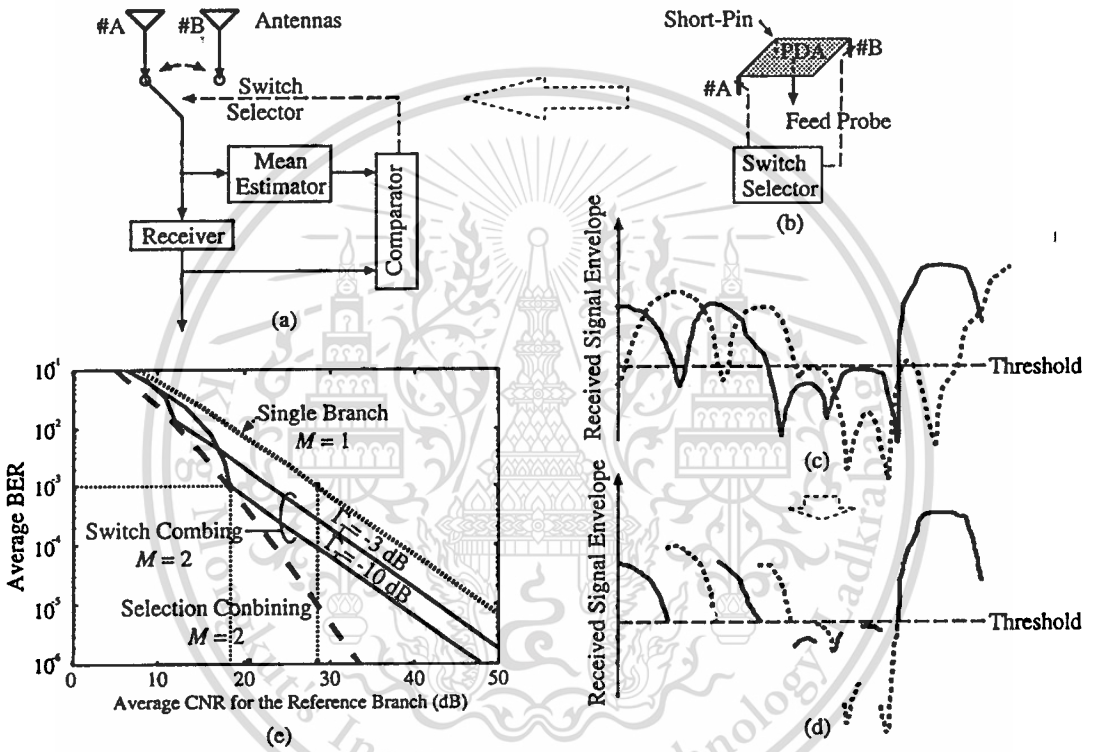

Figure 7.1 Switch-and-stay diversity scheme: (a) circuit diagram, (b) applied to the PDA, (c) received signal envelope of each diversity branch (d) received signal envelope after switch-and-stay combining diversity, and (e) typical CDF of average BER.

To make the selection combining diversity feasible for circuit implementation, the more practical subtypes of selection combining—*switch-and-stay* combining diversity with *delayed detection*, or *switch-and-examine* combining diversity—should be introduced as shown in Fig. 7.1. However, the theoretical analysis in Chaps. 3 and 6, the performance of selection combining may be used to consider as the lower-bound for switch combining with any threshold levels. More details concern with the circuit implementation of switch combining can be found in [66].

The conditional BER expression for other types of modulation techniques (e.g. Gaussian Minimum Shift Keying (GMSK) in Global System for Mobile (GSM), or 8PSK in Time Division-Synchronous Code Division Multiple Access (TD-SCDMA)) may be needed and can be found in [77] if one want to analyze performance of the diversity antenna in different mobile systems. However, the wideband channel model may be necessary for considering the performance of modern mobile communications systems, which are much different from the traditional narrowband systems.

REFERENCES

[1] D. L. Schilling, "Wireless communications going into the 21st century," *IEEE Trans. Veh. Technol.*, vol. 43, no. 3, pp. 645–652, Aug. 1994.

[2] S. Urabe and T. Nojima, "Developments in mobile/portable telephones and key devives for miniaturization," *IEICE Trans. Electron.*, vol. E79-C, no. 5, pp. 600–605, May 1996.

[3] K. Fujimoto, "Overview of antenna systems for mobile communications and prospects for the future technology," *IEICE Trans.*, vol. E-74, no. 10, pp. 3191–3201, Oct. 1991.

[4] P. Keowsawat, K. Meksamoot, and M. Krairiksh, "Performance of a bi-directional polarization diversity antenna using two-perpendicular-probe excited square ring for PCS base station," *Proc. 3rd Int. Symp. Wireless Personal Multimedia Commun.*, Bangkok, Thailand, vol. 1, pp. 306–310, Nov. 2000.

[5] P. Keowsawat, K. Meksamoot, M. Krairiksh, and S. Kosulvit, "The DAG investigation of bi-directional antenna using two-perpendicular-probe excited circular ring for polarization diversity," *Proc. 2000 Asia-Pacific Symp. Broadcasting and Commun.*, Bangkok, Thailand, pp. 268–273, Dec. 2000.

[6] S. Kosulvit, M. Krairiksh, C. Phongcharoenpanich, and T. Wakabayashi, "A simple and cost-effective bidirectional antenna using a probe excited circular ring," *IEICE Trans. Electron.*, vol. E84-C, no. 4, pp. 443–449, Apr. 2001.

[7] S. Kozono, T. Tsuruhara, and M. Sakamoto, "Base station polarization diversity reception for mobile radio," *IEEE Trans. Veh. Technol.*, vol. VT-33, no. 4, pp. 301–306, Nov. 1984.

[8] B. Lindmark and M. Nilsson, "Polarization diversity gain and base station antenna characteristics," *Proc. 49th IEEE Veh. Technol. Conf.*, Houston, Texus, USA, pp. 590–595, May 1999.

[9] R. Vargas, Jr., E. B. Victor, and K. R. Baker, "Polarization diversity for indoor cellular and PCS CDMA reception," *Proc. 47th IEEE Veh. Technol. Conf.*, Phoenix, Arizona, USA, pp. 1014–1018, May 1997.

[10] J. Weitzen and M. Wallace, "Analysis of diversity performance of space diversity and cross polarization for PCS base stations," *Proc. 9th IEEE Int.*

Symp. Personal, Indoor and Mobile Radio Comm., Boston, Massachusetts, USA, vol. 1, pp. 293–297, Sept. 1998.

[11] M. Krairiksh, C. Phongcharoenpanich, K. Meksamoot, and J. Takada, "A circularly polarized conical beam spherical slot array antenna," *Int. J. Electron.*, vol. 86, no. 7, pp. 815–823, July 1999.

[12] N. Kuga, H. Arai, and N. Goto, "A notch-wire composite antenna for polarization diversity reception," *IEEE Trans. Antennas Propagat.*, vol. 46, no. 6, pp. 902–906, June 1998.

[13] K. Fujimoto and J. R. James, *Mobile Antenna Systems Handbook*, Artech House, Norwood, MA, 1994.

[14] M. Ali, M. Okoniewski, M. A. Stuchly, and S. S. Stuchly, "Dual-frequency strip-sleeve monopole for laptop computers," *IEEE Trans. Antennas Propagat.*, vol. 47, no. 2, pp. 317–323, Feb. 1999.

[15] Q. Balzano, O. Garay, and T. J. Manning Jr., "Electromagnetic energy exposure of simulated users of portable cellular telephones," *IEEE Trans. Veh. Technol.*, vol. 44, no. 3, pp. 390–403, Aug. 1995.

[16] M. A. Jansen and Y. Rahmat-Samii, "The electromagnetic interaction between biological tissue and antennas on a transceiver handset," *IEEE Antennas Propagat. Soc. Int. Symp. Dig.*, USA, vol. 1, pp. 367–370, 1994.

[17] M. A. Jansen and Y. Rahmat-Samii, "Performance analysis of antennas for hand-held transceivers using FDTD," *IEEE Trans. Antennas Propagat.*, vol. 42, no. 8, pp. 1106–1113, Aug. 1994.

[18] J. Toftgård, S. Hornsleth, and J. B. Anderson, "Effects on portable antennas of the presence of a person," *IEEE Trans. Antennas Propagat.*, vol. 41, no. 6, pp. 739–746, June 1993.

[19] K. D. Katsibas, C. A. Balanis, P. A. Tirkas, and C. R. Birtcher, "Folded loop antenna for mobile hand-held units," *IEEE Trans. Antennas Propagat.*, vol. 46, no. 2, pp. 260–266, Feb. 1998.

[20] M. Muramoto, N. Ishii, and K. Itoh, "Characteristics of a small planar loop antenna," *IEEE Trans. Antennas Propagat.*, vol. 45, no. 12, pp. 1818–1822, Dec. 1998.

[21] A. Ando, Y. Honma, and K. Kagoshima, "A novel electromagnetically coupled microstrip antenna with a rotatable patch for personal handy-phone system units," *IEEE Trans. Antennas Propagat.*, vol. 46, no. 6, pp. 794–797, June 1998.

[22] N. Herscovici, "New considerations in the design of microstrip antennas," *IEEE Trans. Antennas Propagat.*, vol. 46, no. 6, pp. 807–812, June 1998.

[23] J. T. Rowley and R. B. Waterhouse, "Performance of shorted microstrip patch antennas for mobile communications handsets at 1800 MHz," *IEEE Trans. Antennas Propagat.*, vol. 47, no. 5, pp. 815–822, May 1999.

[24] J. Y. Sze and K. L. Wong, "Slotted rectangular microstrip antenna for bandwidth enhancement," *IEEE Trans. Antennas Propagat.*, vol. 48, no. 8, pp. 1149–1152, Aug. 2000.

[25] T. Amano, N. Chiba, and H. Iwasaki, "A quarter-wavelength shorted microstrip antenna with a slot for dual-frequency operation,". *IEICE Trans. Electron.*, vol. E82-C, no. 7, pp. 1211–1216, July 1999.

[26] Z. D. Liu, P. S. Hall, and D. Wake, "Dual-frequency planar inverted-F antenna," *IEEE Trans. Antennas Propagat.*, vol. 45, no. 10, pp. 1451–1458, Oct. 1997.

[27] T. K. Lo and Y. Hwang, "Bandwidth enhancement of PIFA loaded with very high permitivity material using FDTD," *IEEE Antennas Propagat. Soc. Int. Symp. Dig.*, Atlanta, Georgia, USA, vol. 2, pp. 798–801, June 1998.

[28] H. Nakano, R. Suzuki, and J. Yamauchi, "Low-profile inverted-F antenna with parasitic elements on an infinite ground plane," *IEE Proc.-Microw. Antennas Propagat.*, vol. 145, no. 4, pp. 321–325, Aug. 1998.

[29] N. Odachi, S. Sekine, H. Shoki, and Y. Suzuki, "A novel analytical method for optimizing the terminating impedance of an inverted-F antenna for antenna selection diversity on a hand-held phone," *IEICE Trans. Commun.*, vol. E84-B, no. 1, pp. 89–94, Jan. 2001.

[30] S. G. Pan, T. Becks, A. Bahrwas, and I. Wolff, "N antennas and their applications in portable handsets," *IEEE Trans. Antennas Propagat.*, vol. 45, no. 10, pp. 1475–1483, Oct. 1997.

[31] P. K. Panayi, M. Al-nuaimi, and L. P. Ivrissimtzis, "Tuning techniques for the planar inverted-F antenna," *Proc. 1999 IEE Nat. Conf. Antennas Propagat.*, UK, pp. 259–262, Mar.–Apr. 1999.

[32] C. R. Rowell and R. D. Murch, "A capacitively loaded PIFA for compact mobile telephone handsets," *IEEE Trans. Antennas Propagat.*, vol. 45, no. 5, pp. 837–842, May 1997.

[33] T. Taga and K. Tsunekawa, "Performance analysis of a built-in planar inverted-F antenna for 800 MHz band portable radio units," *IEEE J. Select. Areas Commun.*, vol. SAC-5, no. 5, pp. 921–929, June 1987.

[34] M. S. Tong, M. Yang, Y. Chen, and R. Mittra, "Finite-difference time-domain analysis of a stacked dual-frequency microstrip planar inverted-F

antenna for mobile telephone handsets," *IEEE Trans. Antennas Propagat.*, vol. 49, no. 3, pp. 367–376, Mar. 2001.

[35] K. Meksamoot, M. Krairiksh, and J. Takada, "Polarization diversity PIFA for small portable telephone," *Proc. 1st Int. Symp. Wireless Personal Multimedia Commun.*, Yokosuka, Japan, pp. 304–307, Nov. 1998.

[36] K. Meksamoot, M. Krairiksh, and J. Takada, "Polarization diversity planar inverted-F antenna and its performance in multipath environment," *Proc. 1999 IEEE Int. Symp. Intelligent Signal Processing and Commun. Syst.*, Phuket, Thailand, pp. 709–712, Dec. 1999.

[37] K. Meksamoot, M. Krairiksh, and J. Takada, "Performance of polarization diversity PIFA on portable telephone in multipath environment," *Proc. 1999 Thailand-Japan Joint Symp. Microwaves*, Pattaya, Thailand, pp. 69–75, Sept. 1999.

[38] K. Meksamoot, M. Krairiksh, and J. Takada, "Evaluation of polarization diversity PIFA on portable telephone in multipath environment," *Proc. AP2000 Millennium Conf. Antennas Propagat.*, Davos, Switzerland, vol. 1, p. 362, Apr. 2000.

[39] K. Meksamoot, M. Krairiksh, and J. Takada, "Effect of human interaction on diversity performance of polarization diversity PIFA on portable telephone," *Proc. 2000 Int. Symp. Antennas Propagat.*, Fukuoka, Japan, vol. 3, pp. 1067–1070, Aug. 2000.

[40] K. Meksamoot, M. Krairiksh, and J. Takada, "A Polarization Diversity PIFA on Portable Telephone and the Human Body Effects on Its Performance," *IEICE Trans. Commun.*, vol. E84-B, no. 9, pp. 2460–2467, Sept. 2001.

[41] T. S. Rappaport, *Wireless Communications Principles & Practice*, Prentice Hall PTR, Upper Saddle River, New Jersey, 1996.

[42] M. Hata, "Empirical formula for propagation loss in land mobile radio services," *IEEE Trans. Veh. Technol.*, vol. VT-29, no. 3, pp. 317–325, Aug. 1980.

[43] T. S. Rappaport and C. D. Mcgillem, "UHF fading in factories," *IEEE Trans. Commun.*, vol. 7, no. 1, pp. 40–48, Jan. 1989.

[44] H. H. Xai, H. L. Bertoni, and L. R. Maciel, "Microcellular propagation characteristics for personal communications in urban and suburban environments," *IEEE Trans. Veh. Technol.*, vol. 43, no. 3, pp. 743–752, Aug. 1994.

[45] N. C. Gonçalves and L. M. Correia, "A propagation model for urban microcellular systems at the UHF band," *IEEE Trans. Veh. Technol.*, vol. 49, no. 4, pp. 1294–1302, July 2000.

[46] M. A. Taneda, J. Takada, and K. Araki, "The problem of the fading model selection," *IEICE Trans. Commun.*, vol. E84-B, no. 3, pp. 660–666, Mar. 2001.

[47] M. K. Simon and M. S. Alouini, "A unified approach to performance analysis of digital communication over generalized fading channels," *Proc. IEEE*, vol. 86, no. 9, pp. 1860–1876, Sept. 1998.

[48] R. Steele, *Mobile Radio Communications*, Pentech Press, New York, 1992.

[49] J. H. Winters, J. Salz, and R. G. Gitlin, "The impact of antenna diversity on the capacity of wireless communication systems," *IEEE Trans. Commun.*, vol. 42, no. 2–4, pp. 1740–1751, Feb.–Apr. 1994.

[50] K. Tsunekawa and A. Ando, "Advanced wire grid method for solving the scattered field of a lossy dielectric object," *IEEE Antennas Propagat. Soc. Int. Symp. Dig.*, USA, vol. 2, pp. 797–800, July 1992.

[51] J. D. Parsons, M. Henze, P. A. Ratliff, and M. J. Withers, "Diversity techniques for mobile radio reception," *IEEE Trans. Veh. Technol.*, vol. VT-25, no. 3, pp. 75–84, Aug. 1976.

[52] R. G. Vaughan and J. B. Andersen, "Antenna diversity in mobile communications," *IEEE Trans. Veh. Technol.*, vol. VT-36, no. 4, pp. 149–172, Nov. 1987.

[53] Y. Yamada, K. Kagoshima and K. Tsunekawa, "Diversity antennas for base and mobile stations in land mobile communication systems," *IEICE Trans.*, vol. E-74, no. 10, pp. 3202–3209, Oct. 1991.

[54] K. Cho, T. Hori, and K. Kagoshima, "Effectiveness of four-branch height and polarization diversity configuration for street microcell," *IEEE Trans. Antennas Propagat.*, vol. 46, no. 6, pp. 776–781, June 1998.

[55] K. H. Awadalla, "Direction diversity in mobile communications," *IEEE Trans. Veh. Technol.*, vol. VT-30, no. 3, pp. 121–123, Aug. 1981.

[56] W. F. Young, B. Belzer, and R. G. Olsen, "A two-element antenna for null suppression in multipath environments," *IEEE Trans. Antennas Propagat.*, vol. 48, no. 8, pp. 1161–1174, Aug. 2000.

[57] W. C. Y. Lee and Y. S. Yeh, "Polarization diversity system for mobile radio," *IEEE Trans. Commun.*, vol. COM-20, no. 5, pp. 912–923, Oct. 1972.

[58] R. G. Vaughan, "Polarization diversity in mobile communications," *IEEE Trans. Veh. Technol.*, vol. 39, no. 3, pp. 177–186, Aug. 1990.

[59] U. Wahlberg, S. Widell, and C. Beckman, "The performance of polarization diversity antennas at 1800 MHz," *IEEE Antennas Propagat. Soc. Int. Symp. Dig.*, USA, vol. 2, pp. 1368–1371, July 1997.

[60] S. A. Bergmann and H. W. Arnold, "Polarisation diversity in portable communications environment," *Electron. Lett.*, vol. 22, no. 11, pp. 609–610, May 1986.

[61] T. Taga, "Analysis for mean effective gain of mobile antennas in land mobile radio environments," *IEEE Trans. Veh. Technol.*, vol. 39, no. 2, pp. 117–131, May 1990.

[62] M. G. Douglas, M. Okoniewski, and M. A. Stuchly, "A planar diversity antenna for handheld PCS devices," *IEEE Trans. Veh. Technol.*, vol. 47, no. 3, pp. 747–754, Aug. 1998.

[63] D. H. Schaubert, F. G. Farror, A. Sindoris, and S. T. Hayes, "Microstrip antennas with frequency agility and polarization diversity," *IEEE Trans. Antennas Propagat.*, vol. AP-29, no. 1, pp. 118–123, Jan. 1981.

[64] F. Adachi and J. D. Parsons, "Unified analysis of postdetection diversity for binary digital FM mobile radio," *IEEE Trans. Veh. Technol.*, vol. 37, no. 4, pp. 189–198, Nov. 1988.

[65] W. C. Y. Lee, *Mobile Communications Engineering*, pp. 572–573, McGraw-Hill, Singapore, 2nd Ed., 1998.

[66] W. C. Jakes, *Microwave Mobile Communications*, AT&T IMP Corp., USA, 1974.

[67] J. Ossana Jr., "A model for mobile radio fading due to building reflections: Theoretical and experimental fading waveform power spectra," *Bell Syst. Technical J.*, vol. 43, no. 6, pp. 2935–2971, Nov. 1964.

[68] R. H. Clarke, "A statistical theory of mobile-radio reception," *Bell Syst. Technical J.*, vol. 47, no. 6, pp. 957–1000, July–Aug. 1968.

[69] F. Ikegami and S. Yoshida, "Analysis of multipath propagation structure in urban mobile radio environments," *IEEE Trans. Antennas Propagat.*, vol. Ap-28, no. 4, pp. 531–537, July 1980.

[70] A. M. D. Turkmani, A. A. Arowojolu, P. A. Jefford, and C. J. Kellett, "An experimental evaluation of the performance of two-branch space and polarization diversity schemes at 1800 MHz," *IEEE Trans. Veh. Technol.*, vol. 44, no. 2, pp. 318–326, May 1995.

[71] P. C. F. Eggers, J. Toftgård, and A. M. Oprea, "Antenna systems for base station diversity in urban small and micro cells," *IEEE J. Select. Areas Commun.*, vol. 11, no. 8, pp. 1046–1057, Sept. 1993.

[72] F. Adachi, M. T. Freeney, A. G. Williamson, and J. D. Parsons, "Cross-correlation between the envelopes of 900 MHz signals received at a mobile radio base station," *IEE Proc.*, vol. 133, Pt. F, no. 6, pp. 506–512, Oct. 1986.

[73] T. Taga, K. Tsunoda, and H. Imahori, "Correlation properties of antenna diversity in indoor mobile communication environments," *Proc. 39th IEEE Veh. Technol. Conf.*, San Francisco, CA, USA, pp. 446–451, May 1989.

[74] K. Ogawa and J. Takada, "An analysis of the effective performance of a handset diversity antenna influenced by head, hand and shoulder effects—A proposal for the diversity antenna gain based on a signal bit-error rate and the analytical results for the PDC system," *IEICE Trans.*, vol. J83-B, no. 6, pp. 852–865, June 2000 (in Japanese).

[75] F. Adachi, and K. Ohno, "BER performance owing to random FM noise for QDPSK mobile radio with diversity reception," *Electron. Lett.*, vol. 27, no. 8, pp. 629–631, Apr. 1991.

[76] M. Schwartz, W. R. Bennett, and S. Stein, *Communication Systems and Techniques*, McGraw-Hill, New York, 1966.

[77] M. K. Simon and M. S. Alouini, *Digital Communication over Fading Channels : A Unified Approach to Performance Analysis*, John Wiley&Sons, New York, USA, 2000.

[78] M. Hussein and A. Sebak, "Application of the finite-difference time-domain method to the analysis of mobile antennas," *IEEE Trans. Veh. Technol.*, vol. 45, no. 3, pp. 417–426, Aug. 1996.

[79] L. Chen, T. Uno, S. Adachi, and R. J. Luebbers, "FDTD analysis of a monopole antenna mounted on a conducting box covered with a layer of dielectric," *IEICE Trans. Commun.*, vol. E76-B, no. 12, pp. 1583–1586, Dec. 1993.

[80] M. Analoui and Y. Kagawa, "On the surface-patch and wire-grid modeling for planar antenna mounted on metal housing," *IEICE Trans. Commun.*, vol. E76-B, no. 11, pp. 1450–1455, Nov. 1993.

[81] E. K. Miller, "PCs for AP and other EM reflections: Wire-grid approximations to solid surfaces," *IEEE Antennas Propagat. Mag.*, vol. 39, no. 2, pp. 318–326, Feb. 1997.

[82] N. Ishii and K. Itoh, "A consideration of the thin planar antenna with wire-grid model," *IEICE Trans. Commun.*, vol. E76-B, no. 12, pp. 1518–1525, Dec. 1993.

[83] H. O. Ruoss and F. M. Landstorfer, "Electromagnetic dyadic Green's function for a layered homogeneous lossy dielectric sphere as head model for numerical EMC investigation," *Electron. Lett.*, vol. 32, no. 21, pp. 1935–1937, Oct. 1996.

[84] S. M. Rao, D. R. Wilton, and A. W. Glisson, "Electromagnetic scattering by surfaces of arbitrary shape," *IEEE Trans. Antennas Propagat.*, vol. AP-30, no. 3, pp. 409–418, May 1982.

[85] T. Angkaew, M. Matsuhara, and N. Kumagai, "Finite-element analysis of waveguide modes: A novel approach that eliminates spurious modes," *IEEE Trans. Microwave Theory Tech.*, vol. MTT-35, no. 2, pp. 117–123, Feb. 1987.

[86] J. Cooper, V. Hombach, and A. Schiavoni, "Comparison of computational electromagnetic codes applied to a sphere canonical problem," *IEE Proc.-Microw. Antennas Propagat.*, vol. 143, no. 4, pp. 309–316, Aug. 1996.

[87] G. J. Burke and A. J. Poggio, *Numerical Electromagnetics Code (NEC) — Method of Moments, Parts I–III*, Lawrence Livermore Nat. Lab., Livermore, CA, 1981.

[88] R. F. Harrington, *Field Computation by Moment Methods*, Robert E. Krieger Publishing, Malabar, Florida, 1982.

[89] A. C. Ludwig, "Wire grid modeling of surfaces," *IEEE Trans. Antennas Propagat.*, vol. AP-35, no. 9, pp. 117–120, Sept. 1987.

[90] K. Hirasawa and M. Haneishi, *Analysis, Design and Measurement of Small and Low-Profile Antennas*, Artech House, Norwood, MA, 1992.

[91] C. Hill and T. Kneisel, "Portable radio antenna performance in the 150, 450, 800, and 900 MHz bands outside and in-vehicle," *IEEE Trans. Veh. Technol.*, vol. 40, no. 4, pp. 750–756, Nov. 1991.

[92] W. T. Chen and H. R. Chuang, "Numerical computation of human interaction with arbitrarily oriented superquadratic loop antennas in personal communications," *IEEE Trans. Antennas Propagat.*, vol. 46, no. 6, pp. 821–828, June 1998.

[93] G. F. Pedersen and J. B. Andersen, "Integrated antennas for hand-held telephones with low absorption," *Proc. 44th IEEE Veh. Technol. Conf.*, Stockholm, Sweden, vol. 3, pp. 1537–1541, June 1994.

[94] K. Noguchi, M. Ando, N. Goto, M. Hirose, T. Uno, and Y. Kamimura, "Directional antennas for portable telephones," *IEICE Trans. Commun.*, vol. E79-B, no. 9, pp. 1234–1241, Sept. 1996.

[95] P. Erätuuli, P. Haapala, P. Aikio, and P. Vainikainen, "Measurements of internal handset antennas and diversity configurations with a phantom head," *IEEE Antennas Propagat. Soc. Int. Symp. Dig.*, Atlanta, Georgia, USA, vol. 1, pp. 126–129, June 1998.

[96] M. Okoniewski and M. A. Stuchly, "A study of the handset antenna and human body interaction," *IEEE Trans. Microwave Theory Tech.*, vol. 47, no. 3, pp. 1855–1864, Oct. 1996.

[97] R. G. Vaughan and N. L. Scott, "Evaluation of antenna configurations for reduced power absorption in the head," *IEEE Trans. Veh. Technol.*, vol. 48, no. 5, pp. 1371–1380, Sept. 1999.

[98] M. G. Douglas and R. H. Johnston, "A compact two way diversity microstrip upatch antenna," *IEEE Antennas Propagat. Soc. Int. Symp. Dig.*, Newport Beach, California, USA, vol. 2, pp. 978–981, June 1995.

[99] G. F. Pedersen and S. Skjaerris, "Influence on antenna diversity for a handheld phone by the presence of a person," *Proc. 47th IEEE Veh. Technol. Conf.*, Phoenix, AZ, USA, pp. 1768–1772, May 1997.

[100] K. Fujimoto, A. Henderson, K. Hirasawa, and J. R. James, *Small Antennas*, Research Studies Press, Hertfordshire, England, 1987.

LIST OF PUBLICATIONS

Works Concerning This Thesis

1. K. Meksamoot, M. Krairiksh, and J. Takada, "Polarization diversity PIFA for small portable telephone," *Proc. 1st Int. Symp. Wireless Personal Multimedia Commun. (WPMC'98)*, Yokosuka, Japan, pp. 304–307, Nov. 1998.

2. K. Meksamoot, M. Krairiksh, and J. Takada, "Performance of polarization diversity PIFA on portable telephone in multipath environment," *Proc. 1999 Thailand-Japan Joint Symp. Microwaves (TJMW'99)*, Pattaya, Thailand, pp. 69–75, Sept. 1999.

3. K. Meksamoot, M. Krairiksh, and J. Takada, "Polarization diversity planar inverted-F antenna and its performance in multipath environment," *Proc. 1999 IEEE Int. Symp. Intelligent Signal Processing and Commun. Syst. (ISPACS'99)*, Phuket, Thailand, pp. 709–712, Dec. 1999.

4. K. Meksamoot, M. Krairiksh, and J. Takada, "Evaluation of polarization diversity PIFA on portable telephone in multipath environment," *Proc. AP2000 Millennium Conf. Antennas Propagat.*, Davos, Switzerland, vol. 1, p. 362, Apr. 2000.

5. K. Meksamoot, M. Krairiksh, and J. Takada, "Effect of human interaction on diversity performance of polarization diversity PIFA on portable telephone," *Proc. 2000 Int. Symp. Antennas Propagat. (ISAP2000)*, Fukuoka, Japan, vol. 3, pp. 1067–1070, Aug. 2000.

6. † K. Meksamoot, M. Krairiksh, and J. Takada, "A Polarization Diversity PIFA on Portable Telephone and the Human Body Effects on Its Performance," *IEICE Trans. Commun.*, vol. E84-B, no. 9, pp. 2460–2467, Sept. 2001.

† Reprinted in this chapter.

Related Works

1. P. Keowsawat, K. Meksamoot, and M. Krairiksh, "Performance of a bi-directional polarization diversity antenna using two-perpendicular-probe excited square ring for PCS base station," *Proc. 3rd Int. Symp. Wireless*

Personal Multimedia Commun. (WPMC'00), Bangkok, Thailand, vol. 1, pp. 306–310, Nov. 2000.

2. P. Keowsawat, K. Meksamoot, and M. Krairiksh, "A bi-directional antenna using two-perpendicular-probe excited circular ring for polarization diversity," *Proc. 23rd Electrical Engineering Conf. (EECON-23)*, Chiangmai, Thailand, pp. 321–324, Nov. 2000 (in Thai).

3. P. Keowsawat, K. Meksamoot, S. Kosulvit and M. Krairiksh, "The DAG investigation of bi-directional antenna using two-perpendicular-probe excited circular ring for polarization diversity," *Proc. 2000 Asia-Pacific Symp. Broadcasting Commun. (APSBC'00)*, Bangkok, Thailand, pp. 268–273, Dec. 2000.

Interested Works

1. K. Meksamoot, M. Krairiksh, C. Phongcharoenpanich, and S. Kosulvit, "A planar slot array antenna for Thaicom satellite broadcasting reception," *Proc. 1997 Thailand-Japan Joint Symp. Antennas Propagat. (TJSAP'97)*, Bangkok, Thailand, pp. 55–59, May 1997.

2. C. Phongcharoenpanich, M. Krairiksh, K. Meksamoot, and T. Wakabayashi, "Legendre array," *Proc. 1997 Thailand-Japan Joint Symp. Antennas Propagat. (TJSAP'97)*, Bangkok, Thailand, pp. 195–201, May 1997.

3. C. Phongcharoenpanich, M. Krairiksh, K. Meksamoot, and J. Takada, "Radiation characteristics of a circularly polarized conical beam spherical slot array antenna," *Proc. 1998 Asia-Pacific Microwave Conf. (APMC'98)*, Yokohama, Japan, vol. 3, pp. 1229–1232, Nov. 1998.

4. M. Krairiksh, C. Phongcharoenpanich, K. Meksamoot, and J. Takada, "A circularly polarized conical beam spherical slot array antenna," *Int. J. Electron.*, vol. 86, no. 7, pp. 815–823, July 1999.

Reprinted

平成13年8月25日印刷 平成13年9月1日発行 第117号（毎月1回1日発行） ISSN 0916-8516

IEICE TRANSACTIONS

on Communications

Special Issue on Innovation in Antennas and Propagation for Expanding Radio Systems

VOL.E84-B
NO.9
SEPTEMBER 2001

A PUBLICATION OF THE COMMUNICATIONS SOCIETY
The Institute of Electronics, Information and Communication Engineers
Kikai-Shinko-Kaikan Bldg., 5-8, Shibakoen 3 chome, Minato-ku,
TOKYO, 105-0011 JAPAN

IEICE TRANS. COMMUN., VOL.E84-B, NO.9 SEPTEMBER 2001

PAPER Special Issue on Innovation in Antennas and Propagation for Expanding Radio Systems

A Polarization Diversity PIFA on Portable Telephone and the Human Body Effects on Its Performance*

Komsak MEKSAMOOT†, *Student Member*, Monai KRAIRIKSH†, *and* Jun-ichi TAKADA††, *Regular Members*

SUMMARY A polarization diversity planar inverted-F antenna (PIFA) on portable telephone in the practical use near the operator's body is investigated at 1,800 MHz under multipath urban environment. The antenna structure comprises a center-fed square patch with one permanent short-pin and two RF-switches on three corners. The RF-switches perform as the polarization branch switches for dominantly vertical polarization (VP) or dominantly horizontal polarization (HP) modes. The radiation efficiency of the polarization diversity PIFA is 58% and 53% for VP and HP modes, respectively, which is higher than the 52% efficiency of the reference $\lambda/4$ monopole antenna under the same condition. The mean effective gain (MEG) of VP and HP modes decrease with respect to the increasing cross-polarization power ratio (XPR). The correlation coefficient of two diversity branches is between 0.66 through all the possible XPR ranging from -10 dB to $+10$ dB. The diversity gain is computed from the MEG and correlation coefficient to determine the diversity antenna gain (DAG). The diversity gain, based on 10^{-3} BER for selective combining, is 7.5 dB over non-diversity reception. The DAG is $-1.2\cdots+2.8$ dBi which is approximately 4 dB lower than the case without human body. In other words, the presence of the human body degrades the communication performance by a half.

key words: polarization diversity, PIFA, mean effective gain, correlation coefficient, diversity antenna gain

1. Introduction

At present, personal communications can be considered as a part of daily-life essence. Key devices for transmitting and receiving signal between portable unit and base station are antennas. One of the major problems emerged in mobile communication environment is multipath interference. To overcome deep fading caused by the multipath propagation, there are many alternative schemes on antenna diversity technique [1]. The most commonly used schemes are space diversity and radiation pattern diversity [2], [3] because of their structural simplicity. However, the space diversity requires two or more antenna elements while the radiation pattern diversity may produce undesirable radiation in the direction of the user's head. Additional requirement occurs while using the portable telephone that is the compactness of the unit which implies the small flat built-in antenna. The alternative diversity scheme which will be more suitable is polarization diversity [4]. The compact dimension of an antenna used in this scheme is a significant merit. There were a number of research works dealing with half-wavelength microstrip antenna proposed for polarization diversity [5], [6]. Nevertheless, the dimension of the antenna is not small enough to be mounted on a portable telephone.

In order to mitigate multipath fading while the diversity antenna keeps low-profile, the authors propose a PIFA [7] modified for applying to the polarization diversity [8]. The structure of the antenna is similar to the conventional PIFA, except that it has two semiconductor switches at the orthogonal positions to each other with respect to the short-pin position. By turning either of the switches on, it acts as a short-pin, the polarization of the antenna can be changed by switching. Consequently, the conventional switching diversity schemes can be applied.

The characteristics of the antenna with the portable telephone housing are simulated by the Method of Moments on wire-grid model using the Numerical Electromagnetics Code [9]. Since this antenna is used under the multipath environment, the radiation patterns have no direct meaning of the antenna performance [10], [11]. In previous works, [12]–[14], the investigations were carried out by simulating the human body with only head and hand models. However, Ogawa [15] reported that the additional left-shoulder model, on which the handset was held, considerably effected to the radiation at 900 MHz.

This paper investigates the interaction between the polarization diversity PIFA on portable telephone and the operator's body, from the chest to the head, under the mobile urban environment. The diversity performances of this antenna have been first studied in [16]. This paper improves the results presented in [16] by refining details of the model, changing the angular power distribution from a simple Clarke model to be the extended one [17], adding radiation efficiency, and comparing with $\lambda/4$ monopole antenna. The results are revealed in terms of the radiation patterns, the mean

Manuscript received December 16, 2000.
Manuscript revised March 20, 2001.

†The authors are with the Faculty of Engineering and Research Center for Communications and Information Technology, King Mongkut's Institute of Technology Ladkrabang, Bangkok 10520, Thailand.

††The author is with the Graduate School of Science and Engineering, Tokyo Institute of Technology, Tokyo, 152-8552 Japan.

*Some parts of this paper were presented at ISAP2000, Fukuoka, Japan.

effective gain, the correlation coefficient, the diversity gain, and the diversity antenna gain quantitatively.

2. Configuration and Modeling

2.1 Antenna Structures

The polarization diversity PIFA, will be denoted by PDA (polarization diversity antenna) hereafter, consists of a square metallic patch with the length of 26 mm, to operate at the frequency of 1,800 MHz, located on a conductive telephone box (as ground plane) of dimension $25 \times 45 \times 130\,\text{mm}^3$ as shown in Fig. 1(a). The top-right corner of the patch is shorted to the telephone via a permanent short-pin. Two RF-switches on the top-left (A) and the bottom-right (B) corners which will operate as a short-circuit path, one at a time, results in the radiation of dominantly vertical polarization (VP) or dominantly horizontal polarization (HP) as shown in Figs. 2(a)–(d), respectively.

The numerical results show that the resonant current flows from the short-pin via the edge of the patch and vanishes at the center of the adjacent edge due to the symmetry structure, as depicted in the inset in Fig. 1, i.e., part of periphery $1.5L$ plus height h approximately equals quarter-wavelength $\lambda/4$ [8]. Figure 2(f) shows input impedance of PDA on handset in VP and HP modes with and without human body. Although the input impedance can be matched to 50 Ω if the feed probe is moved toward the short-pin, this paper fixed the feed point at the center to maintain the highest diversity characteristics. Therefore, the PDA in this configuration needs matching circuit beneath the feed probe. The resonant frequency of HP mode is slightly higher than VP mode, it can also be trimmed to obtain the same resonance by slightly lengthening the horizontal dimension of the patch.

A $\lambda/4$ monopole is used for the reference case. It will be omitted while simulating the PDA. Otherwise, it is positioned on the top-left of the telephone box as shown in Fig. 1(a). The radiation pattern, Fig. 2(e), of the dominant polarization is similar to the butterfly shape pattern in xz-plane as noted in [13], [14].

2.2 Human Body Model

The upper-half part of the human body is considered to mostly contribute to the interaction with the mobile handheld antennas. To take into account the interaction of human body, the phantom of the head is modeled and placed on the center of the shoulder. The hand is positioned 5 mm apart from the right-hand side of the head with tilted angle $\alpha = 60°$, and the telephone is in the hand with same orientation as shown in Figs. 3(a) and (b). The cylindrical model of head, parallelopiped model of hand and arm, and trapezoidal

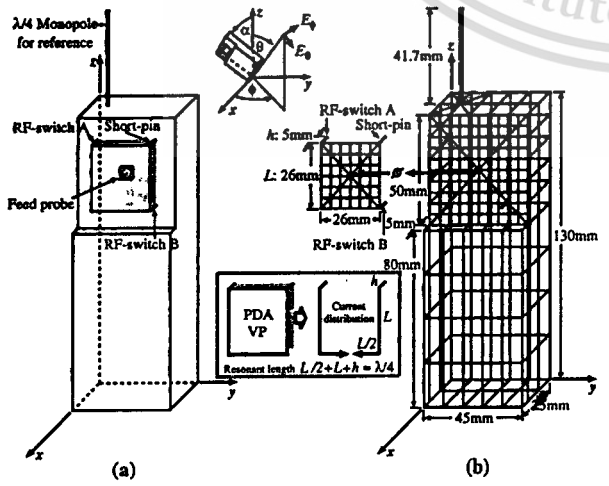

Fig. 1 The PDA on portable telephone and the reference $\lambda/4$ monopole antenna (a) experimental model with portable telephone and (b) wire-grid model.

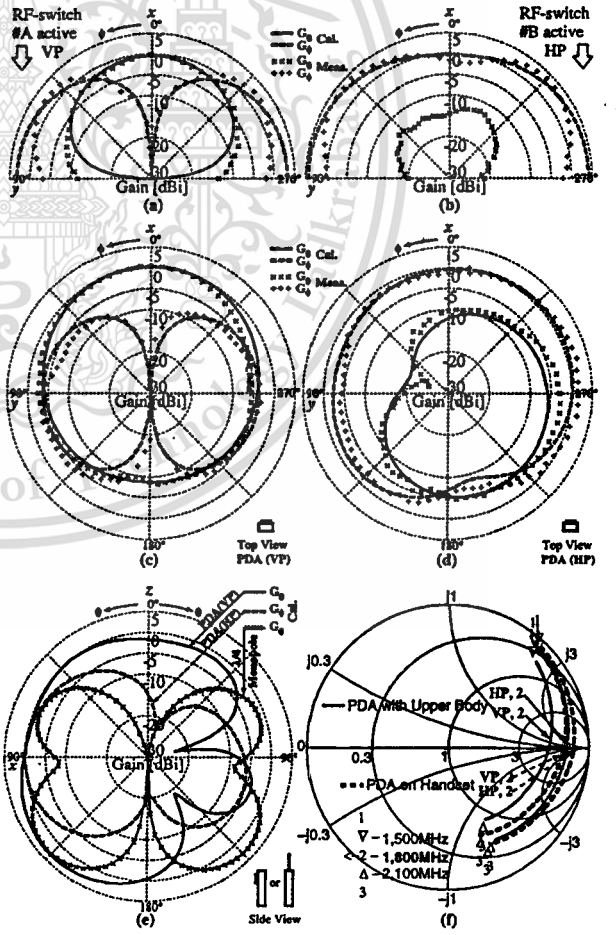

Fig. 2 The radiation patterns, in xy-plane at $\alpha = 0°$, of the PDA on ground plane (a) VP, and (b) HP; PDA on handset (c) VP, and (d) HP; (e) dominant polarizations in xz-plane, compares with $\lambda/4$ monopole; (f) input impedance of PDA.

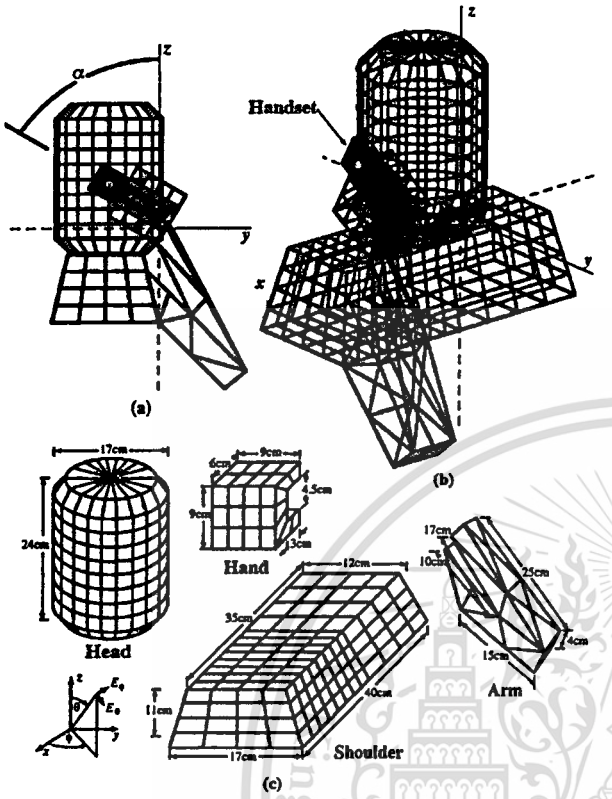

Fig. 3 Wire-grid model of the antenna with human phantom (a) side-view (b) isometric view (c) phantom dimensions.

model of shoulder are assigned by the dimensions as depicted in Fig. 3(c).

2.3 Wire-Grid Modeling

The antenna and telephone are modeled by conductive wire-grid structure as depicted in Fig. 1(b). While the phantoms are modeled by conductive wire-grid loaded with the surface impedance $Z_s = \left(j\omega\mu/(\sigma + j\omega\epsilon)\right)^{1/2}$ [18], where the conductivity $\sigma = 0.85$ S/m and the complex relative permittivity $\epsilon_r = 48 - j30$ averaged for a head [19], and $\sigma = 1.39$ S/m and $\epsilon_r = 54 - j14$ averaged for muscle from FCC, to simulate the dielectric property of the human tissue as depicted in Fig. 3. The short-wire is modeled for the active RF-switch, but none when it is switched off. The choice of the grid-wire radius is based on the equivalent surface area assumption [20]. It is observed that if the grid-wire radius is enlarged or shrinked by 2-fold, the radiation efficiency will decrease or increase by 7%, respectively. The adaptive gridding is employed in the modeling. The grid-size is small for the antennas and nearby structures, e.g., the telephone box part beneath the PIFA patch and at the base of monopole antenna. The larger grid-size is assigned for the structures far from the primarily radiating structures. The segment-length of each wire-grid is assigned adaptively (1 mm–45 mm), likewise. The wire-grid models that are illustrated in Fig. 1(b) and Fig. 3 correspond to the simulation model.

3. Method of Analysis

3.1 Mean Effective Gain

The mean effective gain (MEG), denoted by G_e, is a statistical measure of the antenna gain in mobile environment. It is defined by the ratio between the mean received power of antenna and the total mean incident power over the random route. It can be expressed by [17]

$$G_e = \int_0^{2\pi}\int_0^{\pi}\left(\frac{\mathrm{XPR}}{1+\mathrm{XPR}}G_\theta(\theta,\phi)P_\theta(\theta,\phi) + \frac{1}{1+\mathrm{XPR}}G_\phi(\theta,\phi)P_\phi(\theta,\phi)\right)\sin\theta d\theta d\phi, \quad (1)$$

where $G_\theta(\theta,\phi)$ and $G_\phi(\theta,\phi)$ are the θ- and ϕ-components of the antenna power gain patterns, respectively, and $P_\theta(\theta,\phi)$ and $P_\phi(\theta,\phi)$ are the θ- and ϕ-components of the normalized angular power density functions of incoming plane waves, respectively.

The cross-polarization power ratio (XPR) is defined by the mean incident power ratio P_V/P_H where P_V and P_H are mean incident power of vertically and horizontally polarized waves, respectively. In the suburban outdoor or indoor environment, where there is no line-of-sight signal, the XPR is close to 0 dB. However, in urban outdoor environments, the XPR varies considerably from 0 dB to +10 dB [17], [21].

3.2 Propagation Model

To model the angular power density functions of incoming plane waves in multipath environment, we assume azimuthal distribution $P_{\theta,\phi}(\phi)$ to be uniform and elevational distribution $P_{\theta,\phi}(\theta)$ by Gaussian distributions in the θ direction [17]. For $0 \le \theta \le \pi$

$$P_\theta(\theta,\phi) = A_\theta e^{-\left(\frac{\left(\theta-(\frac{\pi}{2}-m_V)\right)^2}{2\sigma_V^2}\right)} \quad (2)$$

$$P_\phi(\theta,\phi) = A_\phi e^{-\left(\frac{\left(\theta-(\frac{\pi}{2}-m_H)\right)^2}{2\sigma_H^2}\right)} \quad (3)$$

where m_V and σ_V are mean and standard deviation of incident angle of arrival of vertically polarized waves and m_H and σ_H are likewise for horizontally polarized waves (the mean angles are observed from the horizontal direction). A_θ and A_ϕ are the amplitudes of P_θ and P_ϕ, respectively.

The urban outdoor environment model is used in this paper, corresponding to the values of $m_V = 19°, \sigma_V = 20°, m_H = 32°$, and $\sigma_H = 64°$ follow the measurement performed by Taga [17], as depicted in Fig. 4.

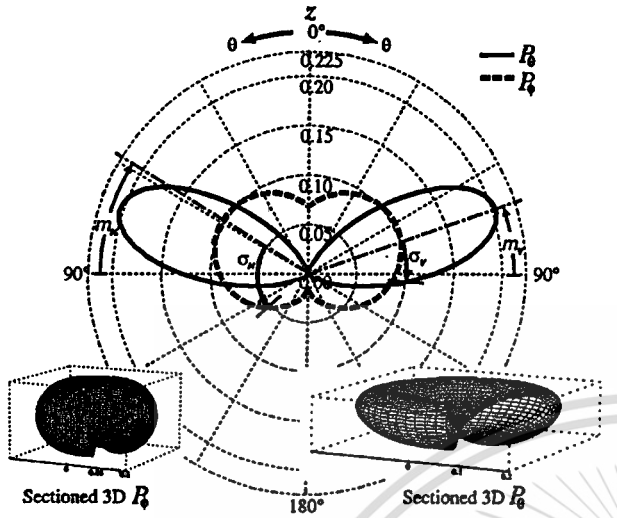

Fig. 4 Angular power density function of waves incident on antenna in the urban environment [17].

3.3 Correlation Coefficient

The envelope correlation coefficient ρ_e of the received signal between two antenna diversity branches can be approximated by the squared magnitude of complex correlation coefficient ρ as [22]

$$\rho_e \approx |\rho|^2 = \frac{|R_{12}|^2}{R_{11}R_{22}}, \tag{4}$$

where the covariance R_{ij} $(i,\ j = 1,\ 2)$ of the two received voltages resulted from $(E_{\theta i}, E_{\phi i})$ and $(E_{\theta j}, E_{\phi j})$ of the complex electric field patterns is

$$R_{ij} = 2KP_H\int_0^{2\pi}\int_0^{\pi}\Big(XPR\cdot E_{\theta i}(\theta,\phi)E^*_{\theta j}(\theta,\phi)P_\theta(\theta,\phi) + E_{\phi i}(\theta,\phi)E^*_{\phi j}(\theta,\phi)P_\phi(\theta,\phi)\Big)\sin\theta d\theta d\phi, \tag{5}$$

where K is a proportionality constant.

When only correlation coefficient is mentioned, this paper refers to the envelope correlation coefficient.

3.4 Diversity Gain

The diversity gain G_{div} is defined as the difference of the average carrier-to-noise power ratio (CNR) at a certain value of the bit-error rate (BER) (usually at 10^{-3}), between the BER curve of the CNR envelope of the diversity combiner output, and that of the single reference antenna output under the Rayleigh fading environment.

The diversity gain with respect to BER is defined by [15]

$$G_{div} = \frac{\Gamma_{div}}{\Gamma_{non}}, \tag{6}$$

where Γ_{non} is the average carrier-to-noise power ratio (CNR) at the prescribed BER when the signals are received by the single branch non-diversity antenna which has the greater CNR of the two branches. Γ_{div} is the average CNR in case of diversity reception.

The average BER $(\overline{P}_e)$ of the diversity antenna due to time varying attenuation can be obtained as

$$\overline{P}_e = \int_0^\infty p_e(\gamma)p(\gamma)d\gamma, \tag{7}$$

where $p_e(\gamma)$ is the conditional BER when the instantaneous CNR at the detector input is γ in the Rayleigh fading channel. $p(\gamma)$ is the probability density (PDF) of the instantaneous CNR after combining. From (7), the average BER can be calculated as follows:

$p(\gamma)$ of the receiving signals for the post-detection two-branch selective combining diversity under unequal median value and correlated signal condition is given as follows [23].

$$p(\gamma) = \frac{d}{d\gamma}\left(1 - e^{\left(-\frac{\gamma}{\Gamma}\right)}Q\left(\sqrt{\frac{2\gamma}{r\Gamma(1-\rho_e)}}, \sqrt{\frac{2\rho_e\gamma}{\Gamma(1-\rho_e)}}\right) - e^{\left(-\frac{\gamma}{r\Gamma}\right)}\left(1 - Q\left(\sqrt{\frac{2\rho_e\gamma}{r\Gamma(1-\rho_e)}}, \sqrt{\frac{2\gamma}{\Gamma(1-\rho_e)}}\right)\right)\right), \tag{8}$$

where Γ is the average CNR of branch A. r is the median value ratio defined by

$$r = \begin{cases} \frac{G_{eA}}{G_{eB}} & (G_{eA} \le G_{eB}), \\ \frac{G_{eB}}{G_{eA}} & (G_{eA} > G_{eB}), \end{cases} \tag{9}$$

where G_{eA} and G_{eB} are the MEG of diversity branches A and B, respectively. Q is the Marcum's Q-function [23].

$p_e(\gamma)$ of the $\pi/4$ shifted Quadrature Phase Shift Keying ($\pi/4$ QPSK) signals with delay detection in the Additive White Gaussian Noise (AWGN) channel is calculated by the following equation [24].

$$p_e(\gamma) = \frac{1}{4\pi\sqrt{2}}\int_0^{2\pi}\frac{e^{-\gamma\left(1-\frac{\cos t}{\sqrt{2}}\right)}}{1-\frac{\cos t}{\sqrt{2}}}dt. \tag{10}$$

By substituting (8)–(10) into (7), the average BER can be calculated by numerical integration.

3.5 Diversity Antenna Gain

The most effective parameter to evaluate the performance of a diversity antenna is the diversity antenna gain (DAG) since it includes the correlation coefficient and the MEG characteristics. The DAG can be considered as the system gain when compared with the reference antenna under the same propagation environment. It is defined as a product of the MEG of the higher branch and the diversity gain as [15]

$$\mathrm{DAG} = \begin{cases} G_{eB}\cdot G_{div} & (r_m \le 1), \\ G_{eA}\cdot G_{div} & (r_m > 1). \end{cases} \tag{11}$$

4. Results and Discussion

The far-field radiation patterns of the PDA and monopole are simulated by the Numerical Electromagnetic Code (NEC2) [9] based on the Method of Moments at the frequency of 1,800 MHz. To validate the simulation results, a PDA on conductive telephone box has been fabricated and measured. The radiation patterns of this antenna were measured via S_{21}-parameter using HP8510C network analyzer in the opened area test site on the rooftop of the building, the antenna was installed at 2.5 m high from the floor, an absorber was installed on the floor between the transmitting antenna (7-E Yagi-Uda antenna) and the AUT to suppress ground reflection. The test range is 5 m.

4.1 Effects of User's Body on Total Gain Patterns

For the case that antenna is mounted on the handset as shown in Figs. 5(a) and (b), the PDA has radiation patterns similar to omni-directional pattern in xy- and xz-plane for HP mode. While VP mode has a null at $\phi = 190°$ in xy-plane and at $\theta = 80°, \phi = 130°$. The monopole on handset has higher gain upto 4 dBi at $\phi = 45°$ and 135° in xy-plane (Fig. 5(b)) whereas in xz-plane (Fig. 5(a)) the gain is high at $\theta = 0°$.

When the head and hand of the user's body are included (Figs. 5(c)–(d)), they absorb the radiation in $-x$ direction (head). The patterns of PDA for VP mode are similar to the patterns of monopole in direction opposite to the head. While the patterns in the direction of head are similar for PDA in VP and HP modes.

When all upper parts of the body are modeled, the radiation patterns are more absorbed in $-z$ direction (shoulder) as can be observed in Fig. 5(e). Arm effects to minor absorption in $+y$ direction (Fig. 5(f)). The quantitative differences can be seen from the radiation efficiency η which is 3% degraded. The radiation efficiency of PDA and monopole on handset approaches 100%. It is reduced to 58.2%, 53.2% and 52.3% for PDA in VP and HP modes and monopole, respectively.

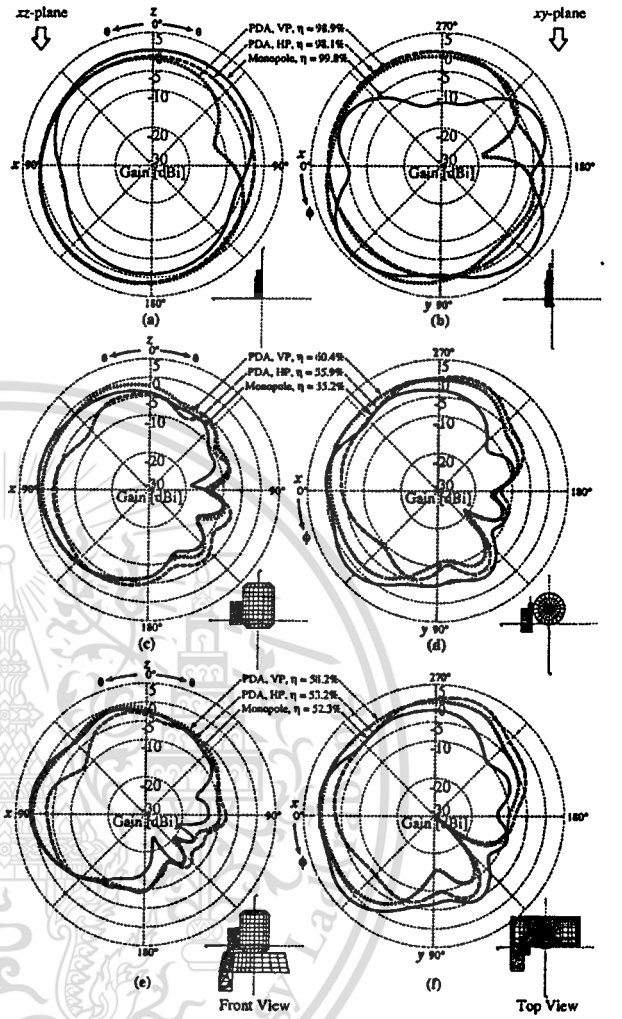

Fig. 5 The total-component-gain patterns of PDA and monopole at tilted angle $\alpha = 60°$; (a) and (b) on handset; (c) and (d) with hand and head; (e) and (f) with upper body. η is the radiation efficiency.

4.2 Polarization Characteristic via Component Gain Patterns

The PDA on handset at tilted angle 60° is firstly investigated, the G_ϕ is higher in the normal direction to the patch for VP mode while G_θ becomes higher for HP mode as shown in Figs. 6(a) and (b), respectively.

When head, hand, arm, and shoulder are cumulatively added, the simulated results show that significant improvement to the radiation patterns (Figs. 6(e) and (f)) is achieved when a head is included with a hand model. Minor improvement to azimuth patterns is obtained when all upper body is modeled (Figs. 6(g) and (h)). These results give the conclusion that the model of shoulder and arm are significant for radiation mechanism at 1,800 MHz as is at 900 MHz [15].

4.3 Mean Effective Gain

The XPR range is chosen to cover all possible value from $-10 \cdots +10$ dB [17], [21]. From Fig. 7, the MEG of PDA for both VP and HP modes and monopole on handset are similar and decrease from $-3 \cdots -2.5$ dBi to $-6 \cdots -5.6$ dBi with respect to the increaseing XPR. When the upper body is included, the MEG of PDA and monopole decrease by 3–4 dB from the previous case and are still in the same trend. The MEG that is degraded by a half is due to the human body blockage to the radiation patterns in almost half space.

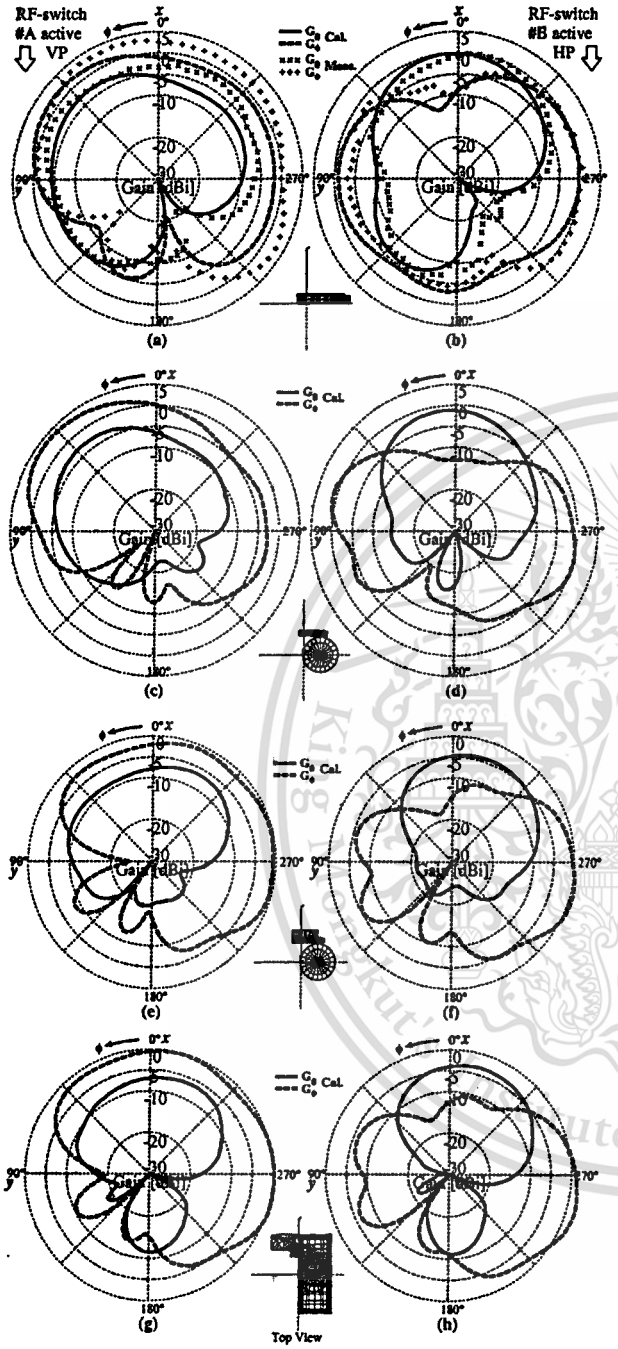

Fig. 6 The G_θ and G_ϕ patterns of the PDA at tilted angle $\alpha = 60°$ in xy-plane; PDA on a portable telephone (a) VP and (b) HP; with head (c) VP and (d) HP; with head and hand (e) VP and (f) HP; with upper body (g) VP and (h) HP.

4.4 Correlation Coefficient

Two diversity branches are considered to be uncorrelated if the correlation coefficient is less than 0.5. However, the reasonable improvement for diversity reception (diversity gain) can be achieved with the correlation coefficient of 0.7 [25]. Figure 8 shows that the correlation coefficient increases to 0.66 if the human body is added. The ρ_e for every case, through all the XPR range, is between 0.32 and 0.66 which is sufficient for practical use. The value of ρ_e in this simulation corresponds to the measurement for the similar structure by Pedersen and Skjaerris [26]. Moreover, results in [8] revealed that ρ_e tends to increase when the inclination angle α of the antenna is increased from 0°. Thus, it might be assumed that ρ_e in Fig. 8 is close to the worst case.

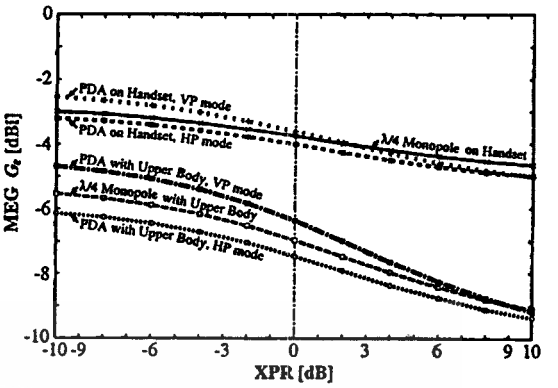

Fig. 7 The differences of MEG of PDA and monopole vs. XPR.

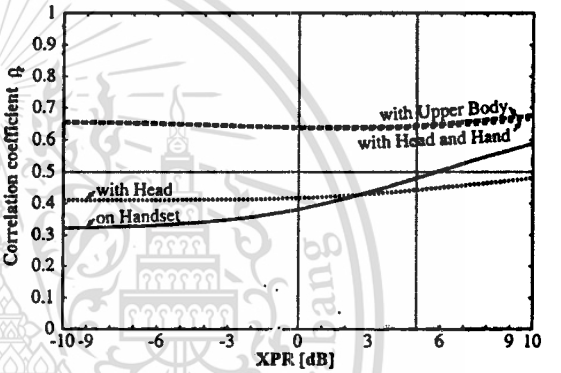

Fig. 8 The differences of correlation coefficient ρ_e of PDA vs. XPR.

4.5 Diversity Gain

The diversity gain of PDA is determined from the MEG differences between VP and HP modes and the correlation coefficient. To show the received average BER improvement from the non-diversity reception, Fig. 9 depicts diversity gain at 10^{-3} BER. The maximum diversity gain for two uncorrelated channels and equal MEG is 10.34 dB. The diversity gain with respect to the XPR is rather constant as shown in Fig. 10. When including the human body, the diversity gain is approximately 1 dB degraded to about 7.5–8.0 dB.

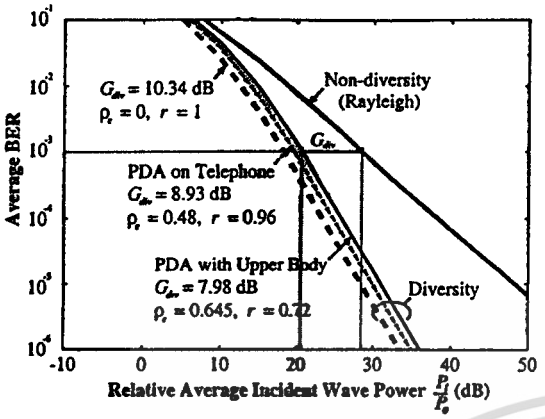

Fig. 9 Diversity gain differences of PDA due to ρ_e and r at XPR = 5 dB.

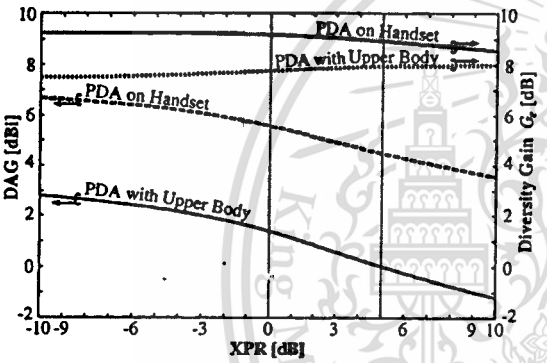

Fig. 10 Diversity antenna gain and diversity gain of PDA vs. XPR.

4.6 Diversity Antenna Gain

The DAG of PDA including human body is approximately degraded 3.8–4.7 dB below the PDA on handset case. It is $2.8 \cdots -1.2$ dBi with respect to the increasing XPR from −10 dB as shown in Fig. 10. Ogawa [15] investigated the selection combining diversity between PIFA and $\lambda/4$ monopole branches at 900 MHz under a similar condition, the DAG of 3 dBi was achieved.

5. Conclusions

Characteristics of a polarization diversity PIFA on a portable telephone have been comparatively investigated without and with the effect of the human interaction. It is found that head, hand, arm, and shoulder modeling are necessary to investigate the interaction to the human body to the far-field radiation at 1,800 MHz. The DAG of the polarization diversity PIFA is close to that of monopole-PIFA diversity antennas [15]. This indicates that the polarization diversity PIFA has similar communication performance to the conventional handset-mounted diversity antenna while the structure can be made to conform to the handset profile.

Acknowledgement

The authors wish to thank Dr. K. Ogawa of Matsushita Electric Industrial Co., Ltd., Japan for his helpful discussion on the diversity parameters and Prof. K. Araki of Tokyo Institute of Technology, Japan for his constructive comments on the angular power distribution model. Thanks also to Ms. P. Keowsawat for her assistance in manipulating diversity data and Mr. N. Kurukitkoson for his assistance in grammatical check.

This work was supported by the National Science and Technology Development Agency (NSTDA), Thailand under the local graduate scholarship program.

References

[1] K. Fujimoto and J.R. James, Mobile Antenna Systems Handbook, ch.2, Artech House, Norwood, MA, 1994.
[2] Y. Yamada, K. Kagoshima, and K. Tsunekawa, "Diversity antennas for base and mobile stations in land mobile communication systems," IEICE Trans., vol.E-74, no.10, pp.3202–3209, Oct. 1991.
[3] K. Ogawa and T. Uwano, "A diversity antenna for very small 800-MHz band portable telephones," IEEE Trans. Antennas & Propag., vol.42, no.9, pp.1342–1345, Sept. 1994.
[4] R.G. Vaughan, "Polarization diversity in mobile communications," IEEE Trans. Veh. Technol., vol.39, no.3, pp.177–186, Aug. 1990.
[5] D.H. Schaubert, F.G. Farror, A. Sindoris, and S.T. Hayes, "Microstrip antennas with frequency agility and polarization diversity," IEEE Trans. Antennas & Propag., vol.29, no.1, pp.118–123, Jan. 1981.
[6] P.M. Haskins and J.S. Dahele, "Four-element varactor diode loaded polarization-agile microstrip antenna array," Electron. Lett., vol.33, no.14, pp.1186–1187, July 1997.
[7] T. Taga and K. Tsunekawa, "Performance analysis of a built-in planar inverted-F antenna for 800 MHz band portable radio units," IEEE J. Sel. Areas Commun., vol.5, no.5, pp.921–929, June 1987.
[8] K. Meksamoot, M. Krairiksh, and J. Takada, "Polarization diversity planar inverted-F antenna and its performance in multipath environment," Proc. 1999 IEEE Int. Symp. on Intelligent Signal Processing and Commun. Syst., pp.709–712, Phuket, Thailand, Dec. 1999.
[9] G.J. Burke and A.J. Poggio, Numerical Electromagnetics Code (NEC)—Method of Moments, Parts I–III, Lawrence Livermore Nat. Lab., Livermore, CA, 1981.
[10] K. Noguchi, M. Ando, N. Goto, M. Hirose, T. Uno, and Y. Kamimura, "Directional antennas for portable telephones," IEICE Trans. Commun., vol.E79-B, no.9, pp.1234–1241, Sept. 1996.
[11] P. Haapala, R. Heiska, M. Honkanen, O. Pekonen, and P. Vainikainen, "Performance evaluation of directive handset antenna in microcellular environment," Electron. Lett., vol.34, no.3, pp.229–230, Feb. 1998.
[12] J. Toftgård, S. Hornsleth, and J.B. Anderson, "Effects on portable antennas of the presence of a person," IEEE Trans. Antennas & Propag., vol.41, no.6, pp.739–746, June 1993.
[13] M.A. Jansen and Y. Rahmat-Samii, "The electromagnetic interaction between biological tissue and antennas on a transceiver handset," IEEE APS Int. Symp. Dig., vol.1,

pp.367–370, 1994.

[14] M.G. Douglas, M. Okoniewski, and M.A. Stuchly, "A planar diversity antenna for handheld PCS devices," IEEE Trans. Veh. Technol., vol.47, no.3, pp.747–754, Aug. 1998.

[15] K. Ogawa and J. Takada, "An analysis of the effective performance of a handset diversity antenna influenced by head, hand and shoulder effects—A proposal for the diversity antenna gain based on a signal bit-error rate and the analytical results for the PDC system," IEICE Trans., vol.J83-B, no.6, pp.852–865, June 2000.

[16] K. Meksamoot, M. Krairiksh, and J. Takada, "Effect of human interaction on diversity performance of polarization diversity PIFA on portable telephone," Proc. 2000 Int. Symp. on Antennas & Propag., vol.3, pp.1067–1070, Fukuoka, Japan, Aug. 2000.

[17] T. Taga, "Analysis for mean effective gain of mobile antennas in land mobile radio environments," IEEE Trans. Veh. Technol., vol.39, no.2, pp.117–131, May 1990.

[18] K. Tsunekawa and A. Ando, "Advanced wire grid method for solving the scattered field of a lossy dielectric object," IEEE APS Int. Symp. Dig., vol.2, pp.797–800, July 1992.

[19] R.G. Vaughan and N.L. Scott, "Evaluation of antenna configurations for reduced power absorption in the head," IEEE Trans. Veh. Technol., vol.48, no.5, pp.1371–1380, Sept. 1999.

[20] E.K. Miller, "PCs for AP and other EM reflections: Wire-grid approximations to solid surfaces," IEEE Antennas & Propag. Mag., vol.39, no.1, pp.94–97, Feb. 1997.

[21] A.M.D. Turkmani, A.A. Arowojolu, P.A. Jefford, and C.J. Kellett, "An experimental evaluation of the performance of two-branch space and polarization diversity schemes at 1800 MHz," IEEE Trans. Veh. Technol., vol.44, no.2, pp.318–326, May 1995.

[22] R.H. Clarke, "A statistical theory of mobile-radio reception," Bell System Technical J., vol.47, no.6, pp.957–1000, July–Aug. 1968.

[23] M. Schwartz, W.R. Bennett, and S. Stein, Communication Systems and Techniques, pp.468–480, McGraw-Hill Book Company, New York, 1966.

[24] F. Adachi and K. Ohno, "BER performance owing to random FM noise for QDPSK mobile radio with diversity reception," Electron. Lett., vol.27, no.8, pp.629–631, April 1991.

[25] W.C.Y. Lee, Mobile Communications Engineering, 2nd ed., pp.572–573, McGraw-Hill, Singapore, 1998.

[26] G.F. Pedersen and S. Skjaerris, "Influence on antenna diversity for a handheld phone by the presence of a person," Proc. 47th IEEE Veh. Technol. Conf., pp.1768–1772, Phoenix, AZ, USA, May 1997.

Komsak Meksamoot was born on April 7, 1972. He received B.Eng. and M.Eng. from Faculty of Engineering, King Mongkut's Institute of Technology Ladkrabang (KMITL) in 1994 and 1997, respectively. He is currently pursuing the D.Eng. degree at the same institute. His research covers planar slot array antennas, microstrip antennas, small antennas for mobile applications, and effect of human interaction on mobile communication performance. He received the Best Paper Award from the 1999 IEEE International Symposium on Intelligent Signal Processing and Communication Systems. Mr. Meksamoot is a student member of IEEE.

Monai Krairiksh was born in Bangkok. He received B.Eng., M.Eng. and D.Eng. from King Mongkut's Institute of Technology Ladkrabang (KMITL) in 1981, 1984 and 1994, respectively. In 1981, he joined the KMITL and presently an associate professor in the Department of Telecommunication Engineering. His main research interests in microwave hyperthermia and antennas for mobile communications. Dr.Krairiksh presently serves as the director of Research Center for Communications and Information Technology (ReCCIT) at KMITL. He is a member of IEEE.

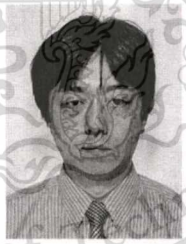

Jun-ichi Takada was born in Tokyo in 1964. He received B.Eng., M.Eng. and D.Eng. degrees from Tokyo Institute of Technology, Japan, in 1987, 1989 and 1992, respectively. In 1992–1994, he was a research associate at Chiba University, Japan. From 1994 he is an associate professor at Graduate School of Science and Engineering, Tokyo Institute of Technology. His current research interests are mobile communication, array signal processing, and numerical simulation of waves. He received the Excellent Paper Award and Young Engineer Award from IEICE Japan in 1993 and 1994, respectively. He is a member of IEEE, ACES and SIAM.

AUTHOR BIOGRAPHY

Author: Mr. Komsak Meksamoot
Date/Place of Birth: 7 April 1972 / Betong, Yala, Thailand

Bachelor Degree: B.Eng. in Telecommunication Engineering (1994)
Undergraduate Research: *Microstrip Patch Coupled with Directors*
Master Degree: M.Eng. in Electrical Engineering (1997)
Master Research: *The Design of Planar Slotted-Waveguide Array Antenna*
Institution: King Mongkut's Institute of Technology Ladkrabang, Thailand

Scholarship:

- Local Graduate Scholarship from the NSTDA (National Science and Technology Development Agency), Thailand (June 1997 – May 2001)
- Visiting Research Scholarships from the INCOCSAT (International Cooperation Center for Science and Technology), TITech (Tokyo Institute of Technology), Japan
  (8–15 Mar. 1998, 16–22 Mar. 1999, 21–30 Mar. 2000, 24–31 Mar. 2001)

Experience:

- Graduate Research Assistant in Steerable Spherical Slot Array Antenna Project under the Career Development Award of the NSTDA (1995–1998)
- Training on Satellite-Mobile Propagation at Satellite Communications Section, Kashima Space and Research Center, Communication Research Laboratory, Japan supported by the ARIB (Association of Radio Industries and Businesses) (4–21 Mar. 1996)
- Training at Takada Laboratory, Mobile Communications Research Group, TITech, Japan supported by the JICA (Japanese International Cooperation Agency), Japan (7 July – 23 Dec. 1998)

Research Awards:

- The Best Paper Award from the 1999 IEEE International Symposium on Intelligent Signal Processing and Communication Systems (ISPACS'99), Phuket, Thailand, Dec. 1999
- The Presentation had been endorsed as the excellent work by the Session Chairs (Session: Human Interaction with Mobile Communication Antennas) in the 2000 International Symposium on Antennas and Propagation (ISAP2000), Fukuoka, Japan, Aug. 2000

Membership:

- The Institute of Electrical and Electronics Engineers (IEEE), USA: Antennas and Propagation Society (AP) and Vehicular Technology Society (VT) (since 1998)
- The Institute of Electronics, Information and Communication Engineers (IEICE), Japan: Communications Society (since 1998)
- National Geographic Society (since 2001)

Special Interests: Photography (since 1988), Lepidopterology (since 1989), and Astronomy (since 1987)